UNIVERSITÀ
DEGLI STUDI
FIRENZE

DOTTORATO DI RICERCA IN
ATOMIC AND MOLECULAR PHOTONICS

CICLO XXVIII

COORDINATORE Prof. Roberto Righini

Entanglement detection via quantum Fisher information in a coupled atom-field system

Settore Scientifico Disciplinare FIS/03

Dottorando:
Safoura S. Mirkhalaf

Tutore:
Prof. Augusto Smerzi

Coordinatore:
Prof. Roberto Righini

Anni 2012/2015

‘‘What makes the desert beautiful,’ said the little prince,
‘is that somewhere it hides a well...’’

Antoine de Saint-Exupéry

To my mom...

Contents

Chapter 1

Introduction

"All in all, it's just another brick in the wall..."
Pink Floyd

Cavity quantum electrodynamics is the study of the interaction between the light and matter [1]. The very first known reference in the field of cavity QED is the abstract of a paper by Edward M. Purcell in 1946 *Physical Review*. This paper was on the changes of decay rate of nuclear magnetic moment transitions at radio frequency, when a spin system is coupled to a resonant electrical circuit [2]. The finding was that if the nuclear magnetic medium is coupled with *small metallic particles* - cavity - the relaxation time drops from about 10^{21} seconds to few minutes. Put simply, the presence of a cavity modifies the decay rate of the emitter.

In 1954, Robert H. Dicke [3] studied the coherent interaction of N atoms with a single mode of the electromagnetic field. The key point of his work was that as a result of coherent interaction, the atoms cannot be regarded as independent emitters if we consider their decay rate. Instead, the ensemble of atoms acts *collectively* with a faster decay rate than N independent individual atoms. This phenomenon is called super-radiance since then. In 1973, it was found the Dicke model exhibits a fascinating phase transition which is itself related to the collective behavior of the particles [4, 5]. More recently, the quantum phase transition of the model in relation to quantum chaos has been investigated [6–9].

Due to lack of intense source of light in 1950's, the experimental realization of the Dicke super-radiance was initially prevented. Nevertheless, after invention of first generations of lasers in 1960 [10], the super-radiance effect was observed in many different laboratories [11–13]. Beside the experimental development, new

techniques were introduced into the cavity QED field such as laser cooling [14, 15] and optical and magneto-optical traps [16–18]. Consequently, more control over the internal/external degrees of freedom of atoms was gained which is still advantageous in the experiments.

In a basic cavity QED scenario, the interaction of the atoms and the electromagnetic fields is inside the cavity. If there is no cavity, an excited atom radiates a photon and decays to the ground state. When the atom is located inside a resonant cavity, the atom radiates the photon to the cavity mode and this photon leaves the cavity mirrors due to dissipation effects. Of course, if the cavity is tuned, the decay rate of the atom will be modified as predicted by Purcell [2]. Nevertheless, in the case of having high quality cavities, the decayed photon can interact repeatedly with the atom before it leaves the cavity. This strong atom-field interaction was studied by Janes and Cummings in 1954 [19]. The Janes-Cumming model was later extended to the case of interaction of collection of atoms with a quantized mode of the field by Tavis and Cumming in 1968 [20]. In fact, the Tavis-Cumming model can be regarded as a Dicke model in the limit of rotating wave approximation (RWA). As a result of employing RWA, the Hamiltonian of the system can be solved analytically.

Since then, thanks to the advancement of lasers and high quality cavities, Janes-Cumming model in number of systems has been realized, such as Rydberg atoms coupled to a microwave resonator [21–24] and alkali atoms inside an optical cavity [25, 26]. Nevertheless, strong limit of interaction needed for the realization of Dicke phase transition was not at hand at the time. It was just recently that thanks to experimental advancement, the strong coupling regime was achieved in systems involving artificial atoms like superconducting qubits [27] or quantum dots [28] embedded in high-quality cavity. Thereafter, in several groups the quantum phase transition and the other properties of the Dicke model has been observed [30–36]. In 2009, the Tavis-Cummings model was implemented by embedding a discrete number of fully controllable superconducting qubits at fixed positions into a transmission line resonator. Consequently, the Vacuum Rabi mode splitting up to three qubits was observed [29]. In 2010, Bose-Einstein condensate coupled to an optical cavity was formed and quantum phase transition and self-organization of a BEC was observed [30]. In a series of experiments by the same group, the different properties of the Dicke phase transition were realized [32, 33]. In another experiment in 2014, the model was implemented in a cavity QED set-up composed of N rubidium atoms inside the high finesse optical cavity [34]. Exploiting two cavity-assisted Raman transitions of the atoms the normal-mode splitting in the Tavis-Cummings model was observed. Moreover, the phase transition in the Dicke model was investigated. Last

year, generalized Dicke models with an ensemble of nitrogen-vacancy (NV) center spins in a diamond sample coupled to a microwave cavity was proposed [36].

Apart from the Dicke phase transition and super-radiance, the coherent coupling of the atoms to a cavity mode, is an interesting testbed of entanglement. In fact, the particles might correlate not by the direct dipole-dipole interaction but via photon exchange processes which serve as a *quantum data bus*. For instance, one may consider the interaction of two ground state atoms coupled with the single mode of the cavity. This is the simplest version of the Dicke model. As a result of interaction with the cavity mode, one atom excites while the other one still is in the ground state. Therefore, due to lack of information, the total state is made of two entangled qubits. Intrinsically, the collective behavior of the atoms in the cavity QED is connected to the concept of multi-particle entanglement.

Quantum entanglement emerged as an controversial issue of quantum mechanics from the very begining. In 1947 A. Einstein in a letter to M. Born called it *"spooky action at a distance"* [37]. Nevertheless, quantum entanglement has found many useful applications in the field of quantum information [38], quantum simulation [39] and quantum metrology [40]. For instance, it has been found that making use of the entangled states as a source of interferometric measurement improves the precision in phase estimation beyond the classical shot-noise limit. Thus, by using entangled states, it is possible to surpass the shot-noise and approach the fundamental Heisenberg limit imposed by quantum theory.

Despite the importance of quantum entanglement, a global - necessary and sufficient - criterion for multi-particle entanglement does not exist. For the case of considering pair(s) of particles in the atomic system, the concurrence has been widely used for quantifying the pair-wise entanglement. Nevertheless, when it comes to more than two particles, different measures are used for different purposes. Thus, the choice of entanglement criterion itself is an issue depending on the application we want to use the entanglement. It has been proved that [41] spectroscopic spin squeezing defined by Wineland *et al* [42] is related to the multi-particle entanglement. Being related to reduction of quantum fluctuations of collective spin vectors, spin squeezing has been used in a number of experiments [43–46]. Nevertheless, it has been proved that spin squeezing as a witness of multi-particle entanglement has its own restrictions [47]. The biggest flow is that it is not detecting a very important family of entangled states, namely *maximally entangled states*. This motivates us to look for measure which might be useful when it come to detection and characterization of the multi-particle entanglement.

In this work, we theoretically study the dynamics of entanglement in a system

of finite numbers of atoms coupled to a single mode of a cavity. Specifically, we consider an initial coherent mode of the cavity which makes it more feasible experimentally. We will detect the multi-particle entanglement dynamics by making use of quantum Fisher information. Quantum Fisher information is an extension of Fisher information which is related to the Cramer-Rao bound of precision in the parameter estimation theory [48]. The Fisher information indicates the maximum amount of information that one can extract from a specific measurement. In this case, the larger the Fisher information, the more precise estimation of a parameter. It has been proved that in a collective spin system, the quantum Fisher information may serve as a witness of multi-particle entanglement [47]. It is also shown that it detects a wider family of entangled states of spins which are not detected by spin squeezing. Last but not least, the quantum Fisher information detects the whole family of entangled states which can be exploited in an interferometric measurement to improve the shot noise limit. Put simply, it detects the useful entanglements [49].

In order to measure the quantum Fisher information collective measurements on the mean spin values shall be done. In other words, having access to the individual particles is not crucial. Therefore, while in this work we consider finite small numbers of particles, it is possible to generalize it to the case of larger ensembles. In that case, we would replace the quantum Fisher information with its classical counterpart.

- In Chapter 2, we briefly introduce the Dicke model and its Hamiltonian; we will neglect the losses both of the cavity and of the atoms. The atomic, quantized field and atomic-field interaction systems and the corresponding Hamiltonians are presented. Thereafter, we introduce the the rotating-wave approximation and give the eigen-states of the Tavis-Cumming Hamiltonian. We finish Chapter 1 with a quite recent realization of the Dicke model for a finite numbers of particles in a circuit QED setup.

- In Chapter 3, we discuss the quantum entanglement detection in a multi-particle system. We begin with introducing the definition of quantum entanglement in a general physical system. Thereafter, we put our focus mainly on the multi-particle entanglement criteria appropriate for collective spin models. We present three criteria of entanglement; namely concurrence, spin squeezing and quantum Fisher information. Specifically, for the spin squeezing and quantum Fisher information, we discuss the relation to the context of precision measurement and parameter estimation.

- In Chapter 4, we make use of the introduced multi-particle entanglement witness in a Dicke model of $N = 2$ particles coupled to the single mode of the

coherent field. Depending on the strength of the initial coherent field population $\bar{n}$ compared to the number of particles N, we will consider the different regime of atom-field interaction: weak field regime ($\bar{n} \ll N$), intermediate regime ($\bar{n} \sim N$) and strong field regime ($\bar{n} \gg N > 1$). For every regime of interaction, we investigate the dynamics of entanglement making use of quantum Fisher information. Moreover, we compare quantum Fisher information with the spin squeezing factor and concurrence. In the two extreme regimes of interaction - the weak and strong field regimes - we derive the analytical expressions for the quantum Fisher information in parallel to numerical simulations. Specifically, by using the factorization approximation, we derive the analytical result for the strong field regime. Lastly, we give examples of detecting the collapse and revival of entanglement by use of quantum Fisher information in the strong field regime.

- In Chapter 5, we extend the case of $N = 2$ particle Dicke model to the case of N (finite) particles. We will employ the same three regimes of interaction as in Chapter 4. The same as the case of having two particles in the system, we employ the approximate approaches to obtain the analytical approximate results for the quantum Fisher information in the two extreme regimes of weak and strong interaction. The dynamics of quantum Fisher information and spin squeezing factor are compared. We also give example of using quantum Fisher information in the strong field regime in order to detection of collapse and revival of Schrödinger cat state for $N = 3$.

Chapter 2

Quantum Dicke Model

"The whole is greater than sum of its parts."
Aristotle

The Dicke model is described by collection of N atoms which cooperatively interact with a single privileged mode of the radiation field. Essentially, the interaction of a single atom with the field is due to coupling of the atomic dipole moment with the the electromagnetic field inside the cavity. Thus, the cooperative interaction is the consequence of the coherent coupling of the N atoms to the common mode of the electromagnetic field.

The Dicke model in the most general form, has it own pros and cons. For example it is linked to an interesting effect of quantum chaos [6, 7]. On the other hand, one disadvantage is that the Hamiltonian is not possible to be solved analytically except under some specific conditions and making use of the suitable approximations, e.g. Holstien-Primakoff approximation [50]. Besides, in order to realize the system is an experiment, one needs to prepare a strong interaction between the atoms and the single mode of the field. This issue is a source of technical difficulties in practice [1].

Nevertheless, it is possible to use the approximation approach to make the system integrable and also make its realization easier experimentally. More precisely, the *rotating wave approximation* - which is in the weak limit of interaction of general Dicke model - has been studied to make the system solvable. Under the RWA, one can solve the system analytically by the expense of loosing some physical effects such as chaos. Also the system can be realized in a more feasible way. Nevertheless,

[1] Today, the strong and deep strong limit can be implemented experimentally.

before using the rotating wave approximation one has to make sure which physical effect of the Dicke model is interesting for him/her.

In this chapter, we introduce the general aspects of the Dicke model, with focus on RWA regime [20]. Moreover, we present the eigen-structure of the Dicke model and finally we look into an experimental realization of the model done by now [29].

2.1 Physical model and Hamiltonians

Our system of interest, Dicke system, is composed of N two-level atoms interacting resonantly with a single mode of the quantized field inside a loss-less cavity. In this section, we introduce the building blocks of the system, atom, field and representation of the Dicke Hamiltonian.

2.1.1 Multi-particle system

Single two-level atom as a spin-1/2 particle

A single two-level atom is one of the simplest physical systems of quantum mechanics. The two-level atom approximation is adequate if the frequency of the external field is tuned close to the transition frequency between the two levels designated by $|g\rangle$ and $|e\rangle$. These internal levels are called the ground and excited levels with corresponding frequencies ω_g and ω_e. It is known that once we attribute the ground state to the eigen-state of s_z with eigen-value of $m_s = -1/2$ and excited state to the eigen-value of $m_s = 1/2$, the dynamics of the two-level atom is interestingly, the same as a spin-half particle in the magnetic field [51]. This was first shown by Feynmann *et al* [52]. In this case, the internal dynamics of a two level atom is fully expressed in terms of Pauli spin operators.
From geometrical point of view, the Bloch representation is conveniently used to visualize the internal state of the atom (like spin-half systems). In this case, any normalized state of a two-level atom can be expressed as a superposition of internal atomic states such that

$$|\theta, \varphi\rangle = \cos\theta|g\rangle + \sin\theta e^{i\varphi}|e\rangle. \tag{2.1.1}$$

where $0 \leq \theta \leq \pi$ and $0 \leq \varphi \leq 2\pi$ are polar and azimuthal angles, respectively. The state given in equation (2.1.1) is called spin coherent state for a two-level atom. The population inversion maps to the z and the coherences represented by the x and y components of spin vector, respectively,

$$
\begin{aligned}
s_x &= (|e\rangle\langle g| + |g\rangle\langle e|)/2 = \sigma_x/2, \\
s_y &= (|e\rangle\langle g| - |g\rangle\langle e|)/2i = \sigma_y/2, \qquad (2.1.2) \\
s_z &= (|e\rangle\langle e| - |g\rangle\langle g|)/2 = \sigma_z/2, \\
s_\pm &= s_x \pm i s_y. \qquad (2.1.3)
\end{aligned}
$$

Here σ_α with $\alpha \in \{ x, y, z\}$ represent Pauli matrices which are the basis of SU(2) algebra. $s_\pm$ are called spin ladder operators. The elementary spin operators obey the following commutation relations,

$$
\begin{aligned}
[s_\alpha, s_\beta] &= i\epsilon_{\alpha\beta\gamma} s_\gamma, \\
[s_z, s_\pm] &= \pm s_\pm, \\
[s_+, s_-] &= 2s_z, \qquad (2.1.4)
\end{aligned}
$$

with $\epsilon_{\alpha\beta\gamma}$ as the Levi-Civita symbol and $\alpha, \beta, \gamma \in \{x, y, z\}$.

In the standard Bloch sphere representation, the pure state (2.1.1) is depicted as a vector pointing from the origin to a point on the surface of the unit sphere. The direction of the state vector (also called Bloch vector) is specified by polar and azimuthal angles with the following coordinates,

$$\vec{a} = (\sin\theta\cos\varphi, \sin\theta\sin\varphi, \cos\theta), \qquad (2.1.5)$$

where $|\vec{a}| = 1$. In general, the state of a two level system is represented by statistical mixture of pure states of the form (2.1.1) (called mixed states). In this case, the state is described by a 2×2 density matrix, involving three real parameters. The state of the system can be depicted as a vector with angles θ and φ but the Bloch vector length smaller than unity, $|\vec{a}| < 1$. Therefore, a mixed state resides in the interior of the Bloch sphere.

The corresponding Hamiltonian for a single two-level atom is given by,

$$
\begin{aligned}
h_a &= \hbar\omega_e/2|e\rangle\langle e| - \hbar\omega_g/2|g\rangle\langle g| \\
&= \hbar\omega_0 s_z. \qquad (2.1.6)
\end{aligned}
$$

where $\omega_0 = \omega_e - \omega_g$ is the atomic transition frequency.

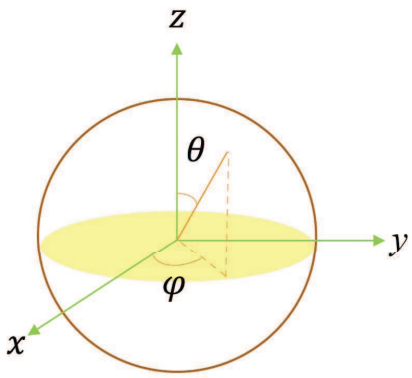

Figure 2.1: Schematic representation of the quantum state $|\varphi, \theta\rangle$ of a spin 1/2 system on the standard Bloch sphere. The definition of the azimuthal φ and the polar angle θ are highlighted and in the following the same notation will be used for the direction of the collective spin on a generalized Bloch sphere.

N two-level atoms as a collective spin $N/2$ particle

Now, let us suppose a collection of N *identical* two level atoms in the system. The generalization of the result of previous section is straightforward. It is convenient to describe the *pure* state of the N qubit systems in terms of the orthonormal Dicke states $|S, M\rangle$ with $S = N/2$ [2]. In order to define Dicke states $|S, M\rangle$, let us firstly introduce the following *collective spin operators* S^2 and S_z

$$\begin{aligned} S_\alpha &= \sum_{i=1}^{N} s_\alpha^{(i)} \\ S_\pm &= S_x \pm i S_y, \\ S^2 &= S_x^2 + S_y^2 + S_z^2. \end{aligned} \tag{2.1.7}$$

in terms of elementary i'th spin operators $s_\alpha^{(i)}$ with $\alpha \in \{x, y, z\}$ given in equations (2.1.3) . The Dicke states are defined as the eigen-states of the S^2 and S_z such that

$$\begin{aligned} S_z|N/2, M\rangle &= M|N/2, M\rangle, \\ S_\pm|N/2, M\rangle &= \sqrt{(N/2 \mp M)(N/2 \pm M + 1)}|N/2, M \pm 1\rangle, \\ S^2|N/2, M\rangle &= N/2(N/2+1)|N/2, M\rangle \end{aligned} \tag{2.1.8}$$

and $-N/2 \leq M \leq N/2$. Collective spin operators (2.1.7) obey the same commuta-

[2] This is provided that we choose to work in a completely symmetric representation.

tion relations as elementary spin operators (2.1.4)

$$\begin{aligned} [S_\alpha, S_\beta] &= i\epsilon_{\alpha\beta\gamma} S_\gamma, \\ [S_z, S_\pm] &= \pm S_\pm, \\ [S_+, S_-] &= 2S_z. \end{aligned} \tag{2.1.9}$$

In fact, Dicke states refer to the collective states which have definite number of particles in ground $|g\rangle$ and excited $|e\rangle$ states,

$$|N/2, M\rangle = \binom{N}{p}^{-1/2} \sum \prod_{k=1}^{p} |g\rangle_k \prod_{l \neq k} |e\rangle_l \,. \tag{2.1.10}$$

Using the collective spin representation, the collection of N two level atoms may be considered as a system of spin-$N/2$ particle. The Hilbert space of such a system, has the Dimension of 2^N. This is due to the fact that the Hilbert space of each single particle has two dimensions. By the way, when there is the symmetry condition in the system like our case, the permutations between particles vanish and the dimension of the Hilbert space of the joint collective system reduces to $N+1$. In this case, the surface of Bloch sphere is no more an exact choice to represent the state of a multi-particle system. By the way, it is convenient to visualize the state of the system in the average form using generalized Bloch sphere with radius $N/2$. In this case, the *mean spin vector* on the Bloch sphere is defined in terms of collective spin averages $\langle S_\alpha \rangle$ as

$$\langle S \rangle = (\langle S_x \rangle, \langle S_y \rangle, \langle S_z \rangle) \tag{2.1.11}$$

with the corresponding length

$$|\langle S \rangle| = \sqrt{\langle S_x \rangle^2 + \langle S_y \rangle^2 + \langle S_z \rangle^2} \tag{2.1.12}$$

In the spherical coordinate the mean spin direction is defined as

$$\vec{n}_{\parallel} = \frac{\langle S \rangle}{|\langle S \rangle|} \tag{2.1.13}$$

$$\equiv (\sin\theta\cos\varphi, \sin\theta\sin\varphi, \cos\theta). \tag{2.1.14}$$

The angles θ and ϕ are given by

$$\theta = \arccos\left(\frac{\langle S_z \rangle}{|\langle S \rangle|}\right) \tag{2.1.15}$$

$$\varphi = \begin{cases} \arccos\left(\frac{\langle S_x \rangle}{|\langle S \rangle| \sin\theta}\right) & \text{if } \langle S_y \rangle > 0; \\ 2\pi - \arccos\left(\frac{\langle S_x \rangle}{|\langle S \rangle| \sin\theta}\right) & \text{if } \langle S_y \rangle \leq 0. \end{cases}$$

The Bloch vector on the surface of the sphere refers to the pure states. For any mixed states of the atomic system (or pure Dicke states of the system such as NOON states), the length of the Bloch vector is less than radius of the sphere $|\langle S \rangle| < N/2$. Figure (2.1) represents the schematic representation of the quantum state $|\varphi, \theta\rangle$ of a spin 1/2 system on the standard Bloch sphere.

There is a point which is worth to mention here. For the standard Bloch sphere introduced previously, θ and φ define the exact state of the atom. Nevertheless, the direction defined by θ and φ on the generalized Bloch sphere, refers only to mean spin direction. This is because of the fact that the state of the system in the collective spin representation has the dimension of $N+1$ while the surface of the Bloch sphere has two dimensions. Of course, in the case of standard Bloch sphere there is a one-by-one correspondence between the points on the sphere and the internal atomic states given previously.

For a system of N two-level atoms with no dipole-dipole interaction, the Hamiltonian is the sum of single two level atom Hamiltonians in equation (2.1.6) such that

$$H_N = \sum_{i=1}^{N} h_i. \tag{2.1.16}$$

For the case of having N identical atoms, the corresponding atomic Hamiltonian simplified to

$$H_N = \hbar\omega_0 S_z. \tag{2.1.17}$$

2.1.2 Quantized field inside a cavity

The quantization of the electromagnetic field inside a cavity yields,

$$\begin{aligned} \vec{E}(\vec{r}) &= i\sum_{\alpha}\sqrt{\frac{2\pi\hbar\omega_\alpha}{V}}\vec{\epsilon}_\alpha a_\alpha u_\alpha(\vec{r}) + H.C., \\ \vec{B}(\vec{r}) &= \sum_{\alpha}\sqrt{\frac{2\pi\hbar c^2}{\omega_\alpha V}}\vec{\nabla}\times\vec{\epsilon}_\alpha a_\alpha u_\alpha(\vec{r}) + H.C., \end{aligned} \tag{2.1.19}$$

where $H.C.$ stands for Hermitian conjugate as the field operator shall Hermitian. The sum is over all the cavity modes ω_α while $\vec{\epsilon}_\alpha$ polarization vector for the corresponding mode α. $u_\alpha(\vec{r})$ denotes the cavity mode function and V is the volume of the cavity. Moreover, $a_\alpha(a_\alpha^\dagger)$ are the annihilation (creation) operator of mode α of the field which satisfy the bosonic commutation relation,

$$[a_\alpha, a_\alpha^\dagger] = 1 \tag{2.1.20}$$

The energy of electromagnetic field is given by

$$U = \frac{1}{8\pi}\int_V [\vec{E}^2(\vec{r}) + \vec{B}^2(\vec{r})]d^3r \tag{2.1.21}$$

After replacing U with the corresponding quantized electric and magnetic field given in (2.1.18), the corresponding Hamiltonian becomes,

$$H_f = \sum_\alpha \hbar\omega_\alpha (a_\alpha^\dagger a_\alpha + \frac{1}{2}). \tag{2.1.22}$$

The contribution $\sum_\alpha \hbar\omega_\alpha/2$ is called the zero point energy of the electromagnetic field. The equation (2.1.22) is the general form of Hamiltonian considering infinite modes of the field. Nevertheless, when we consider the interaction of the field with a two level atom inside the cavity, the field is restricted to the single mode which is close to the atomic transition frequency $\omega = \omega_\alpha \approx \omega_0$. In this case, the field Hamiltonian is reduced to the form

$$H_f = \hbar\omega(a^\dagger a + \frac{1}{2}). \tag{2.1.23}$$

In the following, we drop the zero-point energy as does not change the dynamics.

2.1.3 Interaction of N two-level atoms with single mode of the cavity - Dicke interaction

At this point, Let us consider N identical two-level atoms with ground and excited states $|g\rangle$ and $|e\rangle$ *interacting* with the quantized electromagnetic field inside the cavity,

$$\vec{E}(\vec{r}) = i\sum_\alpha \sqrt{\frac{2\pi\hbar\omega_\alpha}{V}}\vec{\epsilon}_\alpha a_\alpha u_\alpha(\vec{r}) + H.C., \tag{2.1.24}$$

As mentioned before, when atomic transition frequency $\omega_0 = \omega_e - \omega_g$ is close to the frequency of the cavity, the quantized field reduces to the privileged single mode of the cavity,

$$\vec{E}(\vec{r}) = \mathcal{E}\vec{\epsilon}a u(\vec{r}) + \mathcal{E}^*\vec{\epsilon}a^\dagger u(\vec{r}), \tag{2.1.25}$$

where $\mathcal{E} = i\sqrt{\frac{2\pi\hbar\omega}{V}}$ is the field amplitude. In addition, we write the dipole moments of the i'th two-level atom as

$$\begin{aligned} p^{\vec{(i)}} &= p_{eg}^{\vec{(i)}}|e\rangle\langle g| + p_{ge}^{\vec{(i)}}|g\rangle\langle e| \\ &= p_{eg}^{\vec{(i)}} s_+^{(i)} + p_{ge}^{\vec{(i)}} s_-^{(i)}, \end{aligned} \tag{2.1.26}$$

with the atomic spin operators $s_\pm$ given in equations (2.1.7). The ladder spin operators $s_\pm^{(i)}$ satisfy the SU(2) commutation relations (2.1.4). The interaction Hamiltonian of i'th atom with the field is

$$\begin{aligned} H_{int}^{(i)} &= \vec{p}^{(i)}.\vec{E}(\vec{r}) \\ &= \hbar g_i(\vec{r})(a + a^\dagger)(s_+^{(i)} + s_-^{(i)}) \end{aligned} \tag{2.1.27}$$

where the coupling factor is

$$g_i(\vec{r}) = \sqrt{\frac{2\pi\omega}{V\hbar}} i\vec{\epsilon}.\vec{p}_{eg} u(\vec{r}) \tag{2.1.28}$$

In general, the coupling strength is position dependent. By the way, under the *dipole approximation*, i. e. when the wavelength of the radiation is much larger than the size of the atom, it is independent of the atomic position. Therefore, g_i can be considered as a coupling constant. Consequently, the corresponding Hamiltonian for the interaction of the i'th two-level atom with the single mode of the field inside the cavity is given by

$$\begin{aligned} H_{JC} &= H_{int}^{(i)} \\ &= \hbar g_i(a + a^\dagger)(s_+^{(i)} + s_-^{(i)}). \end{aligned} \tag{2.1.29}$$

In order to distinguish the atom-field interaction, the coupling constant g_i shall be stronger than incoherent or dissipative process in the cavity. The main important dissipative processes involved are

- the leakage of photons from the cavity mirrors with the rate of κ, and
- the spontaneous emission of the i'th atom at the rate γ_i.

  The first condition $g_i \gg \kappa$ means that a photon inside the cavity can interact repeatedly with each single atom before it leaves the cavity. While, the second

condition $g_i \gg \gamma_i$ implies that the lifetime of the atom is more than the interaction time with the cavity. In other words, the emission is primarily in the cavity mode rather than the side modes [51]. Under these conditions, the coherent interaction dominates the state dynamics of the system before the dissipation proceses takes place.

Now, we consider N identical atoms which interact with the single mode of the cavity, *independently*. The interaction Hamiltonian is given by

$$H_{int} = \hbar \sum_i g_i (a + a^\dagger)(s_+^{(i)} + s_-^{(i)}). \tag{2.1.30}$$

Here, g_i, being the coupling constant of i'th atom to the single mode of the cavity, varies for each single atom. This situation makes it difficult to find the eigen-values and eigen-functions of the system without using numerical simulations. Nevertheless, for the special cases the interaction strength g_i is independent of i. Specifically, when the system is composed of the particles with inter-distances smaller than the wavelength of the cavity and the atoms being located in the anti-nodes of the cavity. Under these conditions, the coupling constants can be considered the same for all of the particles, say $g_i = g$. Therefor, the Hamiltonian in terms of the collective spin operators (2.1.7) turns into the following form

$$H_{int} = \hbar g (a + a^\dagger)(S_+ + S_-). \tag{2.1.31}$$

This is the general form of the Dicke Hamiltonian. Note that to get the final expression of Hamiltonian (2.1.31), the collection of atoms are supposed to be sufficiently far apart such that the inter-atomic dipole-dipole interactions can be ignored. There are many interesting points concerning the Dicke Hamiltonian. Its connection to quantum phase transition [6–9] chaos [6], quantum entanglement [53–56] and quantum engineering of cat states [56–58] have been extensively studied. Specifically, the role of Dicke interaction in the context of quantum entanglement is interesting. Since, the Hamiltonian (2.1.31) is composed of the both atomic and field operators, it is potentially capable of creating quantum correlations between the cavity and particles under time

evolution. On the other hand, it has been investigated that the Hamiltonian (2.1.31) also generates atom-atom correlations in the system despite the fact that there is no direct short-range interactions among the particles. The reason comes in the following.

In the Dicke model, the single mode of the field acts as a *virtual data bus* which correlates atoms in the long-range. These correlations are apart from the usual dipole-dipole interactions among the atoms which occur in the short-range. Thus, the common electromagnetic field mode supported by an optical resonator mediates the interaction between the atoms. The coupling between particles results in creating quantum correlations such as quantum entanglement in the system.

The system described by the collective Dicke Hamiltonian (2.1.31) has no dissipation in the atomic system; neither decay of the each atom independently nor the damping of the atoms in a collective manner. In the other word, the system is not an *open quantum system* [59]. Interested reader may refer to references [60].

Rotating wave approximation

Adding the unperturbed Hamiltonians of the atomic collection (2.1.17), single mode of the cavity (2.1.23) and atomic-field interaction (2.1.31), we obtain the general Hamiltonian of the system as,

$$H = \hbar\omega_0 S_z + \hbar\omega a^\dagger a + \hbar g(a + a^\dagger)(S_- + S_+). \tag{2.1.32}$$

If there is nearly resonant condition in the system ($\omega \approx \omega_0$) and the light-matter interaction is not very strong (typically $g/\omega < 0.1$), it is a good approximation to drop the counter-rotating terms of the Hamiltonian. Therefore, under *rotating-wave approximation* the Dicke Hamiltonian casts in the following form

$$H = \hbar\omega_0 S_z + \hbar\omega a^\dagger a + \hbar g(aS_- + a^\dagger S_+). \tag{2.1.33}$$

The multi-atom model (2.1.33) is called Tavis-Cummings Hamiltonian [20]. As we mentioned before, for the single atom case this Hamiltonian reduces into the Janes-Cummings Hamiltonian [19]. The Hamiltonian (2.1.33) is interesting as the system is integrable, i. e. it is possible to get the eigen-states and eigen-values of the system analytically (Section 2.2).

Physically speaking, RWA indicates the energy conservation in the system. In fact, the *total excitation operator* of the system

$$L = a^\dagger a + S_z \tag{2.1.34}$$

is conserved as it commutes with Hamiltonian (2.1.33). Another constant of motion is the SU(2) Casimir operator $\mathbf{S}^2 = S_z^2 + (S_+S_- + S_-S_+)/2$. In order to keep the analysis as simple as possible, in the scope of this thesis we always consider the resonant condition, say $\omega = \omega_0$.

2.2 Eigenstructure of the Dicke model

In the following, we present some initial dressed state of the system when the symmetry condition is imposed, $S = N/2$. Under the resonant condition, the Total Dicke Hamiltonian is given by

$$H = \hbar\omega(S_z + a^\dagger a) + \hbar g(aS_- + a^\dagger S_+), \tag{2.2.1}$$

As mentioned before, the total excitation number $a^\dagger a + S_z$ is constant of motion. Therefore, we can make use of this number to label the eigen-states of the system. The smallest eigen-value of S_z is when all of the atoms are in the ground-state, $-N/2$. While, the smallest eigen-value of the photon number operator $a^\dagger a$ is when $|0\rangle$. Consequently, the lowest eigen-state of the system (ground-state) is,

$$|\psi_g\rangle = |\frac{N}{2}, -\frac{N}{2}\rangle \otimes |0\rangle \equiv |-\frac{N}{2}, 0\rangle, \tag{2.2.2}$$

with the energy $E_g = -\hbar\omega\frac{N}{2}$. As under symmetry $S = N/2$ does not change, we drop the first argument of the atomic Dicke states in the following as used in (2.2.2). The next possible eigen-state of the system are when excitation number operator $S_z + a^\dagger a$ has the eigen-value $-\frac{N}{2} + 1$. It is clear that such states would be a superposition of the following Dicke states, $|-\frac{N}{2}, 1\rangle$ and $|-\frac{N}{2}+1, 0\rangle$. Acting the Hamiltonian of (2.2.1) on the relevant bare-states gives,

$$\begin{aligned} H|-\frac{N}{2}+1,0\rangle &= \hbar\omega(-\frac{N}{2}+1)|-\frac{N}{2}+1,0\rangle + \hbar g\sqrt{N}|-\frac{N}{2},1\rangle, \\ H|-\frac{N}{2},1\rangle &= \hbar g\sqrt{N}|-\frac{N}{2}+1,0\rangle + \hbar\omega(-\frac{N}{2}+1)|-\frac{N}{2},1\rangle, \end{aligned} \tag{2.2.3}$$

which can be cast in the form of following 2×2 matrix

$$H = \hbar \begin{pmatrix} \omega(-\frac{N}{2}+1) & g\sqrt{N} \\ g\sqrt{N} & \omega(-\frac{N}{2}+1) \end{pmatrix}, \tag{2.2.4}$$

By diagonalization of the above Hamiltonian, the eigen-states are given by

$$|\psi_0^\pm\rangle = \frac{1}{\sqrt{2}}\big[|-\frac{N}{2}+1,0\rangle \pm |-\frac{N}{2},1\rangle\big], \tag{2.2.5}$$

with the corresponding eigen-values

$$E_0^\pm = \hbar\omega(-\frac{N}{2}+1) \pm \hbar g\sqrt{N}. \tag{2.2.6}$$

Therefore, the *vacuum Rabi splitting*, $E^+ - E^- = 2\hbar g\sqrt{N}$ of the degenerate levels $-\frac{N}{2}+1, 0\rangle$ and $|-\frac{N}{2}, 1\rangle$ to $|\psi_0^\pm\rangle$, depend on the number of atoms N as well as interaction strength. This can be measured with absorption/transmission

spectrum of a weak field [51] which is introduced in the next section. For the next step, we suppose that $S_z + a^\dagger a$ has the eigen-value equal to $-\frac{N}{2}+2$. Using the same procedure as before, we get the eigen-states as

$$\begin{pmatrix} |\psi_1^+\rangle \\ |\psi_1^0\rangle \\ |\psi_1^-\rangle \end{pmatrix} = \begin{pmatrix} (\frac{N-1}{4N-2})^{1/2} & \frac{1}{2^{1/2}} & (\frac{N}{4N-2})^{1/2} \\ (-\frac{N}{2N-2})^{1/2} & 0 & (\frac{N-1}{2N-1})^{1/2} \\ (\frac{N-1}{4N-2})^{1/2} & -\frac{1}{2^{1/2}} & (\frac{N}{4N-2})^{1/2} \end{pmatrix} \begin{pmatrix} |-\frac{N}{2}+2, 0\rangle \\ |-\frac{N}{2}+1, 1\rangle \\ |-\frac{N}{2}, 2\rangle \end{pmatrix}. \tag{2.2.7}$$

with the corresponding eigen-energies,

$$\begin{aligned} E_1^{\pm} &= \hbar\omega(-\frac{N}{2}+2) \pm \hbar g\sqrt{4N-2}, \\ E_1^0 &= \hbar\omega(-\frac{N}{2}+2). \end{aligned} \tag{2.2.8}$$

The ground state of the system $|-N/2, 0\rangle$ represents the quantum state of $|g_1 g_2 ... g_N\rangle \otimes |0\rangle$ (i. e. all of the atoms are in the ground state). The next pair states are combinations of the bare states with single excitation given in (2.2.5). Then, there are triplet dressed-states of equations (2.2.7). By increasing the number of excitations, the number of eigen-levels in each manifold increases up to $N+1$ levels. Afterward, the number of levels remain constant, though the energy-level spacing changes with change of excitations [61, 62].

2.3 Physical realizations

In the following we present a circuit QED set up for realization of the Dicke model done in 2009 by Fink *et al* [29]. But firstly, we present a review of the Rabi splitting in the absorption/transmission of a weak field which will be used later.

2.3.1 vacuum Rabi splitting in the absorption/transmission of a weak field

The standard tool to probe the spectrum of a physical system is the absorption spectroscopy. By examining the absorption of a weak pure field, one can probe the dressed states. Suppose that the atoms/cavity state is initially prepared in the ground-state given in equation (2.2.2). Now, consider the interaction of the atoms with a very weak external field with frequency ω_l. Under the influence of the external field, The atom-field system makes transitions of $|\psi_g\rangle \rightarrow |\psi_0^+\rangle$ and $|\psi_g\rangle \rightarrow |\psi_0^-\rangle$. Clearly, the absorption shall show resonance when

$$\omega_l = \omega_0 \pm g\sqrt{N}, \tag{2.3.1}$$

In the free space $g = 0$, the usual absorption resonance would happen at $\omega_l = \omega_0$. While, when there is the interaction with cavity mode ($g \neq 0$), the doublet of (2.3.1) appears in the absorption spectrum. The resolution of the doublet depends on both number of particles N as well as atomic-field interaction strength g. The width of the peaks depend on the losses of the cavity as well as spontaneous emission of each atom. The peaks of the absorption spectrum are resolvable when the width of each peak in doublet (2.3.1) is much smaller than $2g\sqrt{N}$. In parallel with the external field transitions, there exists dissipation in the forms of cavity leakage and spontaneous emission with the rates κ and γ, respectively. Therefore, for instance the levels $|-N/2, 1\rangle$ and $|-N/2+1, 0\rangle$ both can decay into the ground-state $|-N/2, 0\rangle$ via cavity leakage and spontaneous emission. Therefore the dissipation process would couple the dressed states $|\psi_0^{\pm}\rangle$ to the ground-state. In the limit of large g ($g \gg \kappa, \gamma$), the half-width of each doublet is obtained as [51]

$$\frac{\kappa + \gamma}{2}. \tag{2.3.2}$$

2.3.2 Experimental set-up

The Dicke model corresponding to Hamiltonian (2.1.33) for the small number of qubits inside a high-Q cavity has been realized [29] in a set-up presented in Figure 2.2. In the this experiment, the cavity mode is replaced by a waveguide mode with the first harmonic full-wavelength microwave frequency $\omega/2\pi = 6.7$ GHz and a photon decay rate of $\kappa/2\pi = 6.8$ MHz. While, the atoms are replaced by superconducting qubits positioned at anti-nodes of the first harmonic standing-wave electric field. At the anti-nodes of the standing wave there is maximum amount of interaction with qubits. The experiment is done for up to $N = 3$ qubits. The ground-state of the atomic/cavity system $|ggg\rangle \otimes |0\rangle$ (2.2.2) is prepared by cooling the micro-chip to a temperature of 20 mK in a delusion refrigerator. The qubits are coupled to the field with identical strength of $g/2\pi = 85.7$ MHz with scatter of only a few MHz. Thereafter, the resonant transition of $|g\rangle \rightarrow |\psi_0^{\pm}\rangle$ to the first mode of the cavity has been investigated. This task has been done by exploring the transmission spectrum of the incident weak field introduced previously. When the first atom in resonance with the field (and the two others are far-detuned) the eigen-states of the system are $|\psi_0^{\pm}\rangle = 1/2(|g\rangle \otimes |1\rangle \pm |e\rangle \otimes |0\rangle)$. In fact, for only one tuned qubit in the system the eigen-energy is the same as those of Janes-Cummings [19]. In this case, the excitation is equally shared between the qubit and a photon. The transition spectrum is obtained for one atom in the system. Thereafter, the second qubit added to the system (while the third one still is far-detuned). In this case, the excitation is shared between one photon with probability 1/2 and two qubits with probability 1/4. By radiating light into cavity, the transmission spectrum is obtained. Finally, the third qubit tunes to the already resonantly coupled qubits and the single mode of the cavity. In this case, the eigen-energies of the system $|\psi_0^{\pm}\rangle$ (2.2.5) in terms of atomic levels are $1/\sqrt{2}|ggg\rangle \otimes |1\rangle \pm 1/\sqrt{6}$ $(|egg\rangle - |geg\rangle + |gge\rangle) \otimes |0\rangle$. The doublet state has been observed.

In addition, for the one excitation eigen-states, the N-qubit system acts as one effective spin with effective coupling strength $g_N = g\sqrt{N}$. This can be observed in equation (2.3.1). This quantity for $N = 1 - 3$ has been verified experimentally with a very good agreement with theory [29].

The advantage of using the circuit QED schemes is that they are flexible regard to changing the parameters. Moreover, for mediate number of particles in a similar set-up the w-state entanglement of particles has been observed [63].

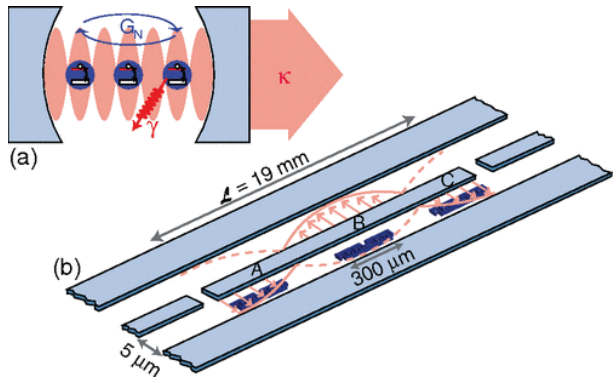

Figure 2.2: Schematic of the experimental set-up. (a) Optical analog. Three two-state atoms are identically coupled to a cavity mode with photon decay rate κ, atomic energy relaxation rate γ and collective coupling strength G_N. (b) Schematic of the investigated system. The coplanar waveguide resonator is shown in light blue, the qubits A, B and C in violet and the first harmonic of the standing wave electric field in red [29].

2.4 Conclusion

In this chapter, we have introduced the Dicke model; The coupling of N two-level atoms with a singe mode of the cavity field. We reviewed the Hamiltonian and the corresponding eigen-structure of the system very briefly. Moreover, we presented an experiment which has been realized the Dicke model for mediate number of particles.

Being composed on an N-particle plus cavity sub-systems, the Dicke model is interesting when it comes to studying the entanglement between different sub-systems such as atom-field entanglement as well as inter-atomic entanglement. Specifically, the atom-atom entanglement, which is a consequence of collective interaction of particles with the same mode of the cavity, is of interest. In fact, Dicke model is possible to be realized both with moderate [29] and many numbers of particles [30, 31] with or without rotating wave approximation. Therefore, it is possible to study the entanglement between particles both in multi-particle and many-body scales. To create entanglement between particles has applications in quantum information as well as quantum metrology. For the same motivation, in the next chapters of this thesis, we will study the multi-particle entanglement in the Dicke model. To this end, in the next chapter, we introduce the quantum entanglement definition. Then, we present three criteria which have been used in order to detect multi-particle entanglement in a N-body system of particles: the concurrence (C), spin squeezing (SSQ)

and quantum Fisher information (QFI). Specifically, we are focused on QFI as it has been proved to be a promising measure in order to detect entanglement with more precision than SSQ.

Chapter 3

Quantum Entanglement detection in a multi-particle system

"Learn how to see. Realize that everything connects to everything else."
Leonardo da Vinci

Quantum entanglement is one of the properties of quantum theory which is important from both theoretical and also experimental points of view. Theoretically, quantum entanglement is in the center of attention when it comes to understanding the fundamental features of quantum theory such as macroscopic/mesoscopic entanglement (Schrödinger cat states), quantum correlations and quantum/classic border. Furthermore, quantum entanglement has found interests also from the experimental viewpoint. Today, entangled states are identified as the very important resources in the fields of quantum information [38], quantum simulation [39] and quantum metrology [40]. It is known that quantum entanglement makes it possible to preform many tasks which are not possible in classical protocols. For example, using entangled states as a resource in quantum metrology, provides the possibility of surpassing the classical limit of measurements (the so-called *shot-noise limit*). This property is very interesting to put parameter estimation protocols [48] into practice.

Depending on the various possible partitioning of a physical system, there might exist different classes of entanglement. For instance, in a system of atom-field coupling, it might be possible to detect the entanglement between

the field and the particles. This *bi-modal entanglement* can be detected by reduced von-Neumann entropy (for the case of pure states) [38]. Moreover, if we concentrate on particle sub-system, there are many other potential classes of entanglement. For example, it is possible to consider the entanglement between every two particles while one can take the entanglement between every single particle with the rest of the atomic system. In addition it is possible to consider the entanglement, between a group of particles to another group of the particles. For different kinds of quantum entanglement in a multi-partite system, various entanglement witnesses have been defined. In the scope of this thesis, we are mainly interested in detecting the dynamics of multi-particle entanglement in the Dicke model making use of quantum Fisher information [47]. Our motivation in exploring the QFI comes as follows.

In the first place, Fisher information is known by its important role in the parameter estimation theory [48]. In fact, it is linked to essential Cramer-Rao Bound which specifies the ultimate limit of precision in estimation a parameter [47, 49]. The more quantum Fisher information of a state is obtained, the more information is available and possible to be extracted by performing an appropriate measurement. Quantum Fisher information, as generalization of Fisher information, is related to the ultimate quantum phase uncertainty in a phase estimation. This property is not limited to systems composed of particles and also is useful in optical interferometers [64].

By the way, beside the importance of QFI is quantum metrology, it has found an interesting application in the context of multi-particle entanglement. QFI has been proved [47] to be a precise multi-particle entanglement witness (detector). A larger quantum Fisher information in a system indicates the presence of more entanglement among the particles. For instance in a collective spin system, the maximally entangled states (such as NOON or GHZ) provide the largest possible QFI of the correspondent state [47]. This result is in contrast to the spin squeezing [42], the other very commonly used multi-particle entanglement witness [41], which is not able to detect entanglement in maximally entangled states [47].

Last but not least, QFI has the capacity to detect the whole family of entangled states which are advantageous for interferometry [47]. This makes more physical sense when we consider the fact that not all entangled states are useful in beating the classical limit of precision [49]. In fact, among all classes of entanglement between particles, there is a very specific family which improves

the precision of phase measurements. The importance of quantum Fisher information is that it detects the whole family of so-called *usefully entangled states*. Obviously, having an criterion which can detect useful entanglement is interesting when it comes to building up an interferometer. We will discuss this properties in more details in the rest of this chapter.

In the this chapter we introduce the QFI and two other witnesses of detecting entanglement in a system of particles. To this end, we first have a look on definition of entanglement. Thereafter, we briefly introduce three measures of entanglement in a multi-particle system: concurrence, spin squeezing and quantum Fisher information. We will use these measures later in order to study the multi-particle entanglement in the Dicke model.

3.1 Quantum entanglement definition

Let us consider two independent (non-interacting) physical systems, say A and B with the corresponding Hilbert spaces $\mathcal{H}_A$ and $\mathcal{H}_B$, respectively. If system A is in the pure state $|\psi_A\rangle$ and system B is in the pure state $|\psi_A\rangle$, the composite system is

$$|\psi_{AB}\rangle = |\psi_A\rangle \otimes |\psi_B\rangle \tag{3.1.1}$$

which belongs to the composite dual Hilbert space, $\mathcal{H}_{AB} = \mathcal{H}_A \otimes \mathcal{H}_A$. States which can be presented in this product form are called *separable (product) states*. The physical property of such states is that any local operations acting on A would not affect B and vice versa. In other words, any measurement on each of the systems does not influence the state of other system. Therefore, one can perform measurement on each system, independently. In the measurement theory language, this translates into the following form, $\langle\psi_{AB}|\hat{\Pi}_{AB}|\psi_{AB}\rangle = \langle\psi_A|\hat{\Pi}_A|\psi_A\rangle \otimes \langle\psi_B|\hat{\Pi}_B|\psi_B\rangle$, where, $\hat{\Pi}_\alpha$'s represent the a positive-operator valued measures which satisfy $\hat{\Pi}_{AB} = \hat{\Pi}_A \otimes \hat{\Pi}_B$ [1] (see Appendix).

Yet, one has to consider that even if the two systems are independent, they can still communicate *classically* with each other. This classical correlation can be

[1] In the rest of this chapter, we drop the hat sign for convenience.

in the form of $|\psi_A^{(k)}\rangle \otimes |\psi_B^{(k)}\rangle$. Thus, the state of the composite system can be written as the following density matrix

$$\rho_{sep} = \sum_k \mu_k |\psi_A^{(k)}\rangle\langle\psi_A^{(k)}| \otimes |\psi_B^{(k)}\rangle\langle\psi_B^{(k)}|. \tag{3.1.2}$$

where μ_k's are the probabilities of k'th incoherent mixture, $\mu_k > 0$ and $\sum_k \mu_k = 1$. By definition, the states which are not possible to be cast in the above convex combination form of product states are called *entangled states*. Quantum entanglement is not being created or destroyed by any kind of local operation and classical communication (LOCC). In other words, If entanglement is detected in the system, it must have been presented in the system before the measurement operation, since local measurements can not generate entanglement [65].

The definition of separability/entanglement can be straightforwardly extended to the case N composite systems in the correspondent Hilbert space, $\mathcal{H} = \mathcal{H}_1 \otimes \mathcal{H}_2 \otimes ... \otimes \mathcal{H}_N$. A state is said to be separable if it can be written as

$$\rho_{sep} = \sum_k \mu_k |\psi_1^{(k)}\rangle\langle\psi_1^{(k)}| \otimes |\psi_2^{(k)}\rangle\langle\psi_2^{(k)}| \otimes ... \otimes |\psi_N^{(k)}\rangle\langle\psi_N^{(k)}|. \tag{3.1.3}$$

In general, when every single sub-system is a mixed state represented by density matrix ρ_i $(i = 1, 2, ..., N)$, the definition of separability turns into the following form,

$$\rho_{sep} = \sum_k \mu_k \ \rho_1^{(k)} \otimes \rho_2^{(k)} \otimes ... \otimes \rho_N^{(k)}. \tag{3.1.4}$$

While the equation (3.1.4) defines the entanglement theoretically, in order to detect it in a specific physical system the only way is to perform some kind of measurements following by using a proper *entanglement criteria (witness)*. Depending on the different kinds of entanglement in the system, many various measures have been introduced by now [65]. In this work, we are interested

in the multi-particle entanglement in the special system of Dicke model introduced in the previous chapter. We consider the entanglement between finite number of atoms ($N \geq 2$) which are in coherent interaction with the single mode of the cavity. It is assumed that particles are indistinguishable. [2] Due to the technical difficulties to address each single particle in the atomic sub-system, we shall use the criteria based on collective spin variables.

In the next section, we briefly introduce the measures of quantum entanglement detection in the multi-particle system based on the collective spin operators.

3.2 Multi-particle entanglement criteria based on collective spin variables

In general, in the multi-particle systems, it is difficult to address each individual qubit Therefore, it is useful to think of the whole system as a single multi-body system. As we discussed in the previous chapter, the collection of N two-level atoms might be treated as a pseudo-spin with $S = \frac{N}{2}$. For the same reason, the entanglement criteria based on the collective spin variables are useful in order to detect entanglement between particles. In this section, we give a introduction on three multi-particle criteria in terms of collective spin variables. Experimentally, these criteria can be evaluated by measurement of expectation values of terms such as $\langle S_\alpha \rangle$ and $\langle S_\alpha S_\beta \rangle$ with $\alpha, \beta = x, y, z$. In the following, we introduce concurrence (C), spin squeezing (SSQ) and quantum Fisher information (QFI) entanglement witnesses. In the next chapter,we will use them frequently in order to detect the multi-particle entanglement in the Dicke model.

3.2.1 Concurrence and pair-wise entanglement

A practical measure of entanglement with a geometrical meaning that can often be calculated easily is concurrence [66]. For pure states it can be written as $C = |\langle \Psi_{12} | \tilde{\Psi}_{12} \rangle|$ where $|\tilde{\Psi}_{12}\rangle = \sigma_y \otimes \sigma_y |\Psi_{12}^*\rangle$ is referred as "state-flipped" state. For a mixed two-qubit state ρ_{12}, it is defined as minimum average pure state concurrence. The required minimum has to be taken over all possible ways of decomposing ρ_{12} into a mixture of pure state $|\Psi_{12}\rangle$.

[2] Symmetry under any permutation of the particles is assumed.

The concurrence, quantifying entanglement of a pair of particle, is given by

$$C = \max\{0, \lambda_1 - \lambda_2 - \lambda_3 - \lambda_4\}, \tag{3.2.1}$$

where λ_i's are the square roots of the eigenvalues of the matrix product

$$\begin{aligned} \varrho_{12} &= \rho_{12}(\sigma_{1y} \otimes \sigma_{2y})\rho_{12}^*(\sigma_{1y} \otimes \sigma_{2y}) \\ &\equiv \rho_{12}\tilde{\rho}_{12}. \end{aligned} \tag{3.2.2}$$

in descending order. In the above equation (3.2.1) ρ_{12}^* denotes the complex conjugate of ρ_{12}, and σ_{iy} are Pauli matrices for the two-level systems. Also, $\tilde{\rho}_{12}$ is called the spin-flipped density matrix. The eigenvalues of ϱ_{12} are real and non-negative even though it is not necessarily Hermitian. The values of the concurrence range from zero for an unentangled state to unity for a maximally entangled state. The *tangle* is calculated directly from concurrence

$$\tau = C^2, \tag{3.2.3}$$

which has been used in some texts instead of concurrence as a measure of entanglement (for instance [67, 68]). Wang and Mølmer have shown [69, 70] that in the case of symmetric multi-qubit system, it is possible to express the elements of the density matrix of a pair of qubit in terms of the expectation value of the collective spin operators,

$$\rho_{12} = \begin{pmatrix} v & x_+^* & x_+^* & u^* \\ x_+ & w & y^* & x_-^* \\ x_+ & y & w & x_-^* \\ u & x_- & x_- & v_- \end{pmatrix} \tag{3.2.4}$$

corresponding to the following matrix elements,

$$
\begin{aligned}
v_{\pm} &= \frac{N^2 - 2N + 4\langle S_z^2\rangle \pm 4\langle S_z\rangle(N-1)}{4N(N-1)}, \\
x_{\pm} &= \frac{(N-1)\langle S_+\rangle \pm \langle [S_+, S_z]_+\rangle}{2N(N-1)}, \\
w &= \frac{N^2 - 4\langle S_z^2\rangle}{4N(N-1)}, \\
u &= \frac{\langle S_+^2\rangle}{N(N-1)}, \\
y &= \frac{2\langle S_x^2 + S_y^2\rangle - N}{2N(N-1)}.
\end{aligned} \tag{3.2.5}
$$

It has been proved [71, 72] that pairwise entanglement is linked to Ueda and Kitagawa spin squeezing [73]. One has to note that the matrix elements of the equations (3.2.5) include the first and second order moments of collective spin operators. Therefore, without necessity to access individual particle, it is straightforward to estimate the entanglement by measurement of the global spins. Nevertheless, as we mentioned before, the concurrence is a useful measure for detecting the entanglement between the pairs of particles. As a matter of fact, in the multi-particle systems such as Dicke or Lipkin-Meshkov-Glick model [74, 75], not only the pair-wise entanglement but also multi-particle entanglement is possible to be observed. Specifically, the latter case is of importance as being a valuable resource for atomic interferometric protocols. Although, concurrence has been used in the form of the rescaled concurrence $C_R \approx (N-1)C$ to detect the entanglement properties in the many-body systems [7, 76, 77], it is not defining the multi-particle entanglement in such systems. In fact, for detecting multi-particle entanglement in a system, there exist other witnesses of entanglement. In the next section, we introduce two more popular criteria of multi-particle entanglement detection, spin squeezing and quantum Fisher information.

3.2.2 Spin squeezing

Definition and perception

In the realm of quantum optics, "as classical states as possible" are called coherent states of the field [78, 79]. In analogy to Glauber coherent states, in

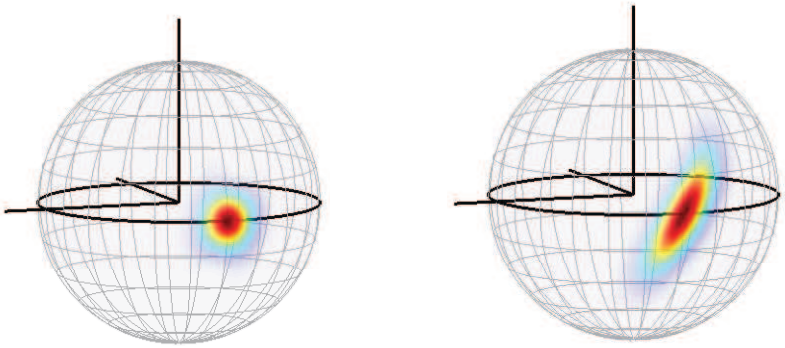

Figure 3.1: Husimi distributions of the spin coherent state (left) and spin squeezed state (right).

a system of collective N spin-1/2 particle (sec. 2.1.1), a coherent spin state is defined as a direct product of single spin states

$$|\theta, \varphi\rangle = \otimes_{k=1}^{N}[\cos\theta|g\rangle_k + \sin\theta e^{i\varphi}|e\rangle_k], \tag{3.2.6}$$

with $|g\rangle$ and $|e\rangle$ being the ground and excited states of the atoms. From the definition (3.2.6), it is clear that there is no quantum correlation among particles. Therefore, the collective spin variances in the perpendicular direction $S_\perp$ to the mean spin direction (given by θ and φ) are equal to the sum of the each elementary spin-half particle. For each elementary spin particle the variance in perpendicular direction of spin direction is isotropic and always equal to ${\Delta s_\perp}^2 = 1/4$ [3]. Therefore, in the case of spin coherent state of $S = N/2$, the variance of collective spin normal to the direction of mean spin vector $\langle S\rangle$ is given by

$${\Delta S_\perp}^2 = N \times 1/4 = N/4. \tag{3.2.7}$$

which is called the *shot-noise limit*. This quantity implies the minimum allowed variance of normal collective spin achievable in classical physics. Moreover, the perpendicular spin variances of a coherent state are called *minimum uncertainty states* of the collective spin system. Spin coherent states can be

[3] where, ${\Delta s_\perp}^2 = \langle s_\perp^2\rangle - \langle s_\perp\rangle^2$

expressed as [71]

$$|\theta, \varphi\rangle = R(\theta, \varphi)|N/2, N/2\rangle, \tag{3.2.8}$$

where $|N/2, N/2\rangle = \otimes_i^N |e\rangle_i$ is the eigen-state of the S_z correspond to eigen-value $N/2$. Also, $R(\theta, \varphi)$ is the rotation operator such that

$$\begin{aligned} R(\theta, \varphi) &= \exp(-i\theta S_n) \\ &= \exp[i\theta(S_x \cos\varphi - S_y \sin\varphi)], \end{aligned} \tag{3.2.9}$$

where S_n is the collective spin state in direction of n in terms of S_x and S_y given in equation (2.1.8).

In addition to the classical-like spin coherent states, another important family of collective spin states have been defined as *spin squeezed states*. The spin squeezed states are considered as non-classical states. This due to the fact that there is quantum correlation between elementary particles which can disturb the isotropic distribution of the spin vector in perpendicular to the mean spin direction (Figure 3.1). By the way, there exist various definitions of spin squeezing in a collective spin states depending on the context we are talking about. For instance, another definition of spin squeezing based on Heisenberg uncertainty limit has been presented [71]. In addition, Ueda and kitagawa [73] have defined a spin squeezing parameter as a ratio of the minimum variance of the spin vector normal to the mean spin direction divided by the shot-noise limit for coherent state ($\Delta S^2_{\perp,SCS} = N/4$)

$$\xi_R^2 = \frac{4\min(\Delta S_\perp^2)}{N}. \tag{3.2.10}$$

Here, $\Delta S_\perp^2$ refers to the spin variance normal to the mean spin direction. It has been proved that there is a close relation between this definition of spin squeezing and concurrence [70]. By the way, we are mainly focused on the definition of spectroscopic spin squeezing defined by Wineland [42] which

is linked to multi-particle entanglement. In quantum metrology, the phase sensitivity of a spin state is defined as the the ratio of the uncertainty of the perpendicular spin directions to the mean spin length

$$\Delta\theta = \frac{\Delta S_{\perp}}{|\langle S\rangle|}. \tag{3.2.11}$$

For the coherent states, $(\Delta\theta)_{SCS} = \frac{1}{\sqrt{N}}$. This is the ultimate phase sensitivity which is achievable within classical physics territory, e. g. interferometry experiments with coherent state arms. By the way, as we will observe in below, the standard quantum limit is not a fundamental limit in quantum mechanics.

Using the phase sensitivity equation (3.2.11), the spin squeezing is defined as the ratio of the phase sensitivity of a general state versus the coherent state one

$$\xi^2 = \frac{(\Delta\theta)^2}{(\Delta\theta)^2_{CSS}} = \frac{N\min(\Delta S^2_{\perp})}{|\langle S\rangle|^2}. \tag{3.2.12}$$

For the case of having coherent spin states $\xi^2 = 1$. Using equations (3.2.11) and (3.2.12), one gets to

$$\Delta\theta = \frac{\xi}{\sqrt{N}}. \tag{3.2.13}$$

If $\xi < 1$, then $\Delta\theta < \Delta\theta_{SCS}$ which means that as long as the state is squeezed, the phase sensitivity beats the shot-noise limit.

On the other hand from the quantum mechanic point of view, there is always an uncertainty on measurement of a parameter. This is due to Heisenberg uncertainty principle of quantum theory. In this case, the uncertainty of collective spin operators is written as

$$(\Delta S_{\perp})^2(\Delta S_{\perp'})^2 \geq |\langle S\rangle|^2/4 \tag{3.2.14}$$

which $S_\perp$ and $S_{\perp'}$ are two normal spin directions to the mean spin direction $\langle S \rangle$ (and also normal to each other, $S_\perp.S_{\perp'}=0$). Let us suppose that the minimum normal spin is along $S_\perp$. If we combine the equation (3.2.12) with (3.2.14), we get $4\xi^2(\Delta S_{\perp'})^2/N \geq 1$. Now, taking advantage of the following chain of inequalities

$$(\Delta S_n)^2 \leq \langle S_n^2 \rangle \leq N^2/4 \tag{3.2.15}$$

the lower-bound of spin squeezing is obtained as

$$\xi^2 \geq \frac{1}{N} \tag{3.2.16}$$

which corresponds to ultimate Heisenberg limit

$$\Delta\theta \geq (\Delta\theta)_{HL} = \frac{1}{N}. \tag{3.2.17}$$

In the rest of this thesis, we will exclusively use the term of the spin squeezing for the spectroscopic definition given in equation (3.2.12). However, we bear in mind that there are many different definitions of spin squeezing which are introduced for different considerations.

spin squeezing and entanglement

It has been proved that the spin squeezing parameter of equation (3.2.12) detects many-body entanglement [41] as long as

$$\xi^2 < 1. \tag{3.2.18}$$

It is possible to prepare large number of entangled atoms in such spin-squeezed states in experiment [43,44]. In the following, we use spin squeezing inequality (3.2.18) as one of the measures of entanglement in the Dicke model. Note that, while spin squeezing has been used widely as a multi-particle entanglement

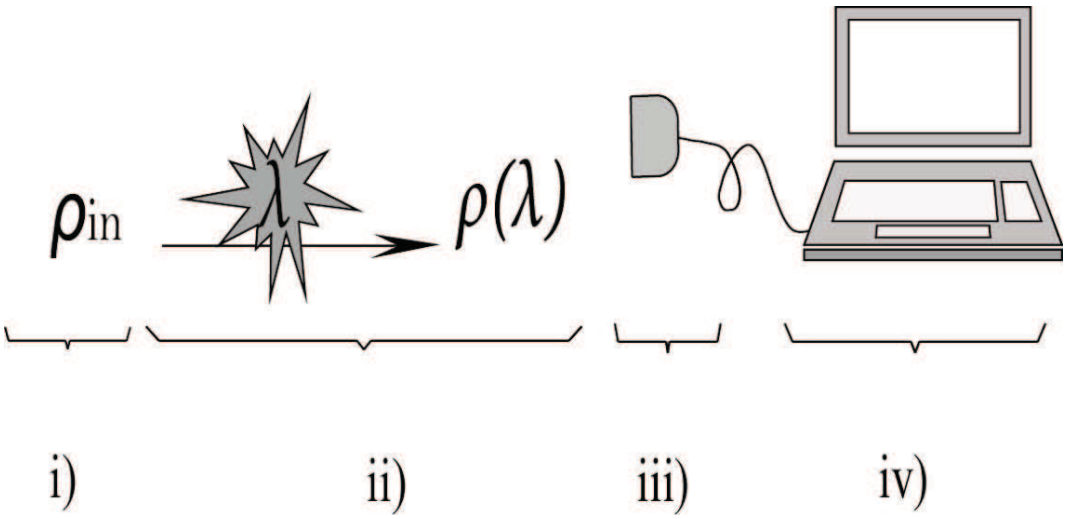

Figure 3.2: **Building blocks of phase estimation.** Here we schematically plot the building blocks of phase estimation: i) the preparation of the probe state ρ_0; ii) the encoding of parameter λ into the system which transform the probe state to $\rho(\lambda)$; iii) the readout measurement $x = \{x_1, x_2, ..., x_i\}$ and finally iv) the mapping from the measurement results to the phase provided by the estimator $E(x)$. The fundamental Cramer-Rao bound (equation 3.2.37), i.e. the statistical variance of the estimator, depends crucially on all these operations.

measure, it is not capable of tracing all kinds of entanglement in a multi-particle system. A very important family of states which are not detected by spin squeezing are maximally entangled Bell states. In fact, while every spin squeezed state is entangled, the vice versa is not necessarily true. In other words, there are many states which are considered entangled states but not included in the family of spin squeezed states.

In the next section, we introduce quantum Fisher information, as a more strong multi-particle entanglement criterion in comparison with spin squeezing.

3.2.3 Quantum Fisher information

Perception and definition

In order to estimate a parameter in physics, one has to perform a proper set of measurements on the prepared physical system and read out the probability distribution of the corresponding parameter. The most natural curiosity afterward is about the best possible measurement precision. Is there any fundamental limit on accuracy attainable in estimation a physical parameter?

For the first time in 1940's it was found [80–83] that there exist a connection between the ultimate precision measurement with *Fisher information*. Fisher information [84, 85], is a factor that measures the maximum amount of information of a parameter achievable from a given probability distribution. In the following we briefly introduce the quantum Fisher information.

In the framework of parameter estimation theory, the central problem is to estimate a parameter λ out of the probability distribution (also called likelihood) $P(x|\lambda)$. Likelihood is the probability of obtaining parameter λ conditioned of having x as the outcome of measurement. Given the set of random variables x, the *estimator* $E(x)$ is defined as any mapping from the experimental measurement outcomes x to the parameter space λ. In other words, an estimator is a generic function which provides a value λ for a given set of experimental results x. In practice, the choice of estimator shall be chosen properly so that λ is as close as possible to the true, unknown value of λ. Being a function of random variables, an estimator itself is a random variable. Thus, it shall be estimated by its statistical mean value

$$\langle E(x)\rangle = \int dx P(x|\lambda)E(x), \tag{3.2.19}$$

which corresponds to the following mean square fluctuation

$$(\Delta E(x))^2 = \int dx P(x|\lambda)[E(x) - \langle E(x)\rangle]^2. \tag{3.2.20}$$

For a given probability distribution of a set of measurement date x, estimators can be defined as the respective mean or its maximum values. As we mentioned above the choice of estimator is important in order to get to the smallest uncertainty in the mean value of the estimator. This family of estimators are called *unbiased estimators* which its statistical average is equal to the true value of the parameter,

$$\langle E(x)\rangle = \lambda, \quad \forall x. \tag{3.2.21}$$

Otherwise, the estimator is called *biased*.

Now, we shall show how the definition of Fisher information magically appears out of the heart of estimation theory. If we use the equations (3.2.19) and (3.2.21) we can write

$$\int dx P(x|\lambda)[E(x) - \lambda] = 0. \tag{3.2.22}$$

Taking derivative of both sides with respect to λ leads to [4]

$$\int dx P(x|\lambda) \frac{\partial L(x,\lambda)}{\partial \lambda} [E(x) - \lambda] = 1, \tag{3.2.23}$$

with definition of *log-likelihood function* $L(x, \lambda)$ as

$$L(x, \lambda) \equiv \ln P(x|\lambda). \tag{3.2.24}$$

Now if we square both sides of the equation (3.2.23) and make use of Cauchy-Schwartz inequality, $|\langle f, g\rangle|^2 \leq \langle f, f\rangle\langle g, g\rangle$, we get the *Cramer-Rao inequality*

$$(\Delta E(x))^2 \geq \frac{1}{f_\lambda}, \tag{3.2.25}$$

where, the *Fisher information* is defined as

$$f_\lambda \equiv \int dx P(x|\lambda)(\frac{\partial L(x,\lambda)}{\partial \lambda})^2 = \int dx \frac{1}{P(x|\lambda)}(\frac{\partial P(x|\lambda)}{\partial \lambda})^2. \tag{3.2.26}$$

the Cramer-Rao bound (3.2.25) implies the fundamental limit of precision at-

[4] we have used the following equation, $\frac{\partial P(x|\lambda)}{\partial \lambda} = P(x|\lambda)\frac{\partial \ln P(x|\lambda)}{\partial \lambda}$

tainable in estimating λ. The equation (3.2.26) shows the ultimate limit of estimation λ is limited by the amount of Fisher information. This of course expresses the physical importance of the Fisher information; The larger Fisher information f_λ, the more information is available to be gained out of the measurement process i. e. the more precise parameter estimation is possible.

Beside the Fisher information, the number of measurement trials affects the estimation precision. In fact, if we repeat the experiment for $\mathcal{N}$ times the equation (3.2.26) turn into the following expression (see Appendix D.)

$$(\Delta E(x))^2 \geq \Delta(E_{CR}(x))^2 = \frac{1}{\mathcal{N} f_\lambda}. \tag{3.2.27}$$

By repeating the measurement for $\mathcal{N}$ times the measurement precision improves by the factor $1/\mathcal{N}$.

Due to probabilistic nature of quantum theory, it is straightforward to generalize the concept of Fisher information to the quantum regime. Given the density matrix of the system $\rho(\lambda)$ [5] and making use of Positive Operator Value Measures (POVM)'s as $\{\Pi_i\}$ (Appendix A.), the quantum counterpart of probability distribution in equation (3.2.19) would be $P_i(x|\lambda) = Tr(\rho(\lambda)\Pi_i)$ with the corresponding derivative $\partial_\lambda P(x|\lambda) = Tr(\Pi_i \partial_\lambda \rho(\lambda))$. Therefore, equation (3.2.26) turns into

$$f_\lambda = \sum_i \frac{Tr[\partial_\lambda \rho(\lambda)\Pi_i]^2}{Tr[\rho(\lambda)\Pi_i]}. \tag{3.2.28}$$

At this point, we define the *symmetric logarithmic derivative operator* L_λ, as the solution of the following equation

$$\frac{\partial \rho(\lambda)}{\partial \lambda} = \frac{1}{2}[\rho(\lambda)L_\lambda + L_\lambda \rho(\lambda)]. \tag{3.2.29}$$

L_λ is Hermitian and uniquely defined only in subspace where $\rho(\lambda)$ in invert-

[5] The density matrix contained the information of parameter λ

ible. By making use of the cyclic permutation properties of the trace and the Hermicity of the operators, we have $Tr[\rho(\lambda)L_\lambda\Pi_i]^* = Tr[L_\lambda\rho(\lambda)\Pi_i]$. Therefore,

$$Tr[\partial_\lambda\rho(\lambda)\Pi_i] = \Re\{Tr[\rho(\lambda)L_\lambda\Pi_i]\} \tag{3.2.30}$$

and equation (3.2.28) results

$$f_\lambda = \sum_i \frac{\Re\{Tr[\rho(\lambda)L_\lambda\Pi_i]\}^2}{Tr[\rho(\lambda)\Pi_i]}. \tag{3.2.31}$$

Quantum Fisher information is defined as the maximum amount of Fisher information over all possible POVM's,

$$F_\lambda(\rho) \equiv \max_{\{\Pi_i\}}\{f_\lambda(\rho,\Pi_i)\} \geq f_\lambda(\rho), \tag{3.2.32}$$

To proceed to find the upper-bound of Fisher information, we make use of the following chain of inequalities,

$$\Re\{Tr[\rho(\lambda)L_\lambda\Pi_i]\}^2 \leq |Tr[\rho(\lambda)L_\lambda\Pi_i]|^2 \leq Tr[\rho(\lambda)\Pi_i]\ Tr[\Pi_i L_\lambda\rho(\lambda)\text{Ł}_\lambda], \tag{3.2.33}$$

which indicate to the $\Re(x)^2 \leq |x|^2 - \Im(x)^2$ and Cauchy-Schwartz inequalities, respectively. Therefore, equation (3.2.28) gives

$$f_\lambda = \sum_i \frac{Tr[\partial_\lambda\rho(\lambda)\Pi_i]^2}{Tr[\rho(\lambda)\Pi_i]} \leq Tr[\Pi_i L_\lambda\rho(\lambda)\text{Ł}_\lambda] \tag{3.2.34}$$

Now, using $\sum_i \Pi_i = I$ (Appendix A.), the upper bound of the Fisher informa-

tion gives

$$F_\lambda = Tr(\rho(\lambda)L_\lambda^2), \tag{3.2.35}$$

which is called the quantum Fisher information (QFI). If we trace out on the complete basis of the density matrix $\rho(\lambda) = \sum_i p_i|\phi_i\rangle\langle\phi_i|$, we get the explicit form of the quantum Fisher information as (see Appendix C.),

$$F_\lambda(\rho) = \sum_i \frac{(\partial_\lambda p_i)^2}{p_i} + 2\sum_{i\neq j}\frac{(p_i - p_j)^2}{(p_i + p_j)}|\langle\phi_i|\partial_\lambda\phi_j\rangle|^2, . \tag{3.2.36}$$

with $|\partial_\lambda\phi_i\rangle \equiv \partial_\lambda|\phi_i\rangle$. There are two point which are worth to mention here. Firstly, the dependence of density matrix on λ and consequently its eigen vectors and eigen-values cause the dependence of quantum Fisher information on λ. At the same time, the quantum Fisher information is always independent of measurement. Another point is that it is not always possible to find the proper physical observable and its correspondence POVM's in experiments. Consequently, quantum Fisher information is not always possible to be measured.

Since quantum Fisher information is the upper bound of Fisher information, The quantum Cramer-Rao bound can be derived by use of equations (3.2.27) and (3.2.32),

$$\Delta E^2 \geq \Delta E_{CR}^2 \geq \Delta E_{QCR}^2 \equiv \frac{1}{\mathcal{N}F_\lambda}, \tag{3.2.37}$$

with $\mathcal{N}$ as the number of independent measurements and $E(x)$ the unbiased estimator of parameter λ. The quantum Cramer-Rao bound provides the ultimate precision limit which is possible to obtain in a set of measurements. By the way, as we mentioned above, it depends on the existence of having efficient estimator.

It has been proved that quantum Fisher information is related to many-body

entanglement [47] in a system of collective spins. In the following, we firstly introduce the explicit form of QFI in the system of collective spins. Thereafter, we present an the useful application of quantum Fisher information as an entanglement witness in a collective spin-1/2 system.

QFI for collective spin systems

Let us return to the system of collective N spin-1/2 particles which is represented by the density matrix operator $\rho(\theta) = \sum_i p_i|\phi_i\rangle\langle\phi_i|$. Specifically, we suppose that θ is the parameter which we are interested to measure as precise as possible. In order to inject the phase in the system, one could have made a rotation on the initial *prepared state* of the system $\rho_0 = \sum_i p_i|\phi_{0,i}\rangle\langle\phi_{0,i}|$ along the direction n. This process is specified as *phase encoding* in the phase estimation language. [6] This interferometric operation is explained by use of a unitary transformation $U(\theta) = e^{-i\theta S_n}$ such that

$$\rho(\theta) = e^{-i\theta S_n}\rho_0 e^{i\theta S_n}. \tag{3.2.38}$$

Here $S_n = \vec{S}.\vec{n}$, being the collective spin operator in the direction of n, is called the *generator of transformation*. Unitary transformation does not change the eigen-values of the initial density matrix while it rotates the initial eigen-vectors such that $|\phi_i\rangle = e^{-i\theta S_n}|\phi_{0,i}\rangle$. Consequently, for collective spin system, the quantum Fisher information (3.2.36) casts in the following form

$$F(\rho(\theta), S_n) = 2\sum_{i\neq j}\frac{(p_i - p_j)^2}{(p_i + p_j)}|\langle\phi_i|S_n|\phi_j\rangle|^2, \tag{3.2.39}$$

which for the special case of pure states simplifies to (Appendix C.)

$$F(\rho(\theta), S_n) = 4\Delta S_n^2, \tag{3.2.40}$$

[6] Let us remind that in order to make a full phase estimation, these two steps have to be completed by read-out and estimation processes which have been already explained. The building blocks of the phase estimation are illustrated in Figure 3.2.2.

with $\Delta S_n^2 = \langle S_n^2 \rangle - \langle S_n \rangle^2$. It is possible to prove that the Fisher information is maximum when the system is in the pure state,

$$F \leq 4\Delta S_n^2 \tag{3.2.41}$$

which by making use of equation (3.2.15) gives the upper-bound of QFI as

$$F \leq N^2. \tag{3.2.42}$$

In fact, it makes a very good physical sense that a system in a pure state contains the most amount of information. In practice by the way, it is difficult to prepare the pure state of the system and consequently very difficult to saturate this bound. From the equation (3.2.39) it is clear that the quantum Fisher information of a system in the state ρ depends on generator S_n and consequently the direction of spin direction $\vec{n}$. Therefore, there is an optimal spin direction which corresponds to maximum value of QFI. For a collective spin system the maximum of QFI is given by $4\zeta_{\max}[M_C]$ where $\zeta_{\max}$ is the maximum eigen-value of the covariance matrix defined as,

$$[M_C]_{lm} = \frac{1}{2} \sum_{ij} \frac{(p_i - p_j)^2}{p_i + p_j} \langle \phi_i | S_l | \phi_j \rangle \langle \phi_j | S_m | \phi_i \rangle. \tag{3.2.43}$$

The above equation reduces to the following form for special case of pure states

$$[M_C]_{lm} = \frac{1}{2} \langle S_l S_m + S_m S_l \rangle - \langle S_l S_m \rangle. \tag{3.2.44}$$

proof - let us take the system in the pure state $\rho = |\phi\rangle\langle\phi|$. For $S_n = \vec{S}.\vec{n}$, from the equation (3.2.40), we have $F = 4\Delta S_n^2 = 4\vec{n}^T.M_C.\vec{n}$. It is known from linear algebra that this expression is maximized by choosing $\vec{n} = \vec{n}_{\max}$ as the eigen-vector corresponding to the maximal eigenvalue. For the general case of mixed states one may refer to Ref. [49].

■

According to (3.2.37), the fundamental Cramer-Rao bound for estimating phase θ in a collective spin systems is given by

$$\Delta\theta^2_{QCR} = \frac{1}{\mathcal{N}F(\rho(\theta), S_n)}. \tag{3.2.45}$$

As quantum Fisher information maximum value is N^2, we get the ultimate precision of $1/N$ if $\mathcal{N} = 1$. On the other hand, from spin squeezing definition given in equation 3.2.10 we have

$$\Delta\theta^2 = \frac{\xi^2}{N}.$$

already given in equation (3.2.13). Now, using (equation 3.2.37) we get

$$\chi^2 \equiv \frac{N}{F} \leq \xi^2, \tag{3.2.46}$$

which we call the parameter χ^2 as *quantum Fisher information flag*.

In addition to spin systems, quantum Fisher information has also been used in optical interferometry [86–88] for detecting non-classical states and precision measurement. Finally, let us mention that while both of χ^2 and ξ^2 are related to phase measurement protocols, they have another important connection trough entanglement perception which we consider as follows.

Quantum Fisher information and entanglement

As we mentioned previously, spin squeezing factor ξ^2 is connected to multi-particle entanglement. Therefore, it is natural to expect a relation between χ^2 factor and entanglement. Considering the system of N spin system, it can be easily proved that the quantum Fisher information flag χ^2 indicates many-body entanglement when

$$\chi^2 < 1. \tag{3.2.47}$$

proof For the separable state of the system in the following form

$$\rho^{(k)} = \rho_1^{(k)} \otimes \rho_2^{(k)} \otimes ... \otimes \rho_N^{(k)} \tag{3.2.48}$$

we have $F(\rho^{(k)}) = 4\Delta S_n^2 = N - 4\sum_{i=1}^{N} \langle s_n^{(i)} \rangle^2 \leq N$. Now, if we consider the general arbitrary mixture of equation (3.1.3)

$$\rho_{sep} = \sum_k \mu_k \rho_1^{(k)} \otimes \rho_2^{(k)} \otimes ... \otimes \rho_N^{(k)} = \sum_k \mu_k \rho^{(k)},$$

and use the convexity property of QFI, $F(\rho_{sep}) \leq \sum_k \mu_k F(\rho^{(k)})$, (see Appendix D.), we obtain

$$F(\rho_{sep}) \leq N. \tag{3.2.49}$$

Consequently, for any entangled state of the system the condition

$$F > N, \tag{3.2.50}$$

or equivalently,

$$\chi^2 = \frac{N}{F} < 1. \tag{3.2.51}$$

is valid. This is the sufficient condition for having multi-particle entanglement in a collective N spin-$\frac{1}{2}$system. In other words, it is not possible to fulfill this condition with a separable state (no matter pure or mixed). The smaller the χ^2, the larger multi-particle entanglement. Of course, the smallest possible value of χ^2 is equal to $1/N$.

■

As we mentioned before ξ^2 is a multi-particle entanglement witness. Nevertheless, equation (3.2.46) implies that χ^2 is a more strong criteria for detecting entanglement in comparison to the ξ^2. In fact, it has been proved [47] that there are families of states which are entangled $\chi^2 < 1$ but not spin squeezed $\xi^2 \geq 1$ such as maximally entangled states. In figure 3.3 we present the Husimi distribution of a typical state on the generalized Bloch sphere which is entangled using χ^2. Nonetheless, it is observed that the S-shape of the state that is not spin squeezed [99]. In the next chapter, we

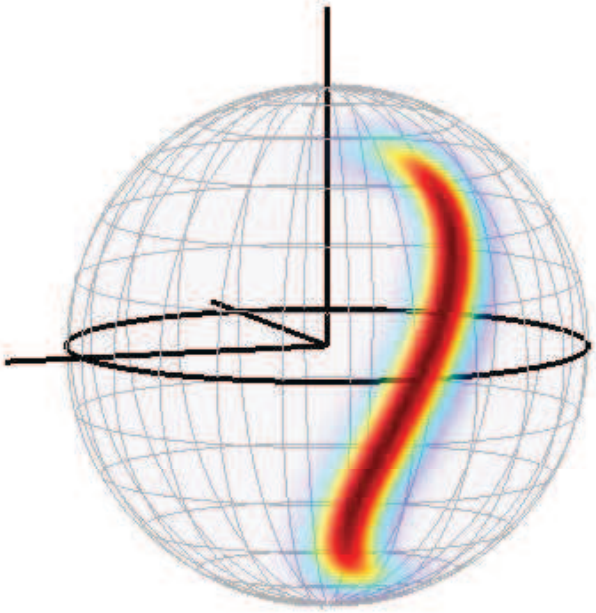

Figure 3.3: Husimi distribution of a typical entangled spin state which is possible to be detected by $\chi^2 < 1$ but is not spin squeezed $\xi^2 > 1$.

observe that there are *entangled-but-not-squeezed* states in the specific system of Dicke model.

In the context of quantum metrology, there is another interesting point regarding χ^2 factor which is worth to be emphasized. It has been proved that the states which fulfill the condition (3.2.51), not only are entangled but necessarily useful-entangled states as a resource in phase estimation protocols. This property is very advantageous, in sub shot-noise interferometry [49].

3.3 Conclusion

In this section, we introduced the concept of quantum entanglement and presented the useful witnesses of multi-particle entanglement. Specifically, we focused on the quantum Fisher information factor due to its capability of detecting a wider family of entangled states than spin squeezing. Nevertheless, one has to note that quantum Fisher information still detects a sub-set of the whole family of entangled states in the collective spin systems. This has illustrated in the Figure 3.4. At the same time, it is proved that QFI is detecting the whole family of usefully entangled states.

In the next chapter, we will use the introduced entanglement measures in the system of Dicke model to detect multi-particle entanglement dynamics. In this regard, we are

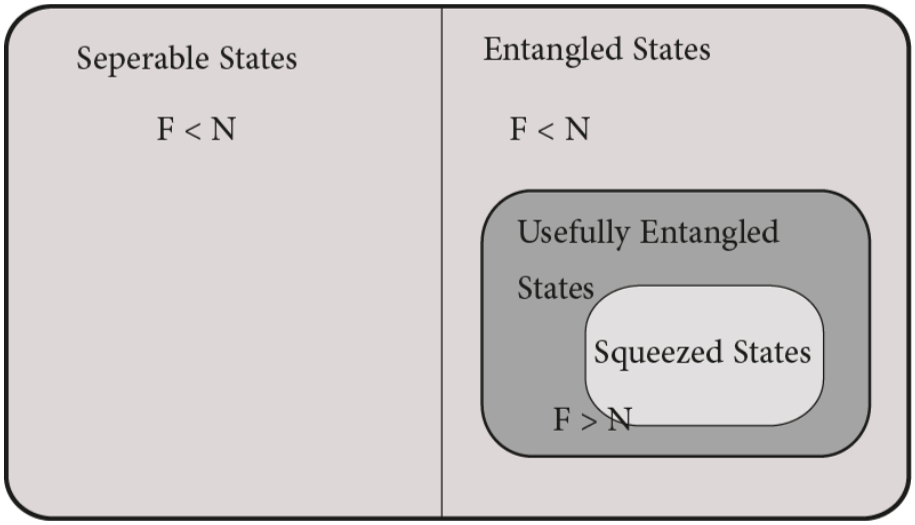

Figure 3.4: Here we illustrate the various kinds of quantum states concerning the entanglement. The vertical line divides entangled and separable states. Every separable state has a Fisher Information $F < N$. On the entangled states side there are some states that are useful for sub shot noise interferometry ($F > N$) and some that are not ($F < N$). A subset of the useful entangled states is the spin squeezed states.

specially interested in the quantum Fisher information as an entanglement witness.

Chapter 4

Entanglement detection via Quantum Fisher Information in the system of Dicke Model I

"What you seek is seeking you."
Rumi

In Dicke model, the single mode of the field acts as a virtual bus which correlates the atoms. This correlations may lead to entanglement between the particles. Up to now, the spin squeezing has been extensively used as a criterion for detecting multi-particle entanglement in the multi-particle systems [43–46]. Nevertheless, as we mentioned before the spin squeezing is just detecting a small class of the multi-particle entangled states. Moreover, the dynamics of (pairwise) entanglement has been explored by concurrence for the Dicke model of N=2 [67] or finite numbers of atoms [68].

On the other hand, quantum Fisher information (QFI) is more stringent measure of multi-particle entanglement than the spin squeezing. QFI gives the sufficient condition for detecting entanglement in a multi-particle system. Also, it is sufficient and necessary criterion for having useful entanglement.

In the following QFI is used as a measure to explore the dynamics of entanglement between two particles interacting with a single coherent mode of the cavity. Dependent on the initial photonic population $\bar{n}$ and number of atoms N, we consider the

different regimes of interaction. For each single regime, we explore the multi-particle dynamics by the quantum Fisher information as witness. We compare it with spin squeezing and occurrence, frequently.

4.1 The model and methods of solution

Let us begin with the system of Dicke model which is already introduced in chapter 2. The system is composed of N resonant two level atoms with ground (excited) energy state $|g\rangle(|e\rangle)$ which are coupled to the single mode of radiation field. We suppose that the atoms are inside a loss-less cavity and also any kind of losses is neglected. The dipole approximation and rotating wave approximation are also imposed.

Considering all the above assumptions, the corresponding Hamiltonian of the system would be of the Tavis-cumming form of equation (2.1.33). The Hamiltonian of the system in the interaction picture is given by,

$$\tilde{H} = g(aS_+ + a^\dagger S_-), \tag{4.1.1}$$

with $\hbar = 1$. Here and in the following we use the interaction picture. In the rest of this work, we suppose the underlying symmetry in the atomic system, i. e. the particles are not distinguishable. As a result, the collective atomic states are restricted to the manifold of $S = N/2$. Since, S is a constant of motion for the Hamiltonian of the system (4.1.1), during the time evolution, the initial manifold of the system does not change. In the other words, the other N manifolds are dark state of the system.

As we mentioned before, interaction Hamiltonian (4.1.1) being composed of the both atomic and field operators, is has naturally the potential of creating the atom-field entanglement in the system which is interesting in creating states with microscopic/macroscopic entanglement, i. e. Schrödinger cat states [57,58]. This bi-modal entanglement, has been studied in various works by now both in the ground as well as dynamical states. On the other hand, as we mentioned in previous chapters, the Hamiltonian (4.1.1) is useful for creating entanglement between the particles. Though, the emergence of multi-particle entanglement is not as obvious as the case of bi-modal entanglement, some works studied the emergence of entanglement even between particles in the Dicke system. As we discussed in section 2.1.3, the appearance of multi-particle entanglement attributes to the presence virtual data bus of

the field inside the cavity. It has also been proved [57, 89] that in the dispersive regime of interaction ($\Delta = |\omega - \omega_0| \gg g$) the above Hamiltonian may be cast in the form of one-axis twisting Hamiltonian $\propto S_x^2$ which creates spin squeezing and consequently the multi-particle entanglement. The possibility of creating spin squeezing (entanglement) using the time-dependent version of Hamiltonian (4.1.1) is also has been considered in Ref. [90].

In the following, we are interested in investigating the detection of multi-particle entanglement dynamics by using the quantum Fisher information as a measure. Depending on the initial photonic population $\bar{n}$ and number of atoms N, we consider three regimes of interaction:

- Weak field regime ($\bar{n} \ll N$),
- Intermediate regime ($\bar{n} \approx N$),
- Strong field regime ($\bar{n} \gg N > 1$).

The model can be analytically solved in the first and third regimes of interaction, approximately. In the intermediate regime we present the numerical results. In the coming section we introduce the initial states of the field and the atomic systems.

4.1.1 Initial state

Initial state of the atomic system

For the case of atomic system, in general, we take all the atoms initially being in the ground state,

$$|\psi(0)\rangle_a = \left|\frac{N}{2}, -\frac{N}{2}\right\rangle. \tag{4.1.2}$$

This initial state is very convenient to be prepared in an atomic system, experimentally. Moreover, it is also interesting to consider the initially entangled states in order to observe effects such as collapse and revival of entanglement or sudden birth or death of entanglement. Therefore, at times, we consider other initial states of the atomic system to investigate the entanglement dynamics.

Initial state of the field

We assume that the initial state of the field is in the coherent state,

$$\begin{aligned} |\psi(0)\rangle_f &= |\alpha\rangle \\ &= e^{-|\alpha|^2/2} \sum_{n=0}^{\infty} \frac{\alpha^n}{\sqrt{n!}} |n\rangle \\ &\equiv \sum_{n=0}^{\infty} c_n |n\rangle. \end{aligned} \tag{4.1.3}$$

with $a^\dagger a|n\rangle = n|n\rangle$. Without loss of generality, we consider only real values of α. A coherent states has a Poissonian number distribution when expressed in a basis of energy eigenstates

$$P_{cs}(n) = |\langle\alpha|n\rangle|^2 = e^{-\bar{n}} \frac{\bar{n}^n}{n!}, \tag{4.1.4}$$

where,

$$\bar{n} = \langle n|a^\dagger a|n\rangle = |\alpha|^2 \tag{4.1.5}$$

is the population of photons in the coherent field.

Considering the initial coherent state for the field is interesting as it is the most convenient field states which might be prepared experimentally. Despite the impressive experimental progress, preparing the Fock state even with few number of photons is still difficult. While, coherent states can be prepared more easily which gives the opportunity to define the different regimes of interaction depending on the strength of the initial field.

Joint system initial state

The initial state of the joint atom-field system is the pure product state of the field and atoms,

$$\begin{aligned} |\psi(0)\rangle &= |\psi(0)\rangle_a \otimes |\psi(0)\rangle_f \\ &= \left|\frac{N}{2}, -\frac{N}{2}\right\rangle \otimes |\alpha\rangle. \end{aligned} \tag{4.1.6}$$

The Hilbert space of the joint atom-field system is given by the tensor product $\mathcal{H} = \mathcal{H}_a \otimes \mathcal{H}_f$ where $\mathcal{H}_a$ and $\mathcal{H}_f$ denote the Hilbert space of atoms and electromagnetic field, respectively. In general the Hilbert space of the atomic state is of dimension of $N+1$ while the Hilbert state of the field is of dimension of ∞. In order to apply the numerical calculations we have imposed a cut-off on the number of bosons in the field such that there is no change in the final results with the change of the cut-off.

It is convenient to carry out the calculations in an interaction representation with the wave function expressed as,

$$|\psi(t)\rangle = \sum_{M=-N/2}^{N/2} \sum_{n=0}^{\infty} C_{M,n}(t) e^{-i\omega(M+n)t} |\frac{N}{2}, M\rangle \otimes |n\rangle. \tag{4.1.7}$$

By applying the Hamiltonian of the equation (4.1.1) on the initial state of (4.1.6), and solving the Schrödinger equation of motion the state of the system at every time is known. Therefore, one may explore the different mean collective spins such as $\langle S_\alpha(t)\rangle$ or $\langle S_\alpha(t) S_\beta(t)\rangle$ with $\alpha, \beta \in \{x, y, z\}$). As a result, it is straightforward to calculate the spin squeezing ξ^2 and quantum Fisher information flag χ^2 during the time evolution.

There is one point which is worth to be mentioned here. It is assumed that the initial state of the system given in (4.1.6) is pure. Furthermore, we consider only the effects of the unitary evolution generated by Hamiltonian (4.1.1), i.e., we do not include the effects of measurement, nor of mixing due to environment-induced decoherence, so that the total system conserves its initial purity (i. e. $Tr[\rho^2(t)] = 1$). By the way, the state of the atomic (field) sub-system in after tracing out the field (atomic)

degrees of freedom does not necessarily remain pure states. This is easily observed by looking into reduced density matrices of the sub-systems when $Tr[\rho_{a,f}^2(t)] < 1$ with $\rho_{a,f}(t) = Tr_{f,a}[\rho(t)]$.

4.2 Interaction of $N = 2$ atoms with the field

In this section we set $N = 2$. This assumption makes it possible to derive the analytical solutions for quantum Fisher information in the weak-field (Sec. 4.2.1) and strong field (Sec. 4.2.3) limits. Furthermore, in Sec. 4.2.2 we present the result of numerical simulation in the intermediate limit since there is no straightforward way to obtain the analytical terms.

Initial state

For the case of having two atoms in the system, the initial state given in equation (4.1.6) simplifies to the following form

$$|\psi(0)\rangle = \sum_{n=0}^{\infty} c_n |1,-1\rangle \otimes |n\rangle, \tag{4.2.1}$$

where c_n's represent the initial state amplitudes of the coherent field of equation (4.1.3). Solving the Schrödinger equation of motion, $i|\dot{\psi}(t)\rangle = H|\psi(t)\rangle$, we obtain the following general time-dependent amplitudes [91],

$$\begin{aligned} C_{-1,n}(t) &= \frac{1}{2n-1}[n-1+n\cos(\sqrt{4n-2}gt)]c_n, \\ C_{0,n}(t) &= -i\sqrt{\frac{n+1}{2n+1}}\sin(\sqrt{4n+2}gt)c_{n+1}, \\ C_{1,n}(t) &= \sqrt{\frac{(n+1)(n+2)}{2n+3}}[-1+\cos(\sqrt{4n+6}gt)]c_{n+2}. \end{aligned} \tag{4.2.2}$$

4.2.1 Weak-field limit

Under the very weak field approximation ($\bar{n} = |\alpha|^2 \ll 1$), we may expand the the coefficients of equations (4.2.2) up to the second orders of α and get to the following expectation values for the spin components [91]

$$\begin{aligned} \langle S_x(t)\rangle &= 0, \\ \langle S_y(t)\rangle &= \sqrt{2}\alpha \sin(\sqrt{2}gt), \\ \langle S_z(t)\rangle &= -[1 - \alpha^2 \sin(\sqrt{2}gt)]. \end{aligned} \tag{4.2.3}$$

Since $\langle S_x\rangle = 0$, the motion of the mean spin vector, is always in the yz plane, with the mean spin length equal to unity, ($|\langle S\rangle| = \sqrt{\langle {S_y}^2\rangle + \langle {S_z}^2\rangle} \approx 1$). Therefore, the plane in which we look for optimal quantum Fisher information as well as spin squeezing is the one defined by the x axis and an axis orthogonal to both x and the instantaneous direction of the mean spin vector $\langle S\rangle$.

In order to calculate the quantum Fisher information, we note that the state of the atomic system during interaction remains almost pure during the time evolution ($|\langle S\rangle| \approx 1$). Therefore, the quantum Fisher information (4.2.4) simplifies to

$$F = 4 \max\{(\Delta S_\perp)^2\}, \tag{4.2.4}$$

and consequently the quantum Fisher information flag is given by,

$$\chi^2 = \frac{N}{4 \max\{(\Delta S_\perp)^2\}}, \tag{4.2.5}$$

where, $\Delta S_\perp^2$ represent the variances of spin operators orthonormal to the mean spin direction $\langle S\rangle$. In addition, the spin squeezing parameter (3.2.12) is given by

$$\xi^2 = \frac{4 \min\{(\Delta S_{\perp'})^2\}}{N}. \tag{4.2.6}$$

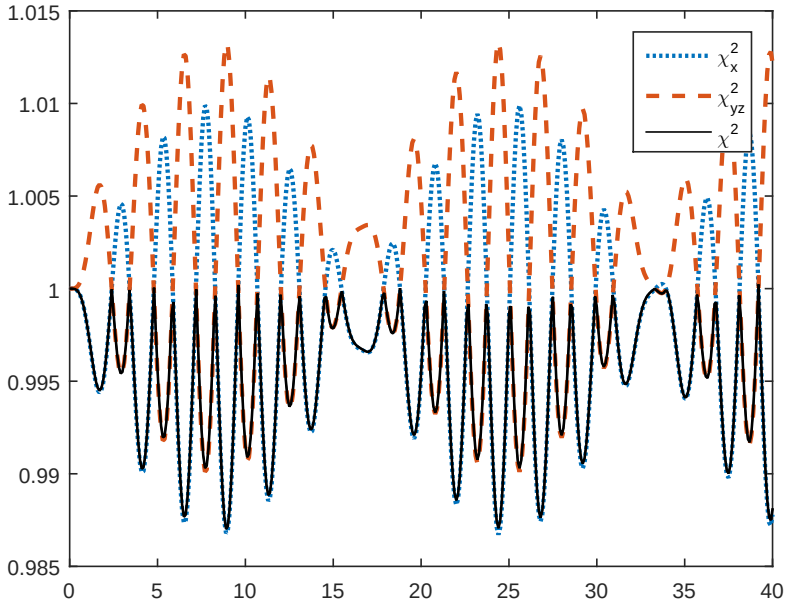

Figure 4.1: Quantum Fisher information flag χ^2 for $N = 2$, $|\alpha|^2 = 0.01$. Three cases of χ^2_x (dashed) and χ^2_{yz} (dash-dotted) and optimal χ^2 (solid) are plotted.

Now let us take an axes yz in the plane perpendicular to the mean spin direction and x. Making appropriate rotations, we can define any vector in the normal plane such that $S_\perp = \cos\theta S_x + \sin\theta S_{yz}$. By optimizing $\Delta S^2_\perp$, we get $\Delta S^2_\perp \geq \max\{\Delta S^2_x, \Delta S^2_{yz}\}$ when $\theta = 0, \pi$. It means that the maximum of spin variances in the normal direction is either along x or yz. In this case we have

$$\chi^2 = \frac{1}{2\max\{(\Delta S_x)^2, (\Delta S_{yz})^2\}}, \tag{4.2.7}$$

and

$$\xi^2 = 2\min\{(\Delta S_x)^2, (\Delta S_{yz})^2\}. \tag{4.2.8}$$

Correspondingly, we get the following following analytical expressions for the spin fluctuations in normal directions

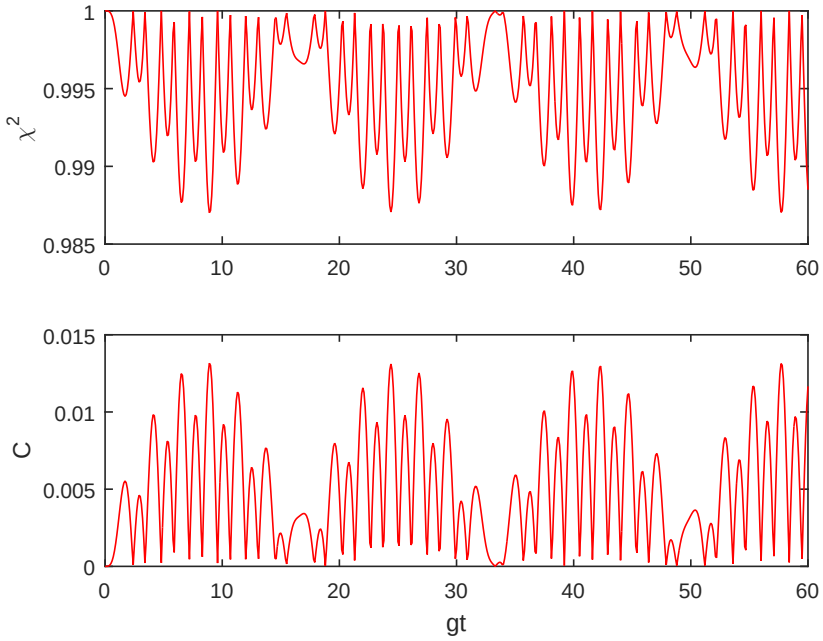

Figure 4.2: Optimal χ^2 (upper) and concurrence C (lower) versus gt for the same values in figure 4.1

$$\begin{aligned} \Delta S_x^2 &\approx \frac{1}{2} + \alpha^2\{\frac{1}{2}\sin^2(\sqrt{2}gt) - \frac{2}{3}\sin^2(\sqrt{6}gt/2)\}, \\ \Delta S_{yz}^2 &\approx \frac{1}{2} - \alpha^2\{\frac{1}{2}\sin^2(\sqrt{2}gt) - \frac{2}{3}\sin^2(\sqrt{6}gt/2)\}. \end{aligned} \tag{4.2.9}$$

Up to the order of $|\alpha|^2$, the uncertainty relation (3.2.14) reduces to

$$\Delta S_x^2 \Delta S_{yz}^2 \approx \frac{1}{4}, \tag{4.2.10}$$

This is the lower-bound of uncertainty relation for three orthonormal spin directions S_z, S_{yz} and S and therefore the state is Gaussian up to the second order of α. in other words, the $\max(\Delta S_x)^2$ corresponds to $\min(\Delta S_{yz})^2$ and vise versa. Therefore, $\chi^2 = \xi^2$.

Figure (4.1) gives the time evolution of optimal quantum Fisher information of

the system for $\bar{n} = |\alpha|^2 = 0.01$ by exact numerical simulations. Furthermore, the analytical quantum Fisher information flag along the x and yz are also given using equations (4.1.6) and (4.2.9). The regular behavior of quantum Fisher information has the period of $gT = 4\pi\sqrt{2} = 17.78$ for the envelope. In order to exactly calculate ξ^2 and χ^2, we have numerically solved the Schrödinger equation of motion for the joint atom-field system. As we mentioned before, in the absence of dissipation the initial pure state of the system (4.1.6) remains pure. By the way, the atomic state is not generally pure anymore as a result of coupling to the field. Thus, one has to find the reduced density matrix of the atomic sub-system, $\rho_a(t) = Tr_f\rho(t)$ at first place. Thereafter, the atomic reduced density matrix shall be used to calculate the mean spin averages given in (3.2.12) and (3.2.39) in order to find the ξ^2 and χ^2 factors.

From equation (4.2.9) it is easy to verify that the minimum of quantum Fisher information flag (and spin squeezing) over time is given by

$$\chi^2_{\min} = \xi^2_{\min} = 1 - \frac{4}{3}\alpha^2 \tag{4.2.11}$$

when

$$\sin\left(\sqrt{2}gt_{\min}\right) = 0 \quad \& \quad \sin^2\left(\sqrt{6}gt_{\min}/2\right) = 1, \tag{4.2.12}$$

which is the same result for the spin squeezing in the weak-field regime calculated in Ref. [91]. Equation (4.2.11) indicates that the minimum amount of χ^2 increases with increasing the amplitude of the coherent field. By the way, as long as $|\alpha|^2$ is small, while there is always entanglement in the system, the amount of it is not considerable ($\chi^2_{\min} \approx 1$). In fact, the maximum amount of entanglement detected by χ^2 is always far from the ultimate Heisenberg limit ($\chi^2_{HL} = 1/2$). The dependence of χ^2 in the small field intensities $|\alpha|^2 \ll 1$ can be seen in Figure 4.4. In order to get this plot we have fixed a cut-off on time at $gt_{cut-off} = 200$ and minimized the χ^2 and ξ^2 over time.

Moreover, based on the equation (4.2.12) the time in which the minimum entanglement occurs does not depend on the strength of the field. Regarding the optimal direction of χ^2 and ξ^2 parameters, we have found that the maximum of quantum Fisher information is along S_y while the minimum spin squeezing occurs in the normal direction of S_x. Note that this is not the most general relation between the

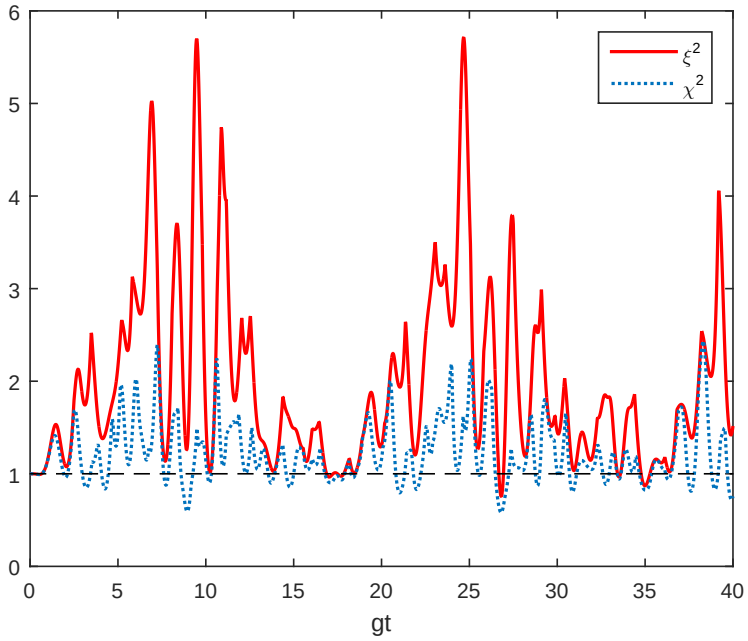

Figure 4.3: The spin squeezing ξ^2 (solid red) and quantum Fisher information flag χ^2 (dotted blue) parameters vs. time gt for $N = 2$,$|\alpha|^2 = 1.2$ and

optimal χ^2 and ξ^2 directions and here is valid due to having the special case of the Gaussian spin states.

In addition, we would like to mention that one could diagonalize the covariance matrices in order to derive the optimal quantum Fisher information (3.2.43) and spin squeezing factors [71], analytically. By the way, we employed the current approach, i. e. considering the spin vectors on the generalized Bloch sphere, since it conveys more visual sense. Of course, using both approaches the results are the same as the expressions given in equations (4.2.9).

Finally, as the atomic system is composed of a pair of particles, it is also interesting to compare the multi-particle entanglement detected by $\chi^2(\xi^2)$ with the pair-wise entanglement measured by concurrence (3.2.1). In Figure 4.2 we have plotted the quantum Fisher information flag χ^2 (upper) and concurrence C (lower). The good agreement in the regular behavior as well as the time in which peaks of parameters occur is observed.

4.2.2 Intermediate-field limit

In the intermediate-field limit, we consider the initial photonic population with the order of number of atoms $\bar{n} \sim N$. In this regime, there is no straightforward analytical way to derive the analytical solutions as it is done in the previous section. By the way, it is possible to get to the exact numerical solutions. Figure 4.3 gives the minimum quantum fisher information flag χ^2 and also spin squeezing parameter ξ^2 as a function of gt for $\bar{n} = |\alpha|^2 = 1.2$. At first glance, one might observe that with increasing $|\alpha|^2$ both spin squeezing and quantum Fisher information lose their regular behaviors in the intermediate-field strength. By the way, for the strong enough field amplitudes, the quantum Fisher information retains the regular behavior. This is what we will discuss in the next section. Moreover, the χ^2 and ξ^2 do not coincide anymore.

Figure (4.4) gives the minimum of quantum Fisher information flag χ^2 and spin squeezing ξ^2 versus coherent field population $|\alpha|^2$. To get this plot, we have put a cut-off on time ($gt_{cutt-off} = 200$) and then have found the minimum of spin squeezing and quantum fisher information over the time span. Moreover, we have replaced any $\chi^2, \xi^2 > 1$ with unity. This is because we are mainly interested in the multi-particle entangled states not the shot-noise nor unentangled states for which $\chi^2, \xi^2 \geq 1$ (section 3.2).

In the weak-field limit which is discussed in previous section 4.2.1, both quantum fisher information and spin squeezing anticipate the same amount of squeezing due to having Gaussian states. Nevertheless, with increasing the field amplitude both measures show increasing of entanglement up to a minimum which occurs around $|\alpha|^2 = 1$.[1] Of course the quantum Fisher information detects more entanglement ($\chi^2_{min} < \xi^2_{min}$) [47] as one would expect based on equation (3.2.46). However, there is a different trend when the field population continues to surpass the minimums. In this case, the spin squeezing decreases and is almost diminished for $|\alpha|^2 \gg 2$. On the other hand, the quantum Fisher information decreases initially but for $|\alpha|^2 \gg 2$ it has almost always considerable non-zero amount with local peaks. This corresponds to presence of entanglement even with if there is moderate coherent fields in the system. All in all, in this regime there is not a regular behavior in the QFI flag and consequently the entanglement dynamics. This is a flow when it comes to measure the entanglement. One has to note that the minimum amount of χ^2 and ξ^2 are not the global and there might exist smaller values for longer times, that is $t > t_{cut-off}$.

[1] This minimum is of order of $\approx O(N/2) = 1$

Nevertheless, the current values for minimum are sufficient to give the general trend of temporal behavior for entanglement measures. Moreover, even if there are smaller values which occurs in very long times, there are essentially not important, from experimental point of view.

The kind of spin squeezing behavior in the intermediate regime of interaction - increasing up to a minimum and then decreasing - has already been studied in the Ref. [91]. As we will see in the next section, the reducing of spin squeezing with increasing the field coherent population is attributed to decreasing the ratio of the collective spin fluctuations to the mean spin length. On the other hand, there is no such dependence in the definition of quantum Fisher information given in equation (3.2.39). Therefore, it seems to be capable of detecting entanglement is the regimes which the spin squeezing is not necessarily available.

In fact, as we mentioned before, as a result of coherently coupling of the particles to the same mode of the field, there exist a quantum bus in the joint atom-field system. This virtual bus causes the quantum correlation between atoms despite of the fact that there in no direct interaction among the particles. Therefore, we naturally expect quantum correlations among the particles even if the coherent field is not small. This fact has been verified in some works, in previous years. For instance, in the case of having strong coherent field, the entanglement dynamics has been studied using the tangle τ (3.2.3) for two [67] and and also few number [68] of particles. Here, with the same motivation, we explore the dynamics of multi-particle entanglement making use of QFI.

Initial single Fock state of the field - Interference effect There is an interesting effect for the special case of initial Fock state $n = 1$. Figure (4.5) gives temporal quantum Fisher information of the atoms. In a periodic manner, the minimum of quantum Fisher information flag $\chi^2 = 1/2$ occur at times $g\tau_{\max} = \frac{\pi}{2\sqrt{2}}$ while there is no spin squeezing [91]. In fact, the system of two atoms interacting with a single Fock state of the radiation field resembles the two-slit experiment. While both of the atoms initiate in the ground state $|gg\rangle$, the single photon has 50% possibility of interaction with each of them and turns it into the excited state. Therefore, the maximally Bell state $|\Psi\rangle = [|ge\rangle + |eg\rangle]/2$ is created at times $\tau_{\max}$ [63]. Nevertheless, there is no way to tell which atom has absorbed the photon. Consequently, the *metaphorical* double-slit experiment occurs as a result of lack of information. We compare QFI flag result with the concurrence (3.2.1) which is also a measure of pair-wise entanglement for mixed states. This effect has been experimentally

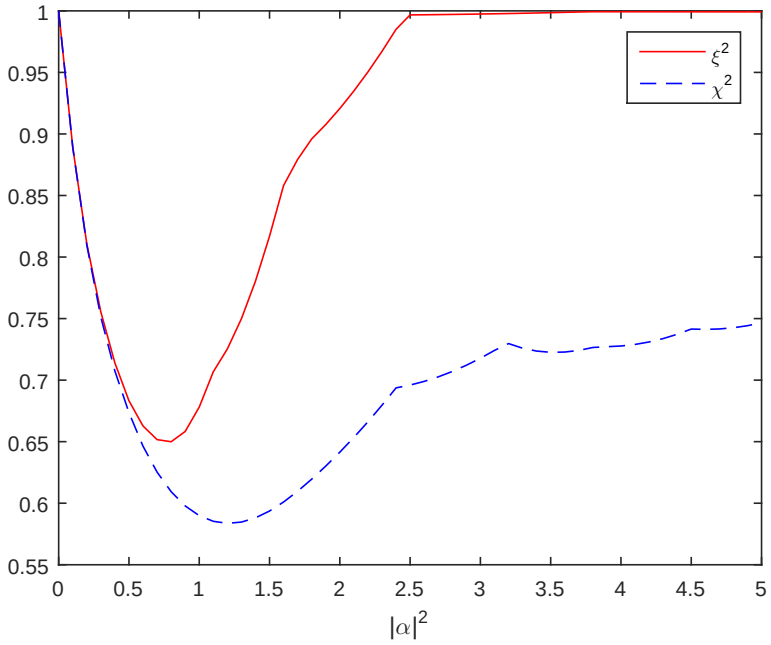

Figure 4.4: The local minimum of spin squeezing and quantum Fisher information flag versus coherent field population $|\alpha|^2$. To get this plot, we have put a cut-off on time span at $gt_{cut-off} = 200$

observed in Ref. [63] in a QED set-up up to three semiconducting qubits coupled with a single photon in a microwave resonator. In this work, the entanglement has been studied by the full state tomography of the density matrix of the atomic system following by the use of an entanglement witness operator. Here, the times in which the two-qubit entangled state $|\Psi\rangle$ detects by χ^2 is in perfect agreement with the result of experiment with 161.8MHz$= 1.05 \times \sqrt{2}g/2\pi$. Note that, the regular behavior of χ^2 is due to regular Rabi dynamics of the system shown in Figure 4.6. It is also verified that in the case of having more than two particle in the system, the interaction of particles with a single number state of the field results in creating the W-state of qubits [92].

4.2.3 Strong-field limit

In this section, we consider the regime in which the photon population of the coherent field is much more larger than the number of atoms, say $\bar{n} = \langle\alpha|a^\dagger a|\alpha\rangle = |\alpha|^2 \gg 2$. It is proved [93, 94] that taking advantage of some approximation in this regime, e. g. factorization approximation or quasi linear approximation, it is possible to derive

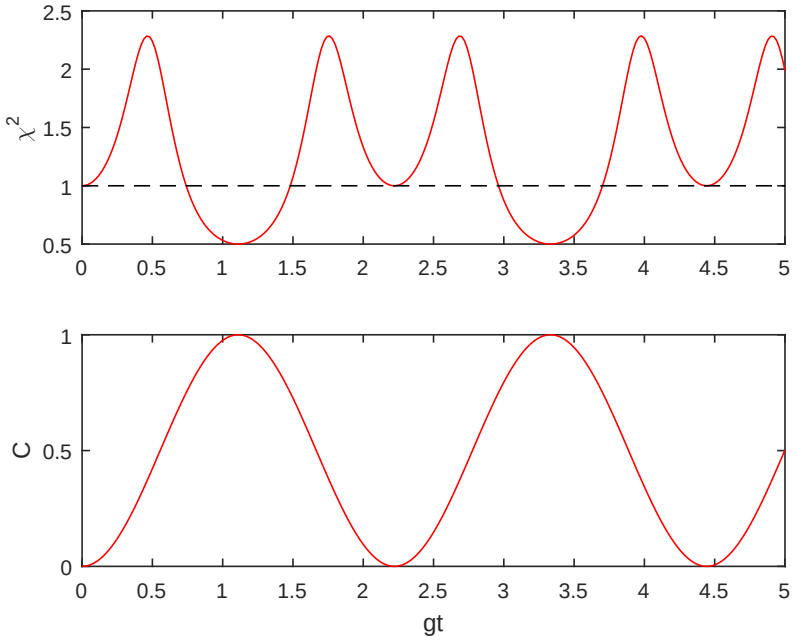

Figure 4.5: Optimal χ^2 (upper) and concurrence C (lower) vs time gt for $N = 2$ and the initial Fock state of the field $n = 1$

the analytical solution for the wave-function of the joint system. Therefore, the expectation values of the collective spins as well as their variances are at hand. As a result, it is possible to get the approximate analytical QFI up to the validity range of the approximation. In the following, we will use the factorization approximation to derive the density matrix of the atomic system. In this case, we firstly give a brief introduction of factorization approximation and its validity region. Afterward, we use the approximation to derive the χ^2 of the atomic system in the strong field regime. We compare the exact numerical solutions with the approximate ones. Moreover, we consider different examples of the initial states which are related to the some specific physical effects in the atomic system. In the following, we will employ the representation of $\bar{n}$ instead of $|\alpha|^2$ frequently to celebrate the memory of nice original literature in the strong-field regime in previous years.

Factorization approximation: "The main idea is to consider the evolution of specially chosen states of the system *atom plus field*. The field has to be initially in a coherent state with a large number of photons. While, the atomic sub-system is chosen is the *semi-classical eigen states* (that is the atomic eigen states in the corresponding classical field). Given such an initial states, the joint system wave function will be approximately factorized for a wide range time. [93] The evolution of an

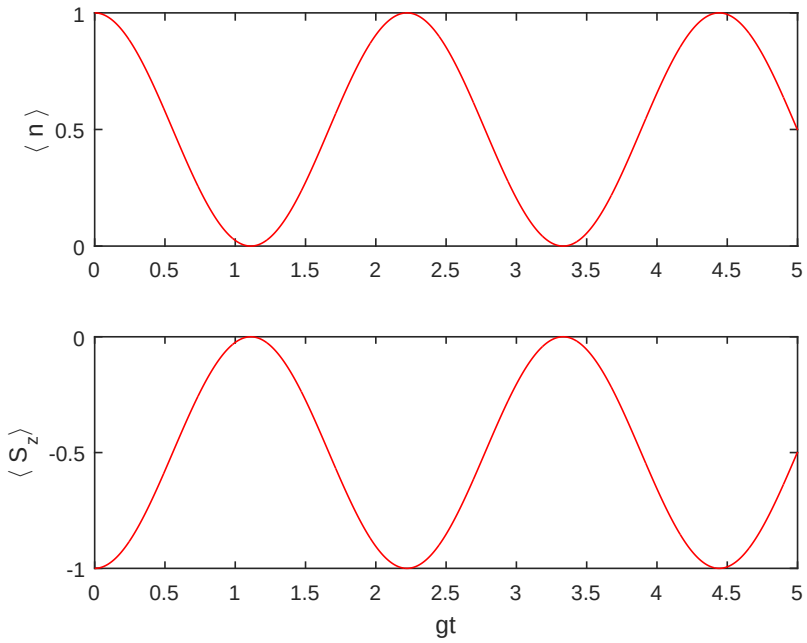

Figure 4.6: The Rabi oscillations of the photonic population $\langle n \rangle = \langle a^\dagger a \rangle$ (upper) and population inversion $\langle S_z \rangle$ (lower) vs. time gt for $N = 2$ and a single initial Fock state of the field.

arbitrary initial atomic state can be described by a superposition of the factorized states. ”

In the following, we give a brief review on what and whereas of this approximation. A short proof of the factorization approximation is given in the Appendix E..

Let us begin with the definition of semi-classical atomic states for the Dicke model. In the *classical field limit* the field operators becomes complex C-numbers,

$$a \to \alpha \equiv \sqrt{\bar{n}} e^{i\phi_f}, \quad a^\dagger \longrightarrow \alpha^* \tag{4.2.13}$$

and the interaction Hamiltonian (4.1.1) becomes proportional to the operator

$$H_{cl}(\phi_f) = (S_+ e^{i\phi_f} + S_- e^{i\phi_f}), \tag{4.2.14}$$

which represent the corresponding semi-classical Hamiltonian of interaction on N two level atoms with an external classical field. In general, the phase ϕ_f is chosen in such a way that coincides with the phase of initial classical field. The semi-classical atomic states are defined as eigen-states of $H_{cl}(\phi_f)$,

$$\begin{aligned} H_{cl}|N/2, m_x(\phi_f)\rangle &= 2m_x|N/2, m_x(\phi_f)\rangle, \\ |N/2, m_x(\phi_f)\rangle &= \exp(i\phi_f S_z)\,|N/2, m_x\rangle. \end{aligned} \tag{4.2.15}$$

The semi-classical states with $\phi_f = 0$ is defined as,

$$S_x\,|N/2, m_x\rangle = m_x\,|N/2, m_x\rangle. \tag{4.2.16}$$

with $-N/2 \leq m_x \leq N/2$. For a system of N two-level atoms, there are $N+1$ semi-classical Dicke states corresponding to $N+1$ eigen-states of S_x. They form a complete basis in space of all symmetrical atomic states.

Now, we assume that the initial field is taken to be in a strong coherent state $|\alpha\rangle$ while the atomic sub-system is initially chosen to be in a semi-classical state. Then, it is possible to prove (see Appendix E.) that the total wave function of the system can be approximately written as a product of its field and atomic parts

$$|\psi(t)\rangle \cong |A_{mx}(t)\rangle \otimes |\Phi_{mx}(t)\rangle. \tag{4.2.17}$$

in such a way that

$$\begin{aligned} |A_{mx}(t)\rangle &= \exp\left(-i\tau(S_z + N/2)\right)|N/2, m_x\rangle\,, \\ |\Phi_{mx}(t)\rangle &= \exp\left(-2im_x gt\sqrt{n - N/2 + 1/2}\right)|\alpha\rangle\,, \end{aligned} \tag{4.2.18}$$

with, $\tau = \frac{gm_x}{\sqrt{\bar{n}-N/2+1/2}}t$.

The factorization approximation is valid for times which are short compared to $t \approx \bar{n}/g$ with a accuracy of order $O(N/\bar{n})$ [94]. In the Appendix E. we have given a

simple proof for this approximation. There is also a more general way of proving the factorization approximation employing the perturbation theory. Interested reader may refer to the Ref. [93].

In order to generalize the approximation to any arbitrary atomic state, we consider the fact that semi-classical states form a complete basis in atomic sub-system. Thus, any initial state of the atomic system can be expanded in terms of semi-classical basis such that

$$|\psi(0)\rangle_a = \sum_{m_x=-N/2}^{N/2} d_{mx}|N/2, m_x\rangle. \tag{4.2.19}$$

Therefore, any arbitrary state of the joint system given by

$$|\psi(0)\rangle = \sum_{m=-N/2}^{N/2} d_{mx}|N/2, m_x\rangle \otimes |\alpha\rangle \tag{4.2.20}$$

Correspondingly, the state of the joint system can be written as a superposition of factorized states at any time t,

$$|\psi(t)\rangle = \sum_{mx=-N/2}^{N/2} d_{mx}|A_{mx}(t)\rangle \otimes |\Phi_{mx}(t)\rangle. \tag{4.2.21}$$

At this point, it is time to make use of factorization approximation explained, in advance. In order to get the analytical expressions for the quantum Fisher information flag χ^2, we consider the specific basis of the three symmetric eigenstates of S_x, which we label by $m_x = -1, 0$, and 1; the singlet state, $S = 0$, is a dark state and thus does not couple to the field. Writing the state of the system as

$$|\psi(0)\rangle = \sum_{mx=-1}^{1} d_{mx}\,|1, m_x\rangle \otimes |\alpha\rangle\,, \tag{4.2.22}$$

and using the factorization approximation, we find that the state of the system up to times up to the order of $\bar{n}/g$ is given by

$$|\psi(t)\rangle = \sum_{mx=-1}^{1} d_{mx} \, |A_{mx}(t)\rangle \otimes |\Phi_{mx}(t)\rangle \tag{4.2.23}$$

where $|A_m(t)\rangle$ and $|\psi_m(t)\rangle$ are the time-evolved atomic and field states, given in equations (4.2.18). Consequently, the reduced density matrix of the two atoms is obtained after tracing out the field degrees of freedom

$$\rho_a(t) = \sum_{mx,lx} d_{mx} d_{lx}^{*} \, |A_{mx}(t)\rangle \, \langle A_{lx}(t)| \, f_{ml}(gt, \bar{n}), \tag{4.2.24}$$

where, $f_{ml}(gt, \bar{n}) = \sum_n \langle n|\Phi_{mx}(t)\rangle\langle\Phi_{lx}(t)|n\rangle$. As explained in Ref. [67], this function has a memory for time scales less than $\sqrt{\bar{n}}/g$ and afterward shows a delta-function behavior. In fact, the presence of large dimensional Hilbert space of the field resembles as a broadband reservoir for the atoms. This Markov approximation is valid up to times on the order $2\pi\sqrt{\bar{n}}/g$, corresponding to the well-known revival time in the Jaynes-Cummings Model [19]. Making this approximation in equation (4.2.24), the atomic states $|A_m(t)\rangle$ act effectively as a "pointer basis" for decoherence of the atomic density matrix. Consequently, one gets the following effective density matrix of atoms [67] in the semi-classical basis as

$$\rho_a(t) = \sum_{mx} |d_{mx}|^2 \, |A_{mx}(t)\rangle \, \langle A_{mx}(t)| \, . \tag{4.2.25}$$

The current case of $N = 2$ with initial state of the both atoms in the ground state $|gg\rangle$ corresponds to

$$d_1 = d_{-1} = \frac{1}{2}, \; d_0 = \frac{1}{\sqrt{2}}, \tag{4.2.26}$$

which gives the following reduced atomic density matrix in the strong field regime

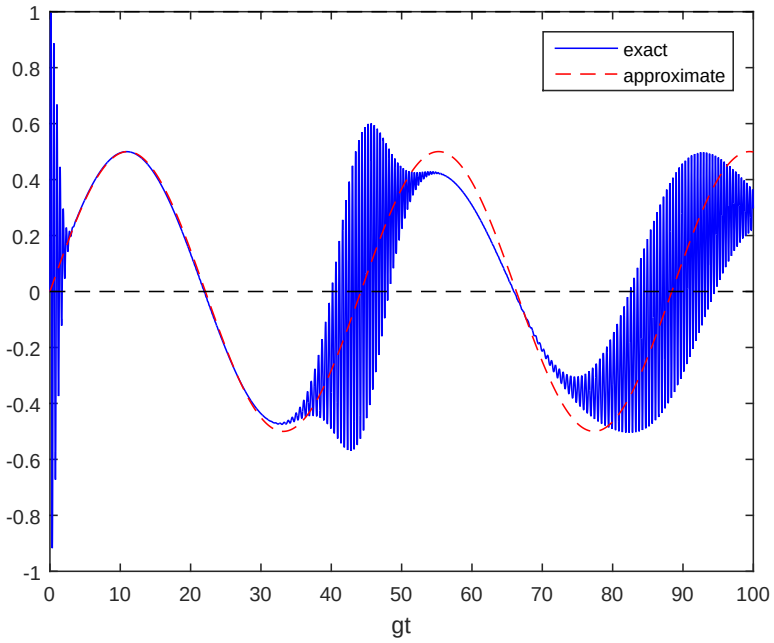

Figure 4.7: The time evolutions of χ^2 and $\sin(2t')/2$ versus time gt in the strong field regime of $|\alpha|^2 = 50$ for $N = 2$ particles.

in the original bare states $|1, M\rangle$ as

$$\rho_a(t) = \begin{pmatrix} \frac{3}{8} & -\frac{i}{4\sqrt{2}}\sin(2t') & \frac{\cos(4t')}{8} - \frac{1}{4} \\ \frac{i}{4\sqrt{2}}\sin(2t') & \frac{2}{8} & -\frac{i}{4\sqrt{2}}\sin(2t') \\ \frac{\cos(4t')}{8} - \frac{1}{4} & \frac{i}{4\sqrt{2}}\sin(2t') & \frac{3}{8} \end{pmatrix}, \tag{4.2.27}$$

with, $t' = \frac{g}{2\sqrt{\bar{n}-1/2}}t$. Note that the reduced density matrix in the semi-classical basis equation (4.2.25) is in a factorized form. Consequently, the density matrix in the original Dicke bare state is not diagonal in general.

Making use of atomic density matrix given in (4.2.27), we obtain the the collective mean spin values as

$$\begin{aligned} \langle S_x(t)\rangle &= 0, \\ \langle S_y(t)\rangle &= \frac{\sin(2t')}{2}, \\ \langle S_z(t)\rangle &= 0. \end{aligned} \tag{4.2.28}$$

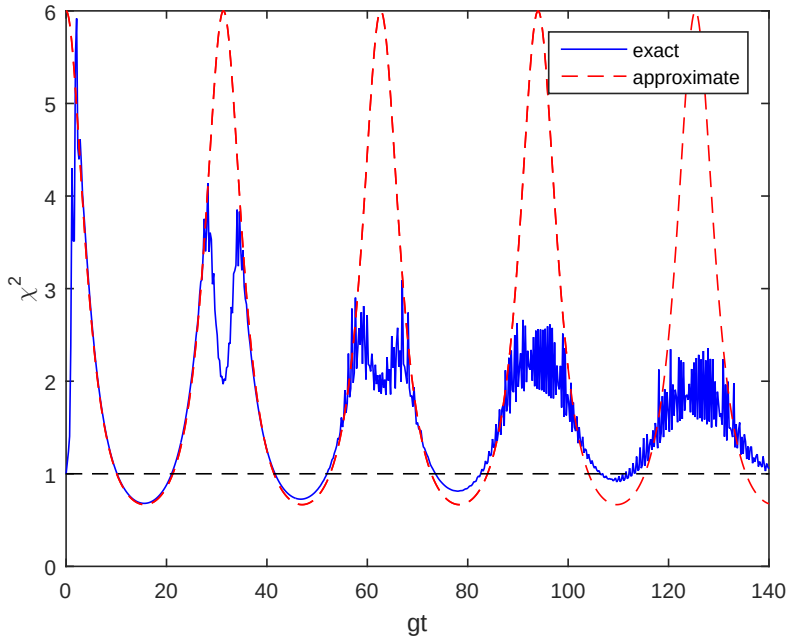

Figure 4.8: The quantum Fisher information flag χ^2 versus gt for initial coherent state $|\alpha|^2 = 100$ interacting with $N = 2$ atom.

and the corresponding variances,

$$\begin{aligned} \Delta S_x^2 &= \frac{\cos(4t')}{8} + \frac{3}{8}, \\ \Delta S_y^2 &= \frac{3}{4}, \\ \Delta S_z^2 &= \frac{3}{4}. \end{aligned} \tag{4.2.29}$$

Note that the average value of S_z is zero since we have used the Markov approximation which is valid as long as $t < 2\pi\sqrt{\bar{n}}/g$. On the other hand, revival time is given by $2\pi\sqrt{\bar{n}}/g$. Therefore, revival does not appears in population inversion, $\langle S_z(t)\rangle$. Nevertheless, we show that even under this approximation, the final expression for χ^2 are in very good agreement with exact numerical solutions. From the equations (4.2.28) it is clear that the mean spin direction $\langle S\rangle \approx \langle S_y\rangle$ has a periodic behavior along y direction with the period $gT = 2\pi\sqrt{\bar{n} - 1/2}$ and always $-1/2 \leq |\langle S\rangle| \leq 1/2$. This periodic behavior is given in Figure 4.7 for both of the numerical and approximate expression in equations (4.2.28). Since the atomic state oscillations are always

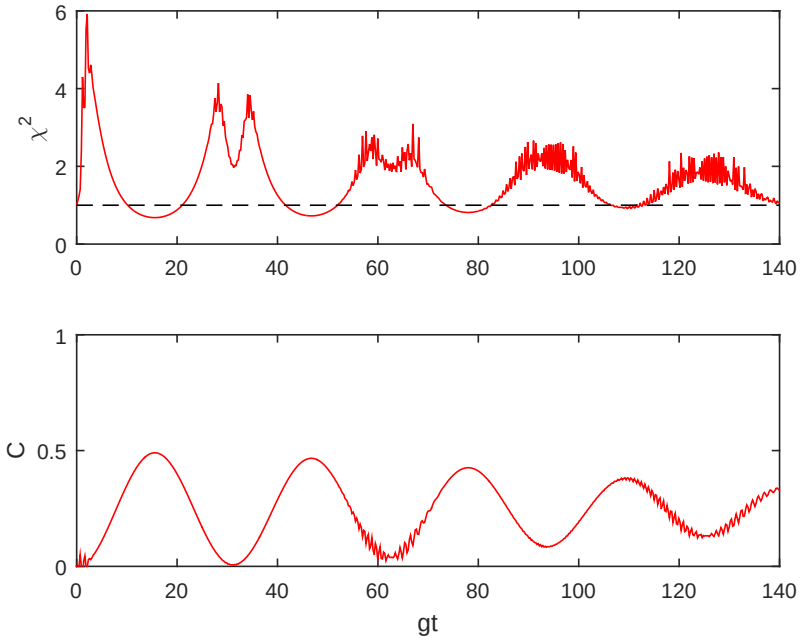

Figure 4.9: Quantum Fisher information flag χ^2 (upper) and concurrence vs. time gt for for initial coherent state $|\alpha|^2 = 100$ interacting with $N = 2$ atom

inside Bloch sphere, the atomic state is always mixed [2]. The natural by-product of this result is that we expect the atomic-field entanglement in the system in the strong-field regime [67].

In order to derive F_Q, we have to use the general definition of F_Q given in equation (3.2.39) for all mixed states. Note that in the weak-field limit we used the simplified form of equation (4.2.4) since the atomic state remains pure during the time evolution. Here, by diagonalization of the 3×3 density matrix equation (4.2.27) following by using equations (3.2.39) and (3.2.51), one gets the analytical expression for the quantum Fisher information flag χ^2. We have not brought the final form of quantum Fisher information due to the lengthiness. Instead, the ultimate result is plotted in the Figure 4.8 as a function of gt. We have also plotted the numerical exact solutions in the same plot. There exist a good agreement between the two solutions in the validity region of approximation. The period of the entanglement function χ^2 is $gT = \pi\sqrt{\bar{n} - 1/2} \approx \pi\sqrt{\bar{n}}$ and the first minimum happens at $t_{min} = \frac{T}{2}$.

From the Figure 4.8 it can be seen that after a number of periods, the entanglement decays as χ^2 is nearly more than unity. This is the typical behavior similar to what happens in the limit of large coherence field in other systems, e.g. squeezing

[2] This can also be verified with $Tr\rho_a^2 < 1$ with using the atomic density matrix (4.2.27).

of quadratures of the field [95]. The decay of entanglement is correlated with the loss of regularities in the behavior of atomic inversion. In fact, as time passes the neighboring revivals begin to spread and finally overlap.

It is also interesting to compare the pair-wise entanglement with the multi-particle entanglement detected by χ^2. In the Figure 4.9 we have plotted the χ^2 (upper) and C (lower) versus time gt. There is a good agreement between the times in which the maximum entanglement occurs by both measures. However, due to basically different nature of entanglement detected by QFI and C, they are not giving the exactly same result.

On the other hand, from the spin squeezing point of view, it is already explained that the spin squeezing vanishes at strong field regime [91]. But is it possible to find the reason that QFI detects the entanglement while no spin squeezing appears? The reason comes in the following. In fact, the definition of spin squeezing given in equation (3.2.12) depends on both mean spin direction and normal spin variances (equation 3.2.12). As we mentioned before, the mean spin length is $|\langle S\rangle| \approx |\langle S_y\rangle| \leq 1/2$ (equations 4.2.3). On the other hand, from equations (4.2.29) it is easy to find the minimum normal variance equal to $\Delta S_x^2 = 1/4$. Therefore, the spin squeezing definition of equation (3.2.12) gives

$$\xi^2 = 2 > 1. \tag{4.2.30}$$

Consequently, the spin squeezing in the limit of strong field strength vanishes. This is also possible to verify this result [91] using the Mollow transformations. In this way, one shall consider the Hamiltonian as a classical field with amplitude α plus a fluctuation field. Creating spin squeezing depends on the ratio of the fluctuations to the average spin strength and decreases with increasing α provided the average number of photons in the field is much larger than N (in this case $N = 2$).

In Figure 4.10 we have used the exact numerical results to plot χ^2 dependent on the strength of the field $|\alpha|^2$. in fact, with increasing $|\alpha|^2$ the minimum of χ^2 decreases, but eventually approaches to an asymptotic value. This limit is what we may get easily from factorization approximation mentioned above. To this end, we consider the fact that the upper bound of QFI is equal to $4\Delta S_z^2$. Making use of equations (4.2.3) and (3.2.51), we get the ultimate bound of $\chi^2 = 0.67$.

Finally, let us put emphasis on the fact that using the classical field does not create

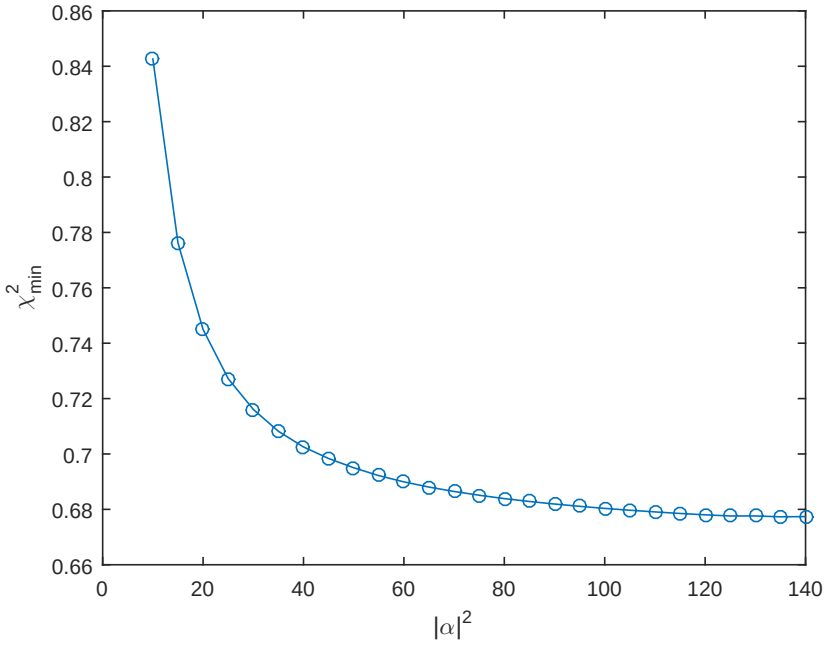

Figure 4.10: Quantum Fisher information flag χ^2 versus initial coherent state $|\alpha|^2 \gg 10$ (strong field limit) interacting with $N = 2$.

entanglement between the particles as one expects. The reason is that in the limit of very large field $\bar{n} \to \infty$, the minimum entanglement happens at very long times $t_{min} \to \infty$ which does not make any physical sense. Moreover, when $\bar{n} \to \infty$ the field operators becomes complex C-numbers (equations 4.2.13). Correspondingly, the interaction Hamiltonian given by equation (4.2.14) which is the semi-classical Hamiltonian of interaction on N two level atoms with an external classical field. Since this Hamiltonian is proportional to S_x which is of course not the type of Hamiltonian capable of creating multi-particle entanglement. As a matter of fact, in order to create entanglement one need to one or two axis twisted Hamiltonian, which contains normally a non-linearity $\propto S^2$ [71]. The semi-classical Hamiltonian however is simply the product of spin operators.

Other initial states and the collapse and revivals of entanglement

In this section we explore the entanglement dynamics of the atomic system in strong field regime for two more initial states. In fact, the unentangled initial state which considered previously is interesting since one can study the *creation* of multi-particle entanglement. On the other hand, considering *initial entangled states* is appealing as provides the possibility to see other properties in dynamics of entanglement. In

particular, by choosing specific initial entangled states of atomic system, we can see the collapse and revival of entanglement i. e. initial entanglement can vanish and return at a later time [68]. The manner that this collapse and revival of entanglement happens depends on the initial entangled state of the atomic system. In the following, we take the initial atomic states linked to these effects and compare the result of QFI flag χ^2 with concurrence C. We would like to see whether the QFI detects such collapse and revival in the dynamics of entanglement?

Example I.

Let us take the initial state of the atomic sub-system as,

$$|\psi(0)\rangle_a = |gg\rangle + |ee\rangle. \tag{4.2.31}$$

This atomic state has been used to study the collapse and revival of entanglement [68]. In the strong-field regime, it has been proved that for a set of initial conditions, the reduced density matrix of the atomic sub-system approaches to that of a pure state at specific times. Since the pure state approach is the same for *a set of initial states* they are called attractors. The set itself is termed basin of attraction. In the same Ref. it has been studied that for the initial atomic states inside the basin of attraction the collapse and revival of entanglement occurs. For the case of $N = 2$ particles the authors have used the tangle as a measure of entanglement. In the Figure 4.11 we have plotted the collapse and revival of entanglement when the qubits started in the maximally entangled state of (4.2.31) for $N = 2$ and $\bar{n} = 100$ using QFI flag χ^2 and concurrence C. It shows that the entanglement in the qubits is initially lost then returns at the first revival peak, $gt = T/2 = 2\pi\sqrt{\bar{n}} = 31.41$. By the way, one has to bear in mind that the QFI flag and concurrence are intrinsically different detectors of the entanglement between particles.

Regarding spin squeezing, the same as the previous case, it is not detecting entanglement in the system as we are in the strong-field regime. In figure 4.12 we give ξ^2 as well as χ^2 versus time gt. In the lower case, it is possible to see that the spin squeezing is divergent exactly at the same points that entanglement detects by χ^2. As discussed previously, we attribute this behavior to the decreasing of the mean spin length.

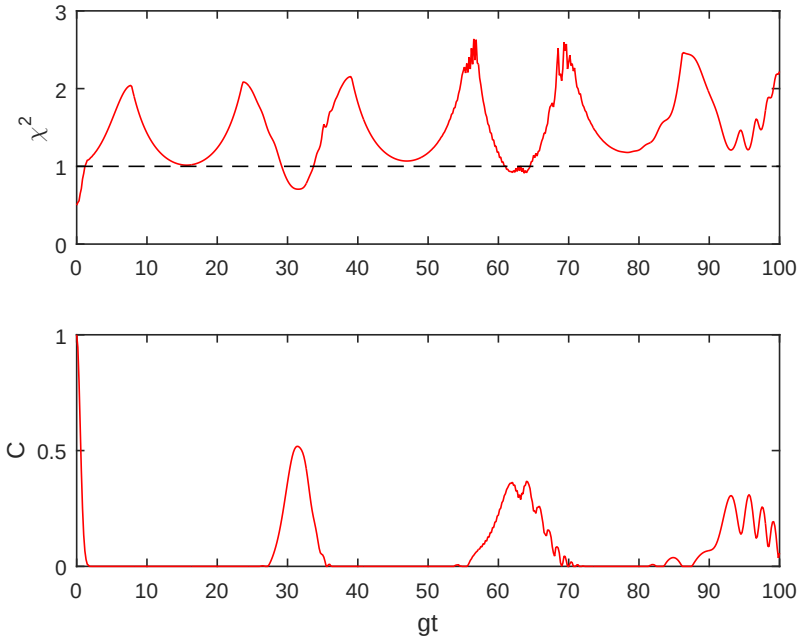

Figure 4.11: Time evolution of (upper) quantum Fisher information flag χ^2 and (lower) concurrence C versus time gt for the initial Bell state $|\psi(0)\rangle_a = |gg\rangle + |ee\rangle$ with $\bar{n} = 100$. The collapse/revival of entanglement is detected by both measures.

Example II.

As another example, we take the initial state as follows

$$|\psi(0)\rangle_a = \sqrt{\frac{19}{20}}|gg\rangle + \sqrt{\frac{1}{20}}|ee\rangle. \tag{4.2.32}$$

This specific initial state is proved to exhibit the sudden death of engagement [67]. In order to distinguish between the case of sudden death and collapse/revival entanglement we use the same terminology as used in Ref. [68]. i. e. the collapse and revival of entanglement appeaser and vanishes with a finite gradient. It has been shown this state is in a family of initial states outside of the basin of attractor may show this behavior provided that they fulfill specific conditions [68]. Unlike the initial entangled state discussed before, for some initial states the concurrence suddenly vanishes with a divergent derivative in concurrence as the eigen-values in equation 3.2.2 get negative and therefore gives the maximum of zero. This is different from what occurs in the previous case in which the entanglement vanishes (revives) gradually with a

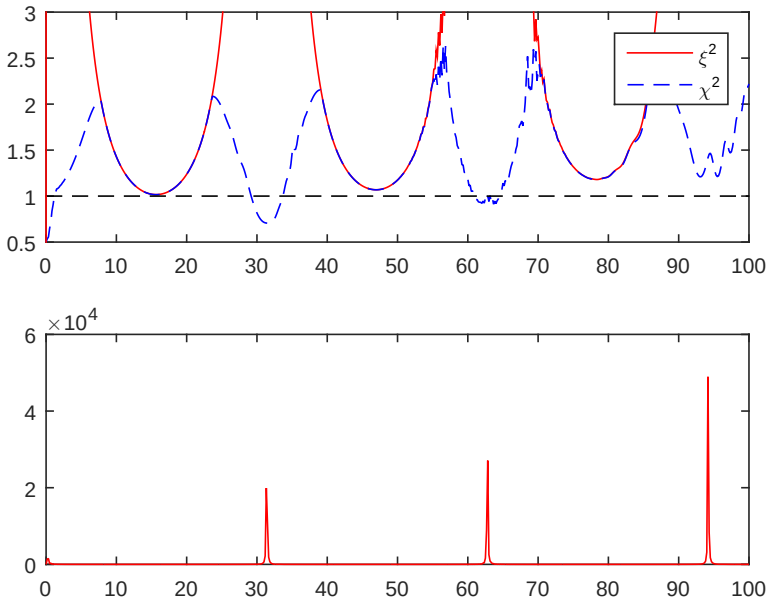

Figure 4.12: ((upper) The spin squeezing and quantum Fisher information flag χ^2 as well as (lower) spin squeezing divergence versus time gt for the initial Bell state. The collapse/revival of entanglement is detected by χ^2 while there is divergences at the same point in spin squeezing.

finite derivative in concurrence. These features are clear comparing the upper parts of Figures 4.11 and 4.13. Moreover, we have also given χ^2 as a function of time gt. The peaks of χ^2 and C are partially in agreement. Nevertheless, as the time passes, the QFI flag does not detect quantum entanglement. The same as the previous case, we attribute this to the fact that QFI detects a more restricted family of entangled states. Compared to the previous case, there is also different times of emergence of peaks of entanglement. In the current case, for both measures the dominant peaks of entanglement occur at $gt = gT/4 = 15.71$ and $gt = 3gT/4 = 47.12$ which is in agreement with Ref. [68] making use of tangle as an entanglement measure. By the way, The smaller peaks in half way of dominant peaks are not detected by χ^2. Moreover, alike other cases after some initial peaks the QFI flag vanishes. At last, one has to notice that while QFI detects entanglement for both cases of collapse/revival and sudden birth/death, it is no strong enough to distinguish between them as concurrence does. By the way, the interesting point about entanglement detected by QFI flag is that it is useful for estimation purposes.

In Figure 4.14 we present the spin squeezing ξ^2 and χ^2 versus time gt. Alike the previous example, in the entanglement points there is not divergence in the manner

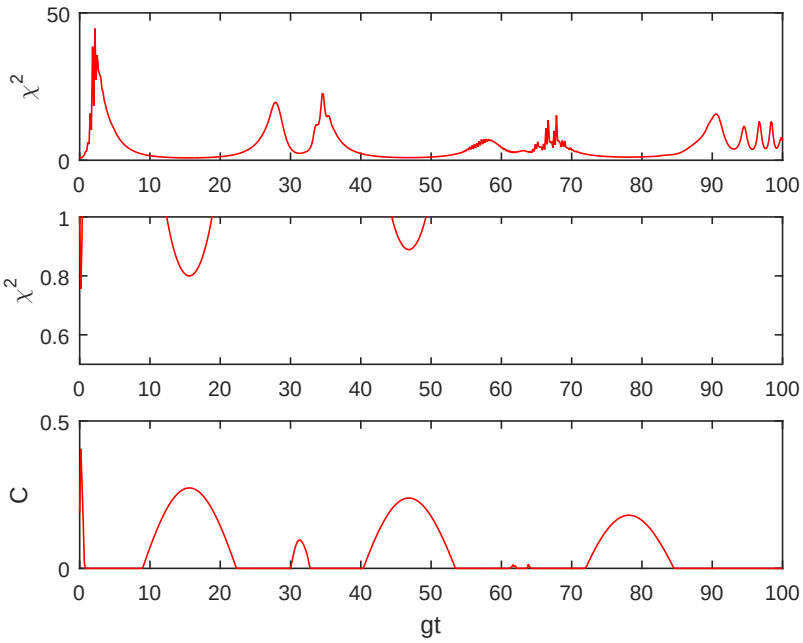

Figure 4.13: (The quantum Fisher information flag χ^2 (upper and middle) and concurrence (lower) versus time gt for a specific initial state $|\psi(0)\rangle_a = \sqrt{\frac{19}{20}}|gg\rangle + \sqrt{\frac{1}{20}}|ee\rangle$. The sudden death of entanglement is detected by both χ^2 and C.

of spin squeezing. By the way, the ratio of variances to the mean spin length is not still sufficient enough to detect the entanglement between particles.

4.3 Conclusion

In this section, we have studied the dynamics of entanglement for the case of interaction of two atoms with single mode of the field. Based on the strength of the initial coherent field, we have defined three regimes of weak, intermediate and strong field interaction. It was shown that the spin squeezing and QFI flag detect the same regular pattern of entanglement for the initial weak field. the minimum amount of entanglement in this case, occurs in the short time $gt_{min} = 4\pi\sqrt{N} = 4\pi\sqrt{2}$.

In the intermediate regime, the detection of entanglement increases by increasing the incident field strength and decreases after a local peak. In the intermediate regime the optimal amount of QFI and spin squeezing occur in longer times than that of the weak regime. In Figure. 4.15 we have given the times in which the minimum of the χ^2 occurs based on a cut-off time fixed on $gt_{cut-off} = 200$. It is clear that

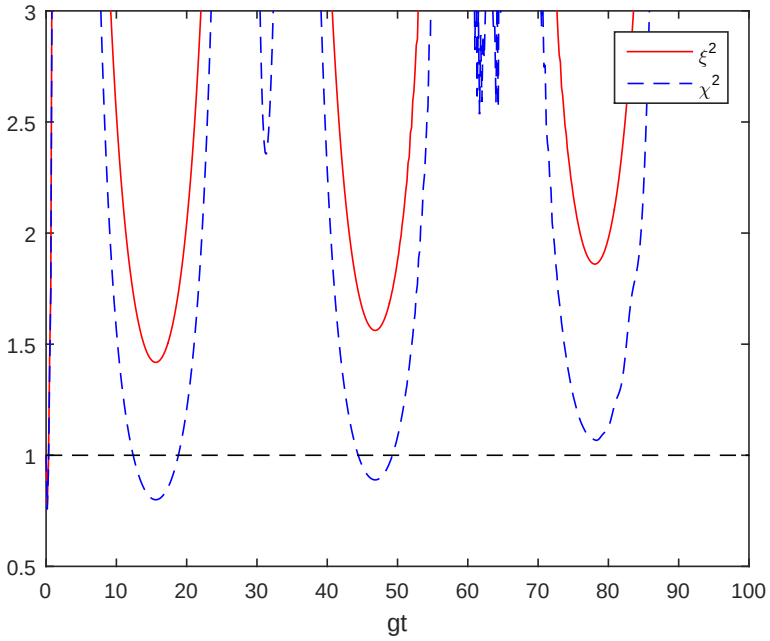

Figure 4.14: (upper) The spin squeezing ξ^2 (solid red) and quantum Fisher information flag χ^2 (dashed blue) versus time gt for the same initial given in Figure 4.13. The sudden death of entanglement is detected by χ^2 but not with ξ^2.

with increasing the coherent field strength the χ^2_{min} is growing while it is found in larger time scales even very close to cut-off time, say 200. Moreover, χ^2 detects much more entanglement in the atomic system for mediate coherent fields as one would expect ($\xi^2_{\min} \leq \chi^2_{min}$). Nevertheless, the qualitative behaviors of the spin squeezing and QFI flag is similar. Neither χ^2 nor ξ^2 have a regular pattern in the intermediate field limit. Moreover, both measure detect the minimum entanglement over the time span when the field strength is $|\alpha|^2 < N = 2$.

Finally, in the strong field regime, the spin squeezing is shown to be decreased drastically while QFI still detects multi-particle entanglement in agreement with concurrence. The multi-particle entanglement in strong field regime is in the short times. For the strong enough fields, employing the factorization approximation, we have got $gt_{min} = \pi\sqrt{\bar{n}}/2$. Moreover, the χ^2 retains a regular pattern of dynamics. We have found an analytical form of χ^2 which is in good agreement with the numerical simulations. For the case of very strong fields, the field is classical and there is no quantum entanglement in the atomic system as expected. Beside using the initial pure atomic state, we have shown that using appropriate initial states of the atomic system, QFI flag also detects the collapse/revival and sudden death of the (useful) entanglement.

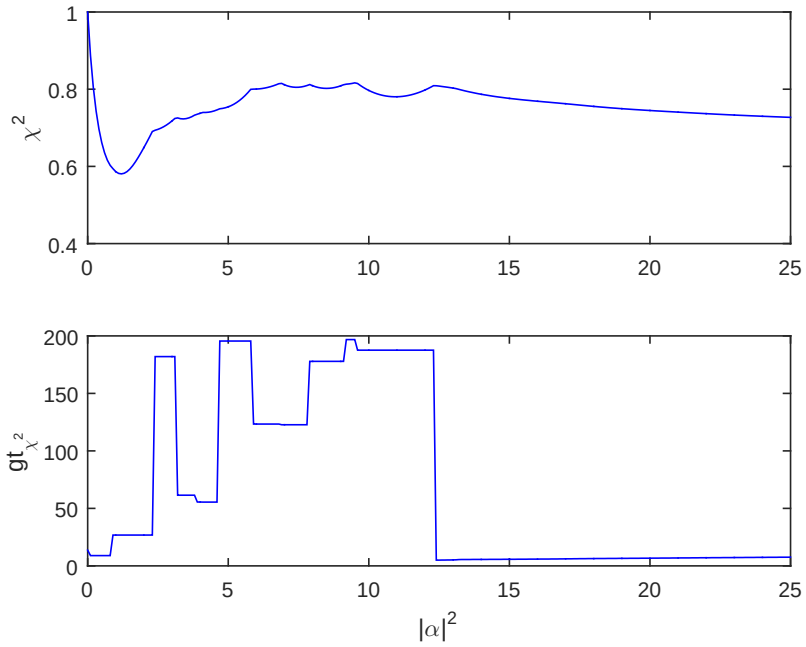

Figure 4.15: (upper) The quantum Fisher information flag χ^2 (lower) time of occurrence of optimal χ^2 versus $|\alpha|^2$. Three regimes of interaction are distinguishable from the time in which minimum over time span occurs. To get this plot, we have put a cut-off on time span at $gt_{cutoff} = 200$. In the weak and strong field regime the optimal χ^2 occurs in short time while in the intermediate regime is in the long time.

Chapter 5

Entanglement detection via Quantum Fisher Information in the system of Dicke Model II

"Everything has beauty, but not everyone sees it."
Confucius

In this section, we will extend the previous case of $N = 2$ atoms to finite number of atoms in order to explore the multi-particle entanglement dynamics. The dynamics of entanglement between small ensemble of particles is interesting from many different points of view including quantum information [96] and Heisenberg limit spectroscopy [97]. Nevertheless, there are many various types of non-equivalent entanglements in a multi-particle system. Correspondingly, for every kind of entanglement in the system there exist different measures of entanglement. The point is that for the case of having more than two particles in the system a universal witness does not exist. Considering this case, as we have seen the good agreements between concurrence and quantum Fisher information predictions, it is a natural step forward to generalize using QFI as a measure of multi-particle entanglement. Thus in the rest of this work, we investigate the entanglement dynamics focusing on quantum Fisher information measure.

5.1 Interaction of N atoms with the field

In the following, we consider the dynamics of entanglement for the Dicke model (section 2.1) of interaction between finite numbers of qubits and a single mode of cavity. In the following, we consider in the same three regimes of interaction; namely, weak field, intermediate and strong field regimes as done in the previous chapter.

Initial state

For a system composed of N two-level atoms interacting with a single mode of the cavity, we consider the initial state of all of the atoms in the ground state while the field is in coherent state (see section 4.1.1). Therefore, the initial state of the joint is the one given in equation (4.1.6)

$$|\psi(0)\rangle = \sum_{n=0}^{\infty} c_n |N/2, -N/2\rangle \otimes |n\rangle,$$

where c_n's indicate the initial state amplitudes of the coherent field of equation (4.1.3). The same as before, we have to solve the Schrödinger equation of motion for $|\psi(t)\rangle$ (4.1.7) which leads to the time-dependent amplitudes $C_{M,n}(t)$ dependent on c_n's.

5.1.1 Weak-field limit

For the very small amplitude radiation field where $|\alpha|^2 \ll 1 < N$, the same as the case of $N = 2$, it is possible to get to the analytical expressions for the time dependent amplitudes $C_{M,n}(t)$. To this end, one has to expand the c_n's and then keep the terms up to the second order of α [91]. Making use of the corresponding amplitudes in the large N limit ($N \gg |\alpha|^2$), one get the average spin components as

$$\begin{aligned} \langle S_x(t)\rangle &= 0 \\ \langle S_y(t)\rangle &= \sqrt{N}\alpha \sin(\sqrt{N}gt), \\ \langle S_z(t)\rangle &= -\frac{N}{2} + \alpha^2 \sin^2(\sqrt{N}gt), \end{aligned} \tag{5.1.1}$$

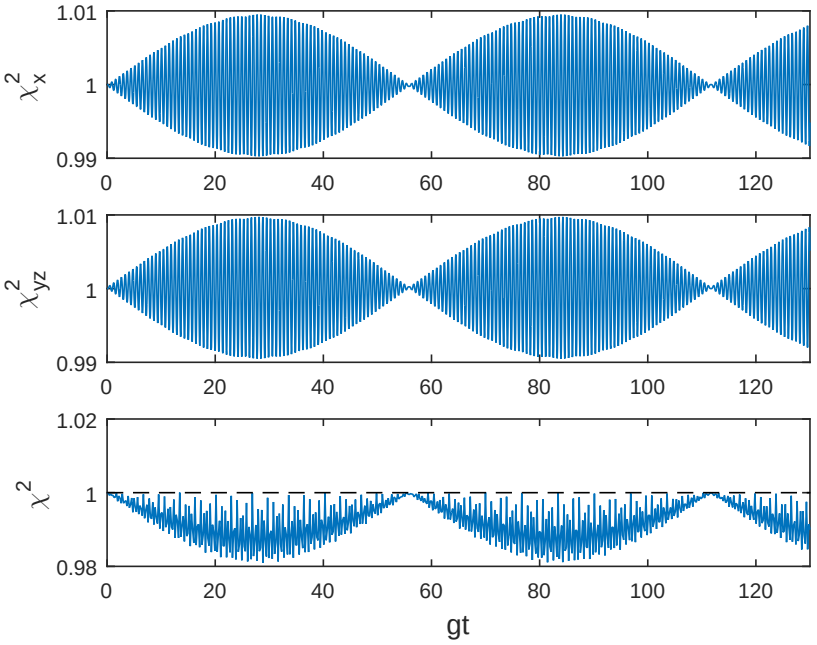

Figure 5.1: The time evolutions of χ^2 (ξ^2) in the weak field regime of $|\alpha|^2 = 0.01$ with $N = 20$ particles.

which gives $|\langle S\rangle| \approx N/2$. Thus, the same as the case of $N = 2$, the atomic state remains pure during the time evolution. in this case, we make use of the equations (4.2.4) for pure states to get the optimal quantum Fisher information flag as

$$\begin{aligned}\chi^2 = \xi^2 &= 1 + \alpha^2\{\frac{N-1}{N}\sin^2(\sqrt{N}gt) \\ &- \frac{2(N-1)}{2N-1}\sin^2(\sqrt{(2N-1)/2}gt)\},\end{aligned} \tag{5.1.2}$$

which simplifies to the following form when N is large,

$$\begin{aligned}\chi^2 &= \xi^2 \\ &\cong 1 + \alpha^2\sin[(2\sqrt{N} - \frac{1}{4\sqrt{N}})gt]\sin(\frac{gt}{4\sqrt{N}}).\end{aligned} \tag{5.1.3}$$

In the limit of $N = 2$ the equation (5.1.2) gives the same result as the equations (4.2.3). The same as before, it is possible to show that for the small initial coherent fields, we have the Gaussian atomic state. As a result, both of the QFI flag and spin

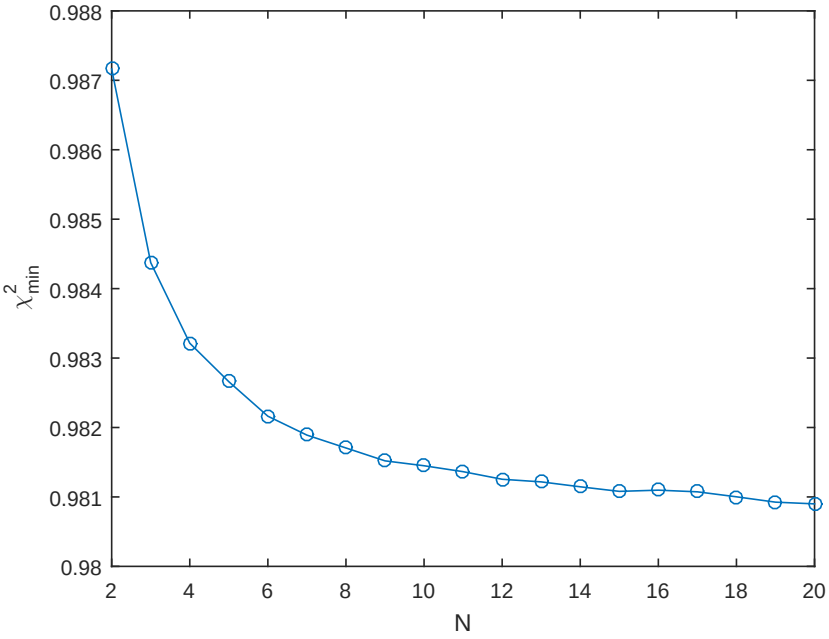

Figure 5.2: The minimum of quantum Fisher information flag χ^2_{min} versus number of particles N for the weak field regime of $|\alpha|^2 = 0.01$ particles. The minimum is calculated numerically up to $gt = 100$.

squeezing parameter still coincide $\chi^2 = \xi^2$. Regarding the optimal directions, the Quantum Fisher information is optimal in -xy plane while spin squeezing is optimal along along x.

Figure 5.1 gives the temporal behavior of the χ^2 for $N = 20$ and $|\alpha|^2 = 0.01$. One observes the numerical exact solutions coincide with the approximate analytical results which is given in equation (5.1.2). Similar to the two-atom case, there is a regular behavior in the dynamics of quantum Fisher information and spin squeezing. From the equation (5.1.3) we get the period of $4\pi\sqrt{N}$ for χ^2 (in the unit of g). This gives the predicted period for the case of $N = 2$, say $4\pi\sqrt{2}$. As before, we observe that there is always a small amount of entanglement in the system. For any finite N, there is a time

$$gt_{min} = 2\pi\sqrt{N} \tag{5.1.4}$$

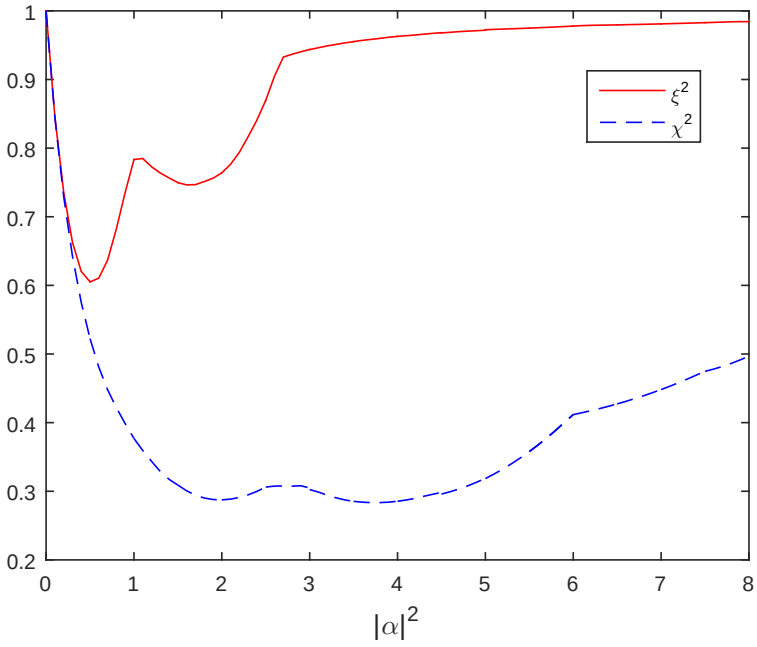

Figure 5.3: The minimum values of ξ^2 and χ^2 versus coherent field population $|\alpha|^2$for $N = 6$. In order to get this plot we have fixed a cut-off on time span at $gt_{cut-off} = 200$.

in which the the minimum of χ^2 occurs of the order of

$$\chi^2_{min} = \xi^2_{min} \sim 1 - \alpha^2. \tag{5.1.5}$$

In the Figure 5.2 we have plotted the minimum of χ^2 versus number of particles N up to $gt = 100$. We can see that with increasing N, the χ^2 decreases rapidly up to $N = 10$ and afterward keeps an asymptotic behavior. This behavior is in agreement with the spin squeezing results given in Ref. [91].

Figures 5.3 and 5.4 give the minimum of QFI flag as a function of $|\alpha|^2$ for $N = 6$ and 20 particles, respectively. Here we have fixed a cut-off on time at $gt_{cut-off} = 200$. For the weak field limit region, we observe the decrease of the χ^2 - which coincides with ξ^2 - with increasing the field strength $|\alpha|^2$. For the stronger fields, the quantum Fisher information flag χ^2 and spin squeezing parameter χ^2 show different behaviors. This is what we discuss in the following.

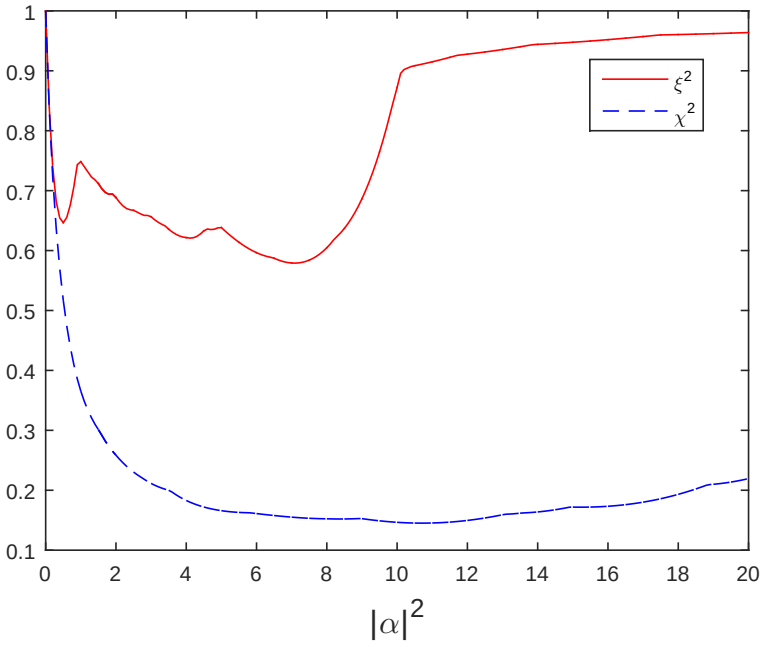

Figure 5.4: The minimum values of ξ^2 and χ^2 versus coherent field population $|\alpha|^2$for $N = 20$. In order to get this plot we have fixed a cut-off on time span at $gt_{cut-off} = 200$.

5.1.2 Intermediate-field limit

In the intermediate field limit in which $|\alpha|^2 \sim N$, It is not possible to derive the analytical solutions. Nevertheless, it is possible to solve the Schrödinger equation of motion numerically to get the dynamics of χ^2. Figures 5.3 and 5.4 present the spin squeezing and quantum Fisher information flag as a function of gt for $N = 6$ and 20 respectively. The points are the optimal values of the χ^2 and ξ^2 for a fixed cut-off on time at $gt = 200$. The same as before to get these plots, we have changed the amplitude of the coherent field $0 \leq |\alpha|^2 \leq N$, and have picked up the minimum of χ^2 and ξ^2 factors. We observe that moving from the weak to intermediate regime of interaction, the χ^2 and ξ^2 begin to give different results. This may be due to the fact that the atomic state is not a Gaussian state anymore. By the way, the overall trend for both entanglement measures - χ^2 and ξ^2 - is similar; that is they both initially decrease up to a minimum value and afterward gradually increase. our numerical results for up to 20 numbers of particles, indicate that the minimums of entanglement of the both measures almost always appear in the field intensities which are of the order of number of atoms N. By the way, for the case of quantum Fisher information the optimal field photon population specifically happens at quantity very close to

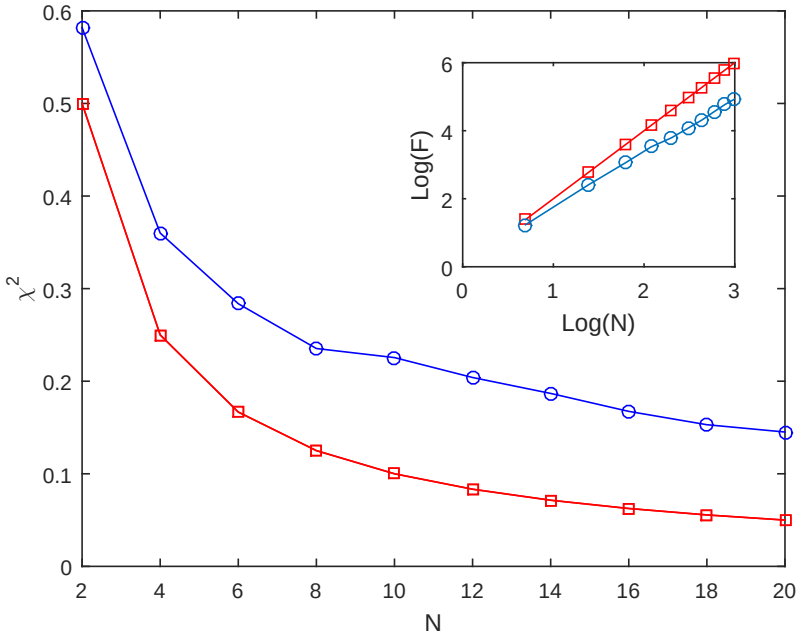

Figure 5.5: **Linearization of intermediate regime of interaction.** The minimum of χ^2 (circled-blue) and χ^2_{HL} (squared-red) versus N for optimal $|\alpha|^2$ during the time span within the cut-off fixed on $gt_{cut-off} = 200$. In the inset we have plotted the $\log F$ and $\log F_{HL}$ versus $\log N$.

the half population of the number of atoms, say $|\alpha|^2 \sim N/2$. On the other hand, we have seen that exactly in the same value spin squeezing decreases drastically. We would like to remind that the minimum values of spin squeezing and quantum Fisher information in Figures (5.3) and (5.4) are obtained considering a cut-off on the time. Therefore, these values are not necessarily the best possible factors if one considers the longer time. Nevertheless, it gives the sense of general trend. Moreover, we have to consider the fact that in principle the possible smaller values which occur at very long times are not interesting from the experimental point of view. Similar plots for the optimal spin squeezing have been reported in Ref. [91].

In Figure 5.5 we have given the optimal value of χ^2 corresponding to the optimal photon population $|\alpha|^2$ as a function of number of atoms in the Dicke system. One may observe that with increasing the number of atoms, the minimum value of χ^2 decreases. By the way, we never saturate the Heisenberg-limit of $1/N$ as it is clear in the Figure. The similar behavior has been reported for the spin squeezing in the presence of finite numbers of atoms in Tavis-Cumming model in Ref. [91]. In the inset the dependence of $\log(F)$ versus $\log(N)$ is given. We have linearized the optimal quantum Fisher information as a function of number of atoms in the system

N and derived the dependence of $F_{opt} = 1.14N^{1.60}$. The maximum quantum fisher information scales as $F_{\max} = N^2$.

Initial single Fock state of the field - W-state creation The same as the previous chapter, it is interesting to investigate the possibility of detection of useful entanglement in the system using a single initial Fock state of the field. The same as the experiment of Ref. [63] we consider the field is populated with a single Fock state interacting with $N = 3$ number of atoms in the ground state, $|ggg\rangle$. In this case, the absorption/emission of the single photon may be done with each single particle in the system. Therefore, the dynamics of the system would put the atomic system in the W-states such as $\Psi_w = 1/\sqrt{3}[|egg\rangle + |geg\rangle + |gge\rangle.]$. As the particles are identical, the lack of information about the internal states of the particle leads to quantum entanglement between particles. In Figure. 5.6, we have used χ^2 to detect the W-state of the system. we have given the χ^2 (upper) versus scaled time gt. Moreover, we have given the probability of the atomic state being in the W-state $P_w(t) = \langle\Psi_w|\rho_a(t)|\Psi_w\rangle$ in the lower part of the same Figure. In Ref. [63] authors have used the entanglement witness to detect the W-state based on the full tomography of the system. It seems that for the case of having more particles in the system quantum Fisher information flag is easier to measure than the entanglement witness.

5.1.3 Strong-field limit

Finally, let us consider the strong-field limit in which $|\alpha|^2 = \bar{n} \gg N > 2$. In this limit the full numerical simulation for the large number of particle is cumbersome due to the significant size of the Hilbert space. By the way, as we discussed in the section 4.2.3, thank to the factorization approximation, it is possible to get the analytical solution for the wave function of the Dicke system composed of N particle in the atomic system [1]. As a result, in principal one can get the collective spin mean values and finally calculate the quantum Fisher information. However, due to the dependence of QFI definition on the eigen-values and eigen-functions of the atomic density matrix, in order to get the χ^2 one first has to diagonalize a $N + 1 \times N + 1$ density matrix. This issue causes some difficulties when N is large. One possible short-cut way is to use the analytical wave-function of the equation

[1] This statement is true up to the validity region of the approximation discussed previously

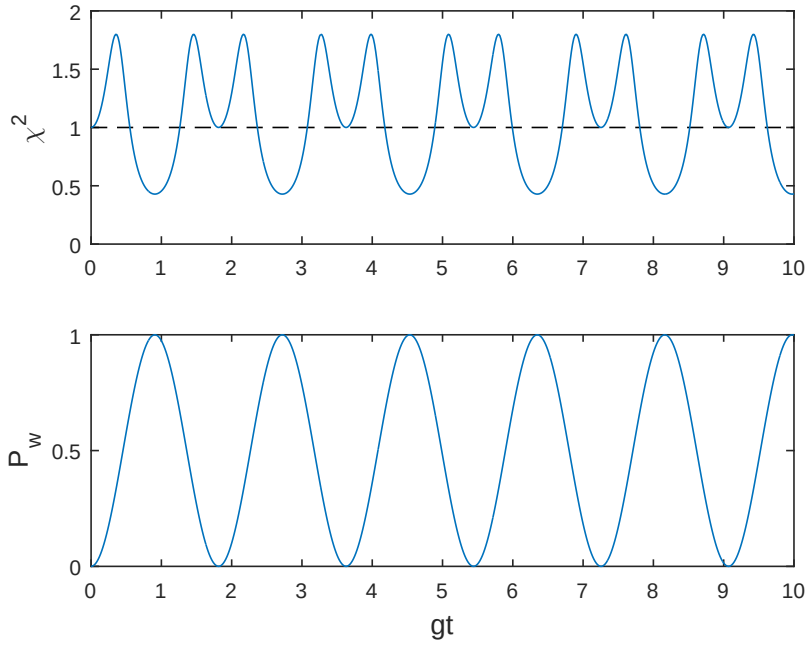

Figure 5.6: The quantum Fisher information flag χ^2 (upper) and the probability of turning the atomic state into w-state $P_w = \langle\Psi_w|\rho_a(t)|\Psi_w\rangle$ (lower) versus scaled time gt for initial single Fock state of the field and $N = 3$.

(4.2.18) and then tracing out the field degrees of freedom numerically. Following by numerically diagonalizing the atomic density matrix of the system and making use of the equations (3.2.39) and (3.2.51), the χ^2 is at hand. Using this *half-analytical* approach, we present the predictions of χ^2 in comparison to the exact full numerical solutions in figures 5.7 to 5.9 for $N = 4, 6, 8$ (for $N = 3, 5, 7$ see Appendix C.). In the validity region of the factorization and Markov approximations we observe a good agreement of analytical/exact predictions. It is interesting to note that in small ensembles of particles χ^2 regain a regular pattern of χ^2 and correspondingly entanglement dynamics when the initial field is strong enough [2]. Of course, there is no necessity to use the Markov approximation and doing the calculations without it might provide a wider range of coincidence between exact/numerical solution. We remind that due to the large size of Hilbert space, one has to balance between the possibility of applying both numerical and analytical approaches.

From the spin squeezing point of view, it is discussed in Ref. [91] that as long as $|\alpha|^2 > N$, with increasing $|\alpha|^2$ the the minimum value of the spin squeezing also increases. This could be due to the increasing the ratio of the collective spin fluctuations to the mean spin length. Consequently, in the strong field regime in

[2]Note that the field must still be a quantum entity not a classical one.

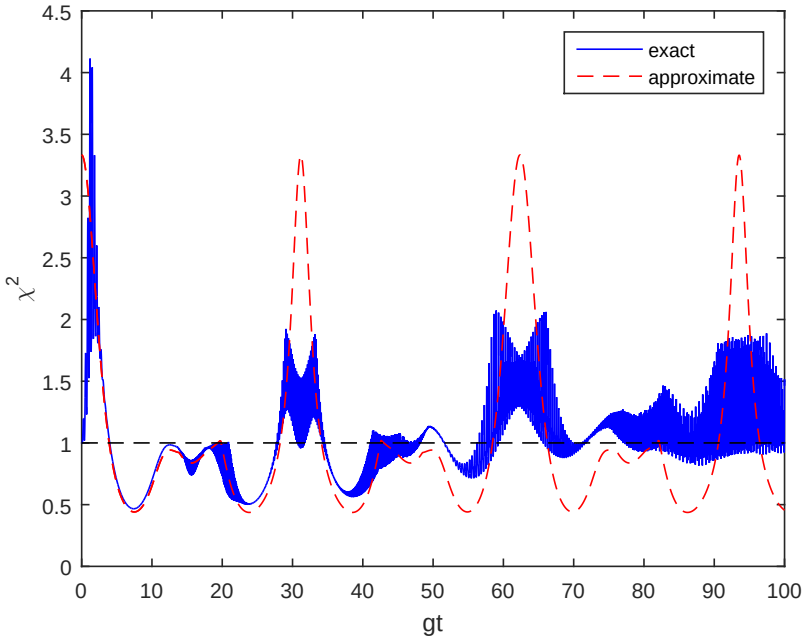

Figure 5.7: The quantum Fisher information χ^2 versus time gt for initial coherent field of population $|\alpha|^2 = 100$ for $N = 4$.

which $\bar{n} \gg N$ the spin squeezing approaches to unity. In the strong field limit, we have checked numerically the spin squeezing factor for the finite numbers of particles and our results are in agreement with the given in Ref. [91].

In Figure. 5.10 we have given the minimum value of quantum Fisher information flag χ^2 dependent on the number of atoms in the system up to $gt_{cut-off} = 200$. The number of atoms is taken up to $N = 20$ and the photonic population is fixed for $|\alpha|^2 = 100$ to satisfy the strong-field condition. One may observe that the amount of entanglement detected by χ^2 is increasing with increasing the number of atoms N. Nevertheless, as the number of atoms increase, the violation from maximum entanglement (HL) also grows. In inset of the same Figure 5.10 we have plotted $\log F$ versus $\log N$. We have found the linear fitting of maximum QFI dependent on numbers of particles as $F_{\max} = 0.98N^{1.59}$. which is considerable when we consider the maximum QFI of N^2 as Heisenberg-Limit. This linearization factor is very close to the value we have found in the intermediate field regime. By the way, the quite regular behavior of the χ^2 in the strong field regime compared to the irregular chaotic trend of intermediate field regime makes it more interesting from the experimental point of view.

It is worth to mention that the regular dynamics of the system of the Janes-

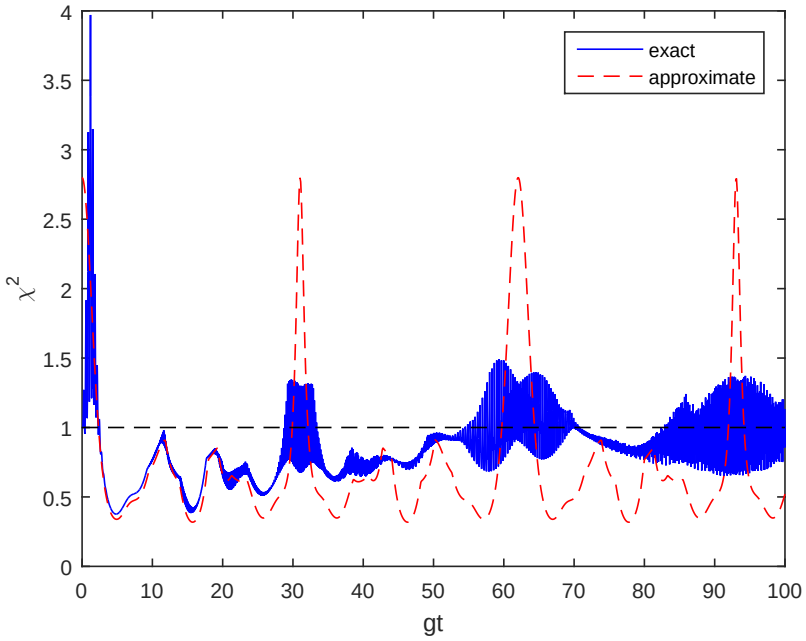

Figure 5.8: The quantum Fisher information χ^2 versus time gt for initial coherent field of population $|\alpha|^2 = 100$ for $N = 6$.

Cummings model - and its extension to the case of Tavis-Cumming model [95] - in the strong field regime has been studied for various parameters; probably the most known effect is the collapse and revival of the population inversion in the atomic system. The dynamics of entanglement in the strong field regime is intriguing when it comes collapse/revival of entanglement for example in the case of Schroödinger cat states studied in Ref. [68].

In Figure. 5.11 we have given the dependence of first minimum if χ^2 versus $|\alpha|^2$ for $N = 6$ particles and a cut-off on time at $t = 200$ (upper) and the corresponding time t_{min} (lower). Similar to the case of $N = 2$ atoms in the system, with increasing the photonic population the minimum value of χ^2 decreases. By the way, in the lower part of the same figure we observe that it is parallel to the increasing the respective time. Therefore, when $\bar{n} \to \infty$ the first minimum appear in vary long time. Therefore, in practice no entanglement appears. From the physical point of view, this is the range where the field is a classical entity not capable of creating entanglement among particle.

Finally, we would like to mention again that in the strong field regime, due to the large size of the Hilbert space, employing full numerical simulations is hardly possible

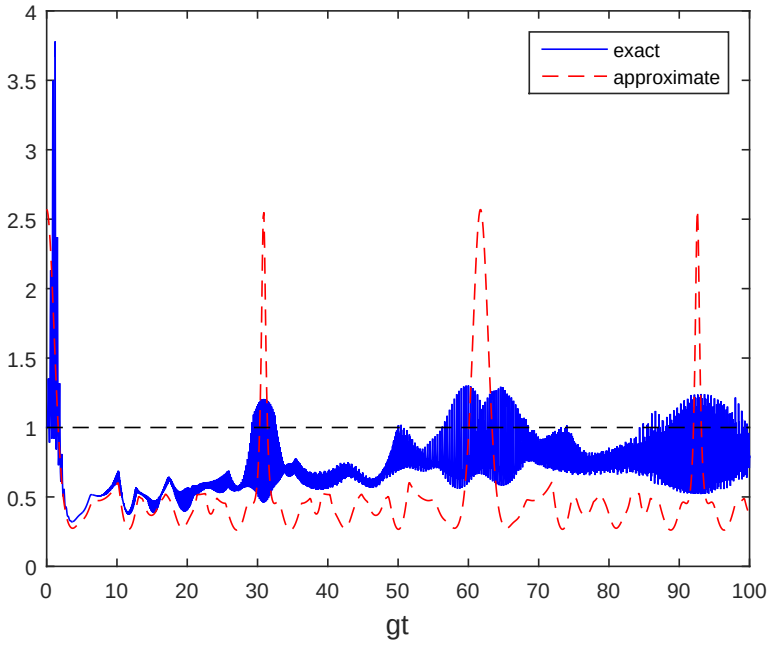

Figure 5.9: The quantum Fisher information χ^2 versus time gt for initial coherent field of population $|\alpha|^2 = 100$ for $N = 8$.

when N is very large[3]. On the other hand, since the numerical approach needs the diagonalization of the $N+1 \times N+1$ atomic density matrix, it is also not very useful in the limit of very large N's. In that case, we propose replacing the quantum Fisher information with its classical counterpart.

Collapse and revival of Schr odinger cat state As an example of usefulness of quantum Fisher information in the strong field regime let us use it in collapse and revival of entanglement discussed in Ref. [68]. In order to check our result with the ones given in the Ref. [68] we take $N = 3$. Moreover, the initial atomic state is a maximally entangled GHZ state and the field is in a coherent strong field state of $\bar{n} = 50$. Figure 5.12 gives the dynamical evolution of quantum Fisher information flag. We can see the revival peaks of χ^2 during scaled time gt. the revival peaks are in the exact agreement with the result of the Ref. [68]. This is despite the fact that in the mentioned reference authors have used different criteria for entanglement dynamics, namely entropy of qubits. We have also checked the results for the case of having more than $N = 3$ atoms and have seen the similar peaks.

[3]Note that $\bar{n} \gg N$.

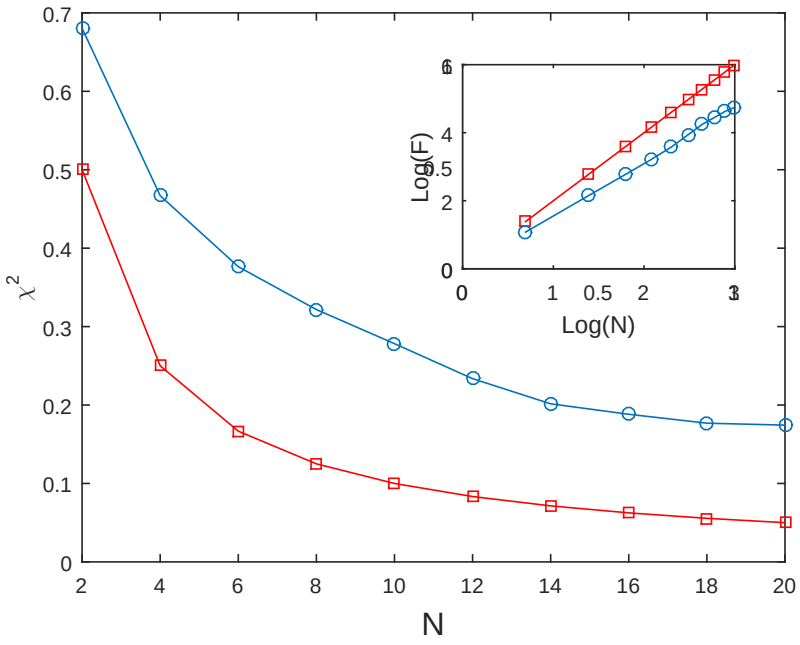

Figure 5.10: **Linearization of strong regime of interaction.** The minimum value of χ^2 (circled-blue) and χ^2_{HL} (squared-red) versus N for optimal $|\alpha|^2$ during the time span within the cut-off fixed on $gt_{cut-off} = 200$. In the inset we have plotted the $\log F$ and $\log F_{HL}$ versus $\log N$.

5.2 Conclusion

In this section, we have used the quantum Fisher information in order to detect multi-particle entanglement in a Dicke system with N atoms. The various interaction regimes have been studied. In the weak field limit χ^2 and ξ^2 give the same result. Nevertheless by increasing the strength of the initial field they begin to behave differently. For the cases of weak and strong interaction limit, the approximate approaches have been used and analytical solutions have been derived. We have observed good agreement between the numerical and analytical results.

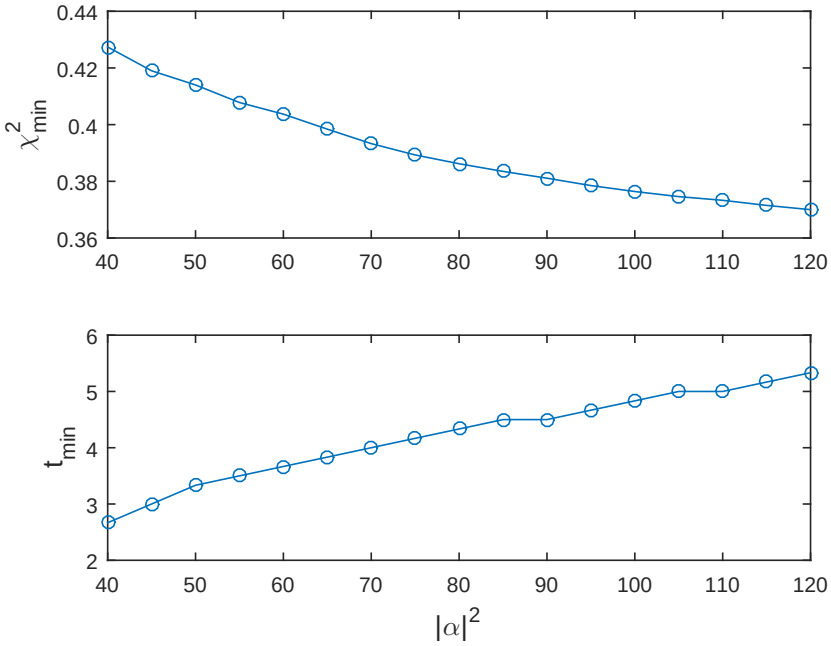

Figure 5.11: The first minimum of quantum Fisher information flag χ^2_{min} (upper) and the corresponding time t_{min} (lower) versus initial coherent field of $|\alpha|^2$ for $N = 6$.

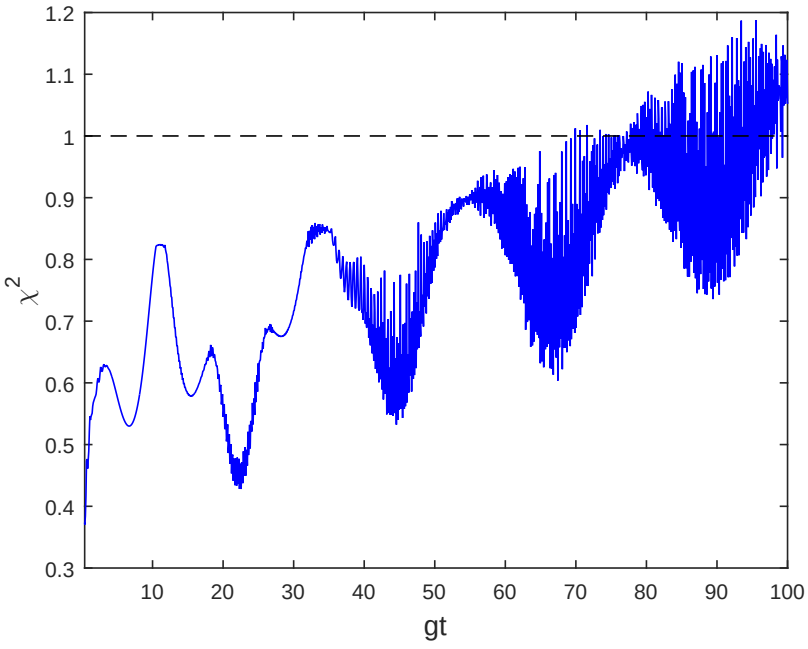

Figure 5.12: Collapse and revival of quantum Fisher information flag χ^2_{min} for the initial field of $|\alpha|^2 = 50$ for for $N = 3$.

Chapter 6

Summary and Conclusion

"Life is a journey, not a destination."
Emerson

In this work we have considered the Dicke system of finite numbers of particles interacting with a single mode of the coherent field inside a loss-less cavity. We have considered the dynamics under rotating-wave approximation and in the resonant condition. Moreover, the initial state of the atomic system is mostly supposed with all the atoms in the ground state[1]. As a result of coherent interaction of particles with the single cavity mode, the atom-atom entanglement appears among the particles in the system. We have studied the dynamics of multi-particle entanglement in the Dicke system considering different strength of the initial coherent field. Specifically, we have focused on the quantum Fisher information as a witness of multi-particle entanglement and have compared our results gained by QFI with other widely used witnesses of particle entanglement, i. e. spin squeezing.

Depending on the strength of the initial coherent field $\bar{n}$ compared to the numbers of particles in the system N, we have considered three regimes of interaction; namely weak $\bar{n} \ll N$, intermediate $\bar{n} \sim N$ and strong $\bar{n} \gg N > 1$ field regime. For the two extreme limits of weak and strong-field interactions, we have used approximated approaches to get the analytical solutions of the atomic wave-function. Consequently, we have found the analytical expressions for the quantum Fisher information flag [2]

[1] In fact, we also employed other initial states frequently but the most of this work has been done considering the initial coherent field of the cavity.

[2] Quantum Fisher information flag is defined as the ratio of the number of particles N to the maximum value of the quantum Fisher information F; that is $\chi^2 = N/F$.

In order to study the dynamics of quantum Fisher information, we have first considered the system of $N = 2$ particles interaction with the coherent mode of the cavity. Being composed of two atoms and a single mode of the quantized field, the system is the simplest extension of the Janes-Cummings model to a multi-partite Tavis-Cumming model. In order to investigate the multi-particle entanglement dynamics, we have started with exploring the interaction of the atomic pair with a weak initial coherent field. Considering the atomic system, we have derived the analytical expression for the quantum Fisher information flag. We have seen excellent agreement between the approximate analytical solutions and the exact numerical ones. Thereafter, we have compared the quantum Fisher information flag χ^2 and spin squeezing factor ξ^2 and have found the same regular periodic patterns of entanglement dynamics in the atomic system. We have shown the agreement between the χ^2 and ξ^2 is due to the fact that the state of the system is Gaussian in the weak field regime of interaction. In addition, beside quantum Fisher information - as a multi-particle entanglement witness - we have employed concurrence - pair-wise entanglement witness - and we have seen an excellent coincidence in the regular behavior of entanglement. Furthermore, we have found that the minimum amount of χ^2 decreases with increasing the initial photonic population $\bar{n} = |\alpha|^2$. By the way, while in the weak field regime we have detected almost always the entanglement between particles, the maximum amount of entanglement is very modest; it is far from the ultimate Heisenberg limit; $\chi^2_{min} \sim 1$.

Secondly, we have considered the interaction of the pair of atoms with an initial coherent field in the intermediate field regime, that is $\bar{n} \sim N = 2$. We have seen that by increasing the value of the initial coherent field, the quantum Fisher information loses its regularity and begin to behave aperiodically. By comparing χ^2 and ξ^2 when we smoothly move from the weak to intermediate field regime, we have seen that they begin to give different values during time. Of course, always the condition $\chi^2 \leq \xi^2$ fulfils. Using the numerical exact simulations, we have explored the optimal minimum values of both quantum Fisher information and spin squeezing versus increasing $|\alpha|^2$ for a fixed duration of time. Qualitatively, we have get the same trend for the spin squeezing and quantum fisher information flag when changing the strength of the initial coherent field; that is decreasing the minimum values of the χ^2 and ξ^2 by increasing the photonic population up to an optimal strength $|\alpha_{opt}|^2$ and afterward increasing it. We have noticed that the smallest value of the spin squeezing appear in smaller field strengths than that of the quantum Fisher information flag. After passing the minima, spin squeezing increases with a high slope while quantum Fisher information increases moderately. We have found the

ratio of minimum amount of the spin squeezing and quantum Fisher information flag to the ultimate values as $[\chi^2]_{min}/\chi^2_{HL} = 1.16$ and $[\xi^2]_{min}/\xi^2_{HL} = 1.30$ which is considerable compared to the weak field limit. By the way, the aperiodicity of the dynamics of entanglement is a flaw when it comes to experimental measurement.

In the intermediate field regime, beside the coherent fields, we have also considered the case of single Fock state of the field. As we have discussed in advance, the interaction of the two two-level atoms with a single Fock state of the field resembles the double-slit experiment in the atomic systems. Therefore, due to lack of information in the internal states of the atoms, the maximally entangled states result. We have used the quantum Fisher information to detect the maximally entangled state which is in agreement with the results of concurrence. Our result also is in agreement with the corresponding experiment in Ref. [63] which has been done by mean of full tomography of the density matrix of the atomic system following by using an entanglement witness. In fact, by increasing the numbers of atoms using quantum Fisher information may appear as an easier experimental task than using the entanglement witnesses. Moreover, the spin squeezing definition given by Wineland *et al* is proved to be insufficient for detecting entanglement when the initial state of the field is a Fock state [91].

Thirdly, we have taken the initial field in the strong field limit; i. e. $\bar{n} \gg N > 1$ [3]. We have employed the factorization approximation, to get the analytical atomic density matrix of the system and derived the approximate quantum Fisher information flag of the atomic system. Our approximate results demonstrate good agreement with the exact numerical simulations in the validity region of the approximation. We have also explored the spin squeezing and as has discussed in . [91]. We have found that as long as $\bar{n} > N$ the spin squeezing increases and finally vanished in the limit of large initial fields. This is related to the fact that in the strong field regime, the atomic system gets very mixed to the field which corresponds to the decreasing of the collective mean spin length of the atomic sub-system. As a result, the ratio of the collective spin fluctuations to the mean spin length increases. In this case, we have given a brief proof using the factorization approximation in parallel to the corresponding numerical simulation results. The interesting point is that, depending on the initial coherent field, we have found a regular behavior for the dynamics of quantum Fisher information flag. This indicates the regular dynamics of the (useful) entanglement among particles. In other words, in the strong field regime the entanglement dynamics regains a regular behavior which had been lost

[3] By the way, the field is still of quantum nature described by the wave-function not a classical one.

in the intermediate regime. The appearance of the regular behavior in dynamics of the observables in the strong field regime is not something new. Perhaps the most interesting features in this context would be the collapse and revival of population inversion which occur in certain times in the system which has been studied for both Janes-Cummings and Tavis-Cummings models. The same behavior has been detected using tangle (square of concurrence) for the case of $N = 2$ [67] and more atoms [68] in the atomic system. We have also calculated concurrence and found the similar predictions for the dynamics of maximum values of entanglement during time. Finally, in the regime of strong field regime, we have considered two initially entangled states of the atomic system and have observed the return of entanglement in later times. Comparing to concurrence, we have found the same dynamics in appearance of the peaks of the reappeared entanglement. By the way, we put emphasis on the fact that the quantum Fisher information and concurrence intrinsically are related to different types of entanglement in the system; the first measure is related to the multi-particle entanglement while the latter is linked to pair-wise entanglement. It has been proved that the concurrence is connected to the spin squeezing definition of Ueda and Kitagawa [73]. On the other hand, the quantum Fisher information is proved to be related to the quantum metrology protocols. With increasing the strength of the initial coherent field in the strong field limit, we have found that the χ^2 decreases and finally shows an asymptotic behavior. By the way, the time in which the optimal χ^2 increases corresponds to the increase of the field. Therefore, in the limit of $|\alpha|^2 \to \infty$ the optimal entanglement appears at very long times; i. e. when practically there is no particle entanglement in the system. This is consistent with what one would expect from interaction of the atomic system with a classical field. Considering a fixed time span, we have found that in the strong field regime as well as weak field regime, the entanglement appears in shorter time scales than the intermediate limit.

In the second part of this thesis, we have extended the study of Dicke model of $N = 2$ atoms to the case of finite numbers of particles N in the system. In this regard, we have discussed the dynamics of the quantum Fisher information flag for the same regimes of interaction; that is the weak, intermediate and strong-field regimes. The importance of studying the dynamics of quantum Fisher information in small ensembles of particles is that it reveals the dynamics of entanglement in the atomic system. To the best of our knowledge, for the spin systems being composed of $N > 2$ particles, a general measure of multi-particle does not exist. By investigating the dynamics of χ^2, we are indeed exploring the multi-particle (useful) entanglement between the particles in the atomic sub-system.

Considering the interaction of a weak coherent field with N particles in the Dicke model, we have derived the analytical expression of the QFI of the atomic system. Based on our results, in the regime of weak field interaction the χ^2 dynamics yields a regular pattern with a specific period proportional to the squared numbers of particles $\sqrt{N}$. The same as the case of $N = 2$ atoms in the system, the atomic density matrix is Gaussian; that is $\chi^2 = \xi^2$. In the weak field regime, with increasing the numbers of particles N, the minimum value of χ^2 decreases[4] and approaches an asymptotic behavior which is in agreement with previous work of Ref. [91]. By the way, the maximum amount of entanglement keeps being inconsiderable, order of $.98 \sim 1$. In addition, we have found that increasing the initial weak field - while keeping the restriction of $\bar{n} \ll 1$ - increases the minimum value of the χ^2. This is in agreement with the results on spin squeezing given in [91]. For the case of intermediate field regime, the numerical results for dynamics of entanglement measures get unwieldy. Alike the case of $N = 2$, the χ^2 and ξ^2 give irregular behavior while always $\chi^2 \ll \xi^2$. It is found that for a fixed N, with increasing $\bar{n}$ both quantum Fisher information and spin squeezing factors give smaller minimum values. Considering different numbers of atoms N, we have observed almost the same patterns of the minimum value of the entanglement measures as given for the case of $N = 2$ [5]. Based on our numerical results, both the quantum fisher information flag and spin squeezing factor decrease when the field strength smoothly increases up to an optimal value corresponding to an optimal initial field strength. Thereafter, both measures begin to increase. Up to $N = 20$, we have always found the optimal value on initial field of χ^2 in stronger optimal fields than ξ^2. For, the stronger fields than the optimal value, both measure begin to increase and approach toward unity. However, with increasing $\bar{n}$, spin squeezing approaches faster toward unity and for the number of particles $2 \leq N \leq 20$ we have observed that up to $\bar{n} \sim N/2$ spin squeezing value gets very small. By the way, quantum Fisher information in the same neighbour demonstrates its minimum value and afterward decreases. Comparing spin squeezing and quantum Fisher information, we have noticed that χ^2 exists for a larger domain of initial coherent field than ξ^2. Taking the minimum possibles values of quantum Fisher information over changing field strength for different N's, we have found that χ^2 decreases with increasing the number of particles. Our numerical results for up to 20 atoms in the system gives the linear fitting of the quantum Fisher information as $F_{opt} \propto N^{1.6}$ in comparison to ultimate Heisenberg limit of $F_{HL} \propto N^2$. Regarding the pros and cons of the intermediate field limit, the best possible value of entan-

[4] It decreases in a sense that gives larger entanglement.

[5] Results are given for a fixed time span for all N's and $\bar{n}$'s.

glement based on quantum Fisher information detections occurs in the intermediate field regime. By the way, the irregular behavior of the χ^2 and correspondingly the entanglement dynamics is a weak point when it comes to experimental purposes.

Last but not least, we have considered the strong field regimes when there are finite numbers of particles in the atomic system. In fact, studying the strong field regime is due to the dominance of the photonic population, in general there is analytical solutions for the dynamics of the system. The factorization approximation let us to calculate the mean spin values and correspondingly the quantum Fisher information as well as spin squeezing analytically [6]. Moreover, it is a good checkpoint for the numerical results. It is known that the strong field regime is connected to the collapse and revival of the dynamics of the atomic system. Therefore, one would naturally expect a parallel effects in the dynamics of entanglement between particles. By the way, due to mix-ness of the atomic state it is in general difficult to find a proper measure to detect the multi-particle entanglement. For these motivations, we have studied dynamic of entanglement in presence of N particle in the system by use of χ^2 measure. We have presented both analytical and numerical results up to 20 numbers of atoms in the system. For the fixed numbers of particles, we have seen the regular behaviors in the dynamics of quantum Fisher information, ξ^2. They demonstrate good agreement to the analytical results in the validity region of the approximation. Moreover, we have found that the appearance of minimum values of entanglement is smaller than the collapse/revival time. Regarding the squeezing parameter, it is already reported in Ref. [91] that for strong field strength $\bar{n} \gg N$ the spin squeezing continues to decrease and approaches to unity. We also have check numerically this issue and have got almost always negligible values of the ξ^2 in the strong field regime. Therefore, it seems that in the strong field regime, spin squeezing is not detecting multi-particle entanglement sufficiently. Also, we have examined the dependence of χ^2 on the initial coherent field strength for fixed numbers of particle N. Based on our results, by increasing the initial coherent field strength, the minimum value of the quantum Fisher information flag improves (namely gets smaller). Nevertheless, the time in which the minimum value appear also increase, in parallel. Consequently, for very strong initial coherent field (classical field), the entanglement happens in very long times (comparing to the collapse/revival time). Thus, there is no practical multi-particle entanglement in the system. In addition, we have considered the effect of increasing the numbers of particles on the entanglement

[6] By the way, since the quantum Fisher information is defined based on the diagonalization of the atomic density matrix with increasing the number of atoms it is quite cumbersome to find explicit terms. In these case, the alternative is to use the Fisher information rather than quantum Fisher information to get the results.

among them. One would expect that with increasing the number of atoms N in the atomic sub-system, by strengthening the role of atomic sub-system, the multi-particle entanglement improves. In this case, our results show that for a fixed initial field strength, increasing the number of particles, the minimum values of the χ^2 increases as well. Nevertheless, by increasing N from 2 to 20, the violation from the ultimate Heisenberg limit $1/N$ also grows. Thus, it seems that the closest value of χ^2 to the Heisenberg-limit is the one for $N = 2$. We have obtained the linear-fit of optimal quantum Fisher information as $F \propto N^{1.56}$ compared to the upper-bound of $F_{HL} \propto N^2$, which is less than the intermediate regime but still quite modest. At last, we have used quantum Fisher information for the case of collapse and revival of the Schrödinger cat state; with strong field and atomic system initiated in an maximally entangled $|\text{GHZ}\rangle$ state. It seems that it is possible to extend the study to the case of more particles in the system. But to prevent difficulties regarding the huge size of the Hilbert space it seems more fruitful to use the Fisher information instead of quantum Fisher information. In that case, employing the Holstein-Primakof approximation probably would be useful as long as $\langle a^\dagger a\rangle \ll N$ to get analytical results. By the way, in the limit of $N \to \infty$ due to coupling of two harmonic oscillators, there is no particle entanglement in the system.

In conclusion, we have investigated the usefulness of quantum Fisher information as a tool to study the dynamics of the finite size Dicke system. Considering the different intensity of the initial coherent field, we have seen that quantum Fisher information appears as a very useful witness for exploring the dynamics of entanglement between (atoms). For the two extreme regimes, we support our numerical results with the analytical ones. We have seen that moving from the weak to strong regimes, there is always useful entanglement *somewhere* in the system. This can be interesting from the atom interferometry point of view. Moreover, we have noticed that the regularity of the entanglement dynamics looses but returns in the strong field regime. In fact, the strong field regime of Dicke model is known for revealing regular behaviours, most interestingly in collapse and revival manner. Moreover, it seems that ξ^2 factor is useful also in presence of the number Fock states of the initial cavity field. Moreover, an entanglement measure seems to work sufficiently well when the atomic density matrix is in the mixed state. In addition, one has to note that the quantum Fisher information is a concept appearing from the heart of parameter estimation theory. Therefore, it is not restricted to the case of spin systems. In fact, we can also use quantum Fisher information for detecting the non-classicality in the bosonic system. Also, it seems possible to generalize it to a measure for investigating the dynamics of the atom-field entanglement in the Dicke system.

Appendix A

Short review of Positive-Operated-Value Measure (POVM) formalism

In this appendix we briefly present the general properties of the POVM formalism used in context of quantum measurement theory.

The 3rd postulate of quantum mechanics concerning the quantum measurement reads as [38]

> " Quantum mechanics are described by a collection $\{M_m\}$ of *measurement operators*. They are operators acting on the state space of the system being measured. The index m referred to the measurement outcome that may occur in experiment. If the state of the quantum system is $|\psi\rangle$ immediately before the measurement then the probability that result m occurs is given by
>
> $$P(m) = \langle\psi|{M_m}^\dagger M_m|\psi\rangle, \tag{A..0.1}$$
>
> and the state of the system by measurement changes as
>
> $$|\psi\rangle \rightarrow \frac{M_m|\psi\rangle}{\sqrt{\langle\psi|{M_m}^\dagger M_m|\psi\rangle}}. \tag{A..0.2}$$
>
> The measurement operator satisfy the completeness equation
>
> $$\sum_m M_m^\dagger M_m = I \tag{A..0.3}$$
>
> which ensures that the probabilities sums to 1 [1]."

Therefore, based on the measurement postulate it is possible to get the *post-measurement* states of the quantum system with the corresponding probability of getting specific outcome. By the way, there are cases in which the post-measurement state of the system is not of importance. For instance, the measurement is in such a way that it is possible to carry out a measurement only once (such as photo-detection when the

[1] Here, I is the Identity operator in the corresponding Hilbert space

photon is destroyed by the measurement process) or simply we are only interested the probability of getting the respective outcome of measurement. In These cases, it is convenient to use the Positive-Operator-Valued Measure (POVM) formalism. This task is done by defining the following operators

$$\Pi_m \equiv M_m^\dagger M_m. \tag{A..0.4}$$

Then from Postulate 3 and elementary linear algebra, Π_m is a positive (non-negative in fact) operator such that $\sum_n \Pi_m = I$ and $P(m) = \langle\psi|\Pi_m|\psi\rangle$. Thus the set of operators Π_m's are sufficient to determine the probabilities of the different measurement outcomes. The operators Π_m are known as the POVM elements associated with the measurement. The complete set $\{\Pi_m\}$ is known as a POVM.

In general, the elements of a POVM are not necessarily orthogonal, with the consequence that the number of elements in the POVM, can be larger than the dimension, of the Hilbert space they act in. In fact, the POVM formalism is the generalization of the standards projective measurement when the orthogonality condition is imposed,

$$\Pi_m \Pi_{m'} = \delta_{m,m'} \Pi_m. \tag{A..0.5}$$

In this case, the projective property for each element $\Pi_m^\dagger \Pi_m = \Pi_m$ is fulfilled *per se*. (as soon as we apply A we get to B).

By the way, the state of the system is not pure in general, but is a mixed state presented by the density matrix $\rho = \sum_i p_i |\psi_i\rangle\langle\psi_i|$ where p_i is the probability of being in the i'th possible pure state. In this case, the probability of obtaining the result m provided that the system is in $|\psi_i\rangle$ reads

$$P(m|i) = \langle\psi_i|\Pi_m|\psi_i\rangle = Tr(\Pi_m|\psi_i\rangle\langle\psi_i|) \tag{A..0.6}$$

and consequently, the probability of having m as result of measurement on ρ is given by

$$
\begin{aligned}
P(m) &= \sum_i P(m|i)p_i \\
&= \sum_i p_i Tr(\Pi_m|\psi_i\rangle\langle\psi_i|) \\
&= Tr(\rho\Pi_m), \qquad \text{(A..0.7)}
\end{aligned}
$$

where, in the first line we have used a property of conditioned probabilities while in the second line we have used A..0.6.

Appendix B

Deriving the explicit form of QFI

Here we derive the quantum Fisher information given in equation (3.2.35) in terms of complete basis of density matrix $\rho(\lambda) = \sum_i p_i |\phi_i\rangle\langle\phi_i|$ such that $p_i \geq 0$ and $\sum_i p_i = 1$. Note that since density matrix is dependent on λ in general p_i's and $|\phi_i\rangle$'s are also functions of λ. By the way, we do not show explicitly this dependence in the notation in following. In the density matrix basis the equation (3.2.35) is written as

$$F_\lambda(\rho) = \sum_{i,j} p_i |\langle\phi_i|L_\lambda|\phi_j\rangle|^2 = \sum_{i,j} \frac{p_i + p_j}{2} |\langle\phi_i|L_\lambda|\phi_j\rangle|^2. \tag{B..0.1}$$

Thus, in order to derive QFI one has to find the matrix elements of $\langle\phi_i|L_\lambda|\phi_j\rangle$ such that $p_i + p_j > 0$. Using definition of symmetric logarithmic derivative operators given in equation (3.2.29) we get

$$\langle\phi_i|L_\lambda|\phi_j\rangle = \frac{2\langle\phi_i|\partial_\lambda\rho|\phi_j\rangle}{(p_i + p_j)} \tag{B..0.2}$$

Therefore, equation (C..0.1) turns into

$$F_\lambda(\rho) = \sum_{i,j} \frac{2}{(p_i + p_j)} |\langle\phi_i|\partial_\lambda\rho|\phi_j\rangle|^2 \tag{B..0.3}$$

where the summation includes the term for which $(p_i + p_j) > 0$. Now, we use the following derivative chain rule

$$\partial_\lambda\rho = \sum_i (\partial_\lambda p_i)|\phi_i\rangle\langle\phi_i| + \sum_i p_i |\partial_\lambda\phi_i\rangle\langle\phi_i| + \sum_i p_i |\phi_i\rangle\langle\partial_\lambda\phi_i|, \tag{B..0.4}$$

where $|\partial_\lambda \phi_i\rangle \equiv \partial_\lambda |\phi_i\rangle$. Therefore, we have

$$\langle \phi_i|\partial_\lambda \rho|\phi_j\rangle = (\partial_\lambda p_i)\delta_{i,j} + (p_i - p_j)|\partial_\lambda \phi_i\rangle\langle\phi_j|. \tag{B..0.5}$$

where we have used $\partial_\lambda \langle\phi_i|\phi_j\rangle = \langle\partial_\lambda \phi_i|\phi_j\rangle + \phi_i|\langle\partial_\lambda \phi_j\rangle = 0$. Using equations (B..0.5) and (B..0.5) we get to the explicit expression for the quantum Fisher information as

$$F_\lambda(\rho) = \sum_{i=1}^{k} \frac{(\partial_\lambda p_i)^2}{p_i} + \sum_{i\neq j}^{k} \frac{2(p_i - p_j)^2}{(p_i + p_j)} |\langle\phi_i|\partial_\lambda \phi_j\rangle|^2, \ (k \leq n). \tag{B..0.6}$$

which is given in equation (3.2.36).

Appendix C

Calculating QFI for pure states - upper-bound

In order to find the explicit form of QFI we start from general form of equation (3.2.39). Consider the quantum system is in the pure state $\rho = |\phi_i\rangle\langle\phi_i|$ with $p_i = 1$ and $p_j = 0, \forall j \neq i$. We then apply the following displacement on the generator, $S_n \to S_n - \langle S_n\rangle$. This transformation does not make any change on the original Fisher information value since it depends on the $p_i - p_j$ in the denominator. Making this transformation, the Quantum Fisher information (3.2.39) gives

$$F(|\phi_i\rangle\langle\phi_i|, S_n) = 2\sum_{i\neq j} p_i|\langle\phi_i|S_n - \langle S_n\rangle|\phi_j\rangle|^2 = 4\Delta S_n^2. \tag{C..0.1}$$

To get to the second equality we have used the identity condition, $|\phi_i\rangle\langle\phi_i| = 1 - \sum_j |\phi_j\rangle\langle\phi_j|$. Now, we suppose that the quantum state is a general mixed state with density matrix $\rho = \sum_i |\phi_i\rangle\langle\psi_i|$. Using the inequality $\frac{(p_i-p_j)^2}{p_i+p_j} \leq p_i + p_j$ in equation 3.2.36 with (C..0.1) yields

$$F(\rho, S_n) \leq 4\Delta S_n^2. \tag{C..0.2}$$

This inequality implies the upper bound of QFI. i.e., any arbitrary mixed state of the system ρ has the smaller value of QFI than its value in pure state. It makes a good physical sense because a system in the mixture of pure states provides less information than when is in pure state.

Appendix D

Some useful properties of QFI

In this appendix we present some properties of quantum Fisher information we have already used in Chapter 3.

- **Convexity** - Let us consider the general state $\rho = \sum_i \mu_i \rho_i$ with $\mu_i > 0$ and $\sum_i \mu_i = 1$. From $Tr[\Pi(x)\rho(\lambda)] = \sum_i \mu_i Tr[\Pi(x)\rho_i]$ we get the probability of getting λ provided on having the experimental set of data x as

$$P(x|\lambda) = \sum_i \mu_i P_i(x|\lambda). \tag{D..0.1}$$

Based on Cauchy-Schwartz inequality we get

$$(\frac{\partial P(x|\lambda)}{\partial \lambda})^2 = (\sum_i \mu_i \frac{\partial P_i(x|\lambda)}{\partial \lambda})^2 \leq \sum_i \mu_i P_i(x|\lambda) \sum_i \mu_i \frac{1}{P_i} (\frac{\partial P_i(x|\lambda)}{\partial \lambda})^2. \tag{D..0.2}$$

Thus

$$\frac{1}{P(x|\lambda)} \leq \sum_i \mu_i \frac{1}{P_i} (\frac{\partial P_i(x|\lambda)}{\partial \lambda})^2 \tag{D..0.3}$$

After integrating the both sides of the above inequality over x and using the equation (3.2.26) we get

$$f_\lambda \leq \sum_i \mu_i f_\lambda^{(i)} \tag{D..0.4}$$

with $f_\lambda^{(i)} = \int dx \frac{1}{P_i(x|\lambda)} (\frac{\partial P_i(x|\lambda)}{\partial \lambda})^2$ as the Fisher information of i'th sub-state. Since, quantum Fisher information is the maximum fisher information over all possible POVM's, it can be proved that also quantum Fisher information is convex,

$$F(\rho) = F(\sum_i \mu_i \rho_i) \leq \sum_i \mu_i F(\rho_i). \tag{D..0.5}$$

- **Additivity** - For $\mathcal{N}$ independent sub-system and independent measurement we have

$$f_\lambda = \sum_{i=1}^{\mathcal{N}} f_\lambda^{(i)} \tag{D..0.6}$$

where $f_\lambda^{(i)} = \int dx \frac{1}{P_i(x|\lambda)} (\frac{\partial P_i(x|\lambda)}{\partial \lambda})^2$. is the Fisher information for i'th sub-system with summation over all measurement results x. In the case of identical sub-systems and identical POVM's we get

$$f_\lambda = \mathcal{N} f_\lambda^{(i)} \tag{D..0.7}$$

and Cramer-Rao bound as

$$\Delta E_{CR}^2 = \frac{1}{\mathcal{N} f_\lambda}, \tag{D..0.8}$$

which is given in equation (3.2.27).

Appendix E

Factorization approximation - a brief proof

In this appendix we present a proof for factorization approximation we have used in section 4.2.3.

- **proof** Let us introduce the transformation

$$Q = \exp[i\hat{\phi}(S_z + N/2)], \tag{E..0.1}$$

where $\exp(\pm i\hat{\phi})$ are the field phase operators defined as [93]

$$\begin{aligned} \exp(i\hat{\phi}) &= (aa^\dagger)^{-1/2}a, \\ \exp(-i\hat{\phi}) &= a^\dagger(aa^\dagger)^{-1/2} \end{aligned}$$

Applying Q on the bare atomic states $Q|N/2, M\rangle = M|N/2, M\rangle$ following by using the completeness property of the Dicke states, we obtain

$$Q = \sum_{M=-N/2}^{N/2} e^{iM\hat{\phi}}|N/2, M\rangle\langle N/2, M|. \tag{E..0.2}$$

In general, $[Q, Q^\dagger] = |N/2, 0\rangle\langle N/2, 0|$. However, as long as $\bar{n} \gg N \geq M$, Q is unitary operator. The following commutation properties of the Q will be used later

$$\begin{aligned} f(\hat{n})Q^\dagger &= Q^\dagger f(\hat{n} + S_z + N/2), \\ Qf(\hat{n}) &= f(\hat{n} + S_z + N/2)Q, \\ QS_+Q^\dagger &= \exp(i\hat{\phi})S_+, \\ QS_-Q^\dagger &= \exp(-i\hat{\phi})S_-. \end{aligned} \tag{E..0.3}$$

(E..0.4)

where, $\hat{n} = a^\dagger a$. We have not dropped the hat sign $\hat{}$ for the number and phase field operators to prevent mixing them up with the corresponding eigen-values. to stress it is being an operator. Acting on the bosonic operators we have

$$\begin{aligned} Q^\dagger \hat{n} Q &= \hat{n} - S_z - N/2, \\ Q^\dagger a Q &= \sqrt{\hat{n} - S_z - N/2 + 1} e^{i\hat{\phi}}. \end{aligned} \tag{E..0.5}$$

Applying the Q transformation to the Dicke interaction Hamiltonian 4.1.1, we will have the following transformed Hamiltonian

$$\begin{aligned} \tilde{H}_{int} &= Q^\dagger H_{int} Q \\ &= g(\sqrt{\hat{n} - S_z - N/2 + 1} S_+ + S_- \sqrt{\hat{n} - S_z - N/2 + 1}). \end{aligned} \tag{E..0.6}$$

in the regime of strong-field limit (in a sense $\hat{n} \gg S_z$), one can expand the transformed Hamiltonian in terms of power series of small parameter $(\hat{n} - N/2 + 1/2) \ll 1$ such that,

$$\tilde{H}_{int} = 2g\sqrt{\hat{n} - N/2 + 1/2} S_x - \frac{g[S_z, S_x]_+}{\sqrt{\hat{n} - N/2 + 1/2}} + ... \tag{E..0.7}$$

here $[]_+$ denotes the anti-commutator. It has been shown that even the first zeroth-order term

$$\tilde{H}_{int} \cong 2g\sqrt{\hat{n} - N/2 + 1/2} S_x, \tag{E..0.8}$$

suffices for well-describing the essential quantum phenomena such as collapse and revival of the atomic inversion, the wave function factorization at evolution of the Q-function. Now, the question is *what is the corresponding wave-function?* The answer comes in the following.

The original time evolution operator in terms of transformed Hamiltonian E..0.8 is given by

$$U(t) = Q\tilde{U}(t)Q^\dagger, \tag{E..0.9}$$

where,

$$\tilde{U}(t) = \exp(-2igt\sqrt{\hat{n} - N/2 + 1/2}S_x), \tag{E..0.10}$$

is the time evolution related to the effective Hamiltonian E..0.8. Using the above operator, we can write the time evolved wave function of the system as

$$\begin{aligned} |\psi(t)\rangle &= U(t)|\psi(0)\rangle \\ &= Q\tilde{U}Q^{\dagger}|\psi(0)\rangle. \end{aligned} \tag{E..0.11}$$

For some specific reason which will be clear later, let us take the specific atomic initial state as a semi-classical state,

$$|\psi(0)\rangle = |N/2, m_x\rangle \otimes |\alpha\rangle. \tag{E..0.12}$$

For the matter of convenience, we have replaced the capital letters for collective spin eigen-values M_x with small ones m_x. The phase operator acting on the coherent sate gives

$$e^{\pm i\hat{\phi}k}|\alpha\rangle = |\alpha\rangle + \frac{k\Delta\hat{n}}{2\bar{n}} + O(\frac{k}{\sqrt{\bar{n}}})^2. \tag{E..0.13}$$

Therefore, we have,

$$\begin{aligned} Q^{\dagger}|\psi(0)\rangle &= |N/2, m_x\rangle \otimes |\alpha\rangle - \frac{k\Delta\hat{n}}{2\bar{n}}(S_z + N/2)|N/2, m_x\rangle \otimes |\alpha\rangle \\ &\cong |N/2, m_x\rangle \otimes |\alpha\rangle \end{aligned} \tag{E..0.14}$$

In the second line we have ignored the second term as of the order of $O(k/\sqrt{\bar{n}})$ and compare to the first terms has no principal contribution to the results. Therefore, the initial state does not change, under the transformation Q. Next, we apply the operator $\tilde{U}$ on the transformed unitary initial state

$$\begin{aligned}\tilde{U}|N/2,m_x\rangle\otimes|\alpha\rangle &\approx \exp\{-2igt\sqrt{\bar{n}-N/2+1/2}S_x\}|N/2,m_x\rangle\otimes|\alpha\rangle \\ &= \exp\{-2im_xgt\sqrt{\hat{n}-N/2+1/2}\}|N/2,m_x\rangle\otimes|\alpha\rangle.\end{aligned} \tag{E..0.15}$$

Now, making use of Eq. E..0.14 and apply Q on the above equation we obtain

$$|\psi(t)\rangle \cong \exp(2im_xgt\sqrt{\hat{n}+S_z+1/2})|N/2,m_x\rangle\otimes|\alpha\rangle. \tag{E..0.16}$$

The last step is to apply the expansion of the square root ($\hat{n}\gg S_z$)

$$\begin{aligned}\sqrt{\hat{n}+S_z+1/2} &\approx \sqrt{\hat{n}-N/2+1/2}-\frac{S_z+N/2}{2\sqrt{\hat{n}-N/2+1/2}} \\ &+ O(\frac{N^2}{\bar{n}^3/2}) \qquad \text{(E..0.17)} \\ &. \qquad \text{(E..0.18)}\end{aligned}$$

In the above equation the first two terms are most dominant parts. Thus, we just keep these terms and neglect the rest. Note that the first and second terms commute. Thus, they act separately on the photonic and atomic parts of the wave function which yields

$$\begin{aligned}|\psi(t)\rangle &= \exp(-2igtm_x\sqrt{\hat{n}-N/2+1/2})|\alpha\rangle \\ &\otimes \exp(\frac{-im_xgt(S_z+1/2)}{\sqrt{\bar{n}-N/2+1/2}}),\end{aligned} \tag{E..0.19}$$

which coincides with equation (4.2.18) if

$$\begin{aligned}|\Phi_{mx}(t)\rangle &\equiv \exp\left(-2im_xgt\sqrt{\hat{n}-N/2+1/2}\right)|\alpha\rangle, \\ |A_{mx}(t)\rangle &\equiv \exp\left(-i\tau(S_z+N/2)\right)|N/2,m_x\rangle,\end{aligned} \tag{E..0.20}$$

with, $\tau=\frac{gm_x}{\sqrt{\bar{n}-N/2+1/2}}t$.

■

Appendix F

Plots for QFI in Strong-field limit for $N = 3, 5, 7$

Here, we present the plots for the χ^2 versus scaled time gt in the strong field regime of Chapter 5. The number of atoms are $N = 3, 5, 7$ and the photonic population is always set to $|\alpha|^2 = 100$ in order to preserve the strong field limit of $|\alpha|^2 = \bar{n} \gg N$. By increasing the number of atoms in the system, the analytical approximate begin to violate from the exact results. It worth to remind that in the factorization approximation is valid when $\bar{n} \gg N$. With increasing the number of particles, one has to increase the strength of the coherent field accordingly. Paradoxically, using the large photonic population $\bar{n}$ makes it difficult to apply the numerical simulations.

F. Plots for QFI in Strong-field limit for $N = 3, 5, 7$

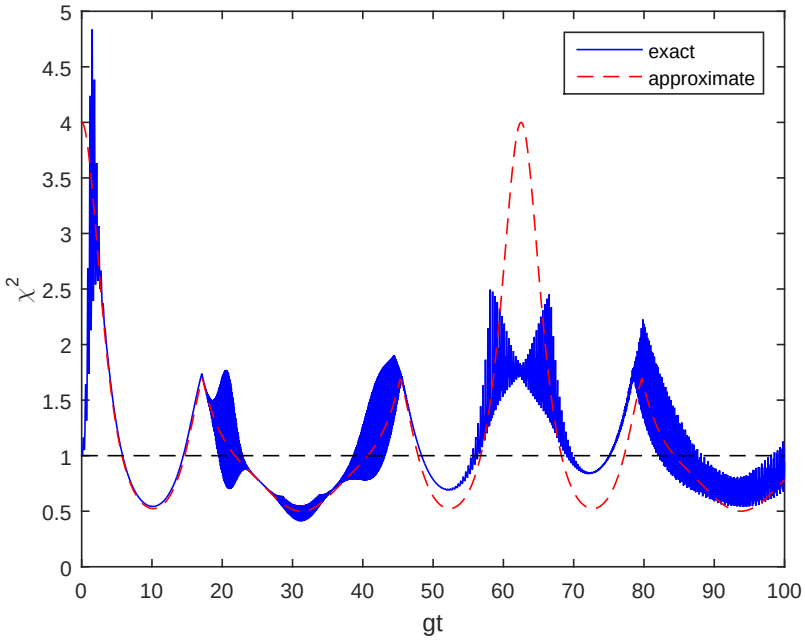

Figure F..1: The quantum Fisher information ξ^2 versus time gt for initial coherent field of population $|\alpha|^2 = 100$ for $N = 3$

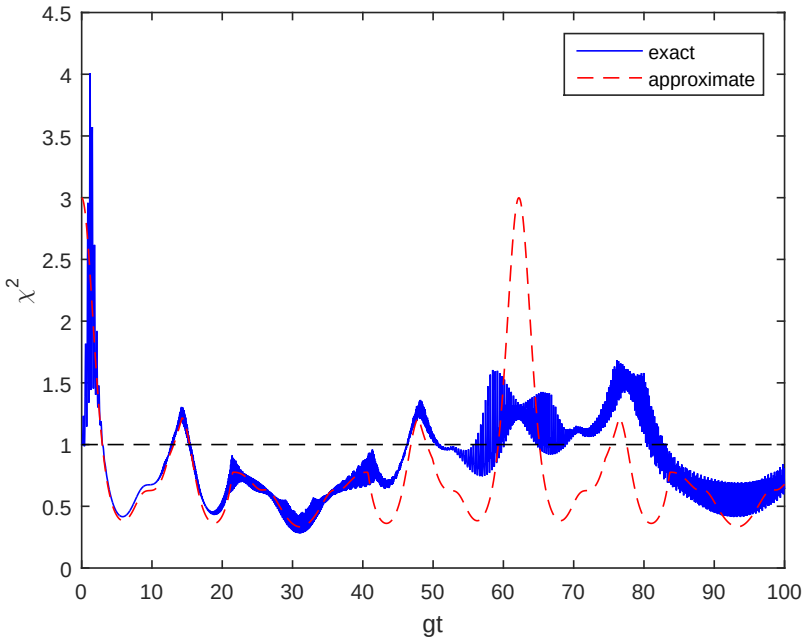

Figure F..2: The quantum Fisher information ξ^2 versus time gt for initial coherent field of population $|\alpha|^2 = 100$ for $N = 5$

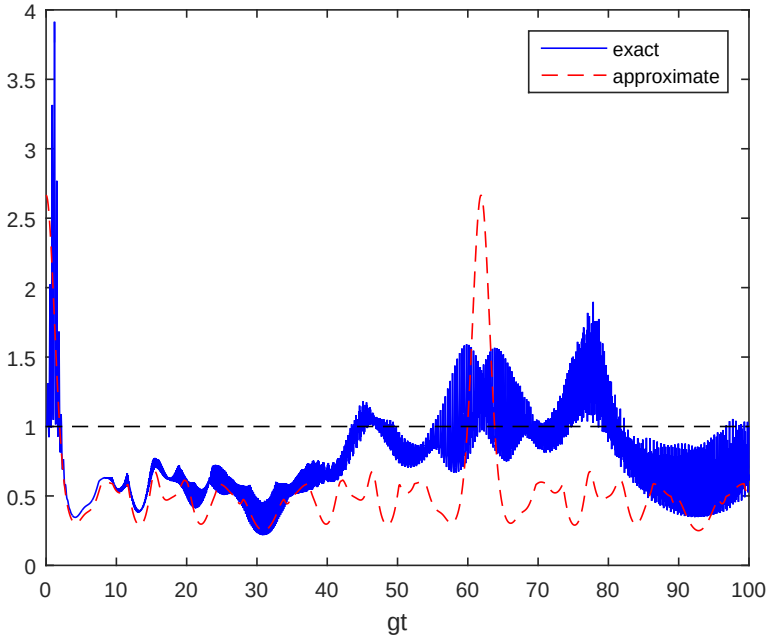

Figure F..3: The quantum Fisher information ξ^2 versus time gt for initial coherent field of population $|\alpha|^2 = 100$ for $N = 7$

Bibliography

[1] *Quantum Electrodynamics: the strange theory of light and matter*, R. P. Feynman (Princetone Univercity Press, 2006).

[2] E. M. Purcell, Phys. Rev. **69** 681 (1946).

[3] R. H. Dicke, Phys. Rev. **93**, 99 (1954).

[4] K. Hepp and E.H. Lieb, Ann. Phys. N.Y.**76**, 360 (1973).

[5] Y. K. Wang and F. T. Hioe, Phys. Rev. A 7, **831** (1973).

[6] C. Emary and T. Brandes, Phys. Rev. E, **67**, 066203 (2003). Phys. Rev. Lett. **103**, 083601 (2009).

[7] N. Lambert, C. Emary, and T. Brandes, Phys. Rev. Lett. **92**, 7 (2004).

[8] N. Lambert, C. Emary, and T. Brandes, Phys. Rev. A **71**, 053804 (2005).

[9] V. M. Bastidas, C. Emary, B. Regler, and T. Brandes Phys. Rev. Lett. **108**, 043003 (2012).

[10] T. H. Maiman Nature **187** (4736), 493 (1960).

[11] N. Skribanowitz, I. P. Herman, J. C. MacGillivray and M. S. Feld. Phys. Rev. Lett. **30** (8), 309 (1973).

[12] M. Gross, C. Fabre, P. Pillet and S. Haroche. Phys. Rev. Lett. **36** (17), 1035 (1976).

[13] A. Flusberg, T. Mossberg and S. R. Hartmann. Phys. Lett. A, **58** (6), 373 (1976).

[14] W. D. Phillips and H. Metcalf, Phys. Rev. Lett. **48** 596 (1982).

[15] P. D. Lett, R. N. Watts, C. I. Westbrook, W. D. Phillips, P. L. Gould, and H. J. Metcalf, Phys. Rev. Lett. **61** 169 (1988).

[16] E. L. Raab, M. Prentiss, A. Cable, S. Chu, and D. E. Pritchard, Phys. Rev. Lett. **59**, 2631 (1987).

[17] A. Ashkin, J. M. Dziedzic, J. E. Bjorkholm, and S. Chu, Opt. Lett. **11** 288 (1986).

[18] J. P. Gordon and A. Ashkin, Phys. Rev. A **21** 1606 (1980).

[19] E. T. Janes and F. W. Cummings, Proc. IEEE **51**, 89 (1963).

[20] M. Tavis and F. W. Cummings, Phys. Rev. **170**, 379 (1968).

[21] Y. Kaluzny, P. Goy, M. Gross, J. M. Raimond and S. Haroche. Phys. Rev. Lett. **51** (13), 1175 (1983).

[22] P. Goy, J. M. Raimond, M. Gross and S. Haroche. Phys. Rev. Lett. **50** (24), 1903 (1983).

[23] D. Meschede, H. Walther and G. Müller. Phys. Rev. Lett. 54(6), 551 (1985).

[24] G. Rempe, H. Walther and N. Klein. Phys. Rev. Lett. **58** (4), 353 (1987).

[25] G. Rempe, R. J. Thompson, R. J. Brecha, W. D. Lee and H. J. Kimble. Phys. Rev. Lett. **67** (13), 1727 (1991).

[26] R. J. Thompson, G. Rempe and H. J. Kimble, Phys. Rev. Lett. **68** (8), 1132 (1992).

[27] A. Wallraff, D. I. Schuster, A. Blais, L. Frunzio, R.-S. Huang, J. Majer, S. Kumar, S. M. Girvin, and R. J. Schoelkopf, Nat. 431, 162 (2004).

[28] G. Khitrova, H. M. Gibbs, M. Kira, S. W. Koch and A. Scherer. Nat. Phys. **2** (2), 81 (2006).

[29] J. M. Fink, R. Bianchetti, M. Baur, M. Goppl,, L. Steffen, S. Filipp, P. J. Leek, A. Blais, and A. Wallraff, Phys. Rev. Lett. **103**, 083601 (2009).

[30] K. Baumann, C. Guerlin, F. Brennecke and T. Esslinger, Nature, **464**, 1301 (2010).

[31] D. Nagy, G. Kónya, G. Szirmai, and P. Domokos, Phys. Rev. Lett. **104**, 130401 (2010).

[32] K. Baumann, R. Mottl, F. Brennecke, and T. Esslinger Phys. Rev. Lett. **107** 140402 (2011).

[33] F. Brennecke, R. Mottl, K. Baumann, R. Landig, T. Donner, and T. Esslinger, PNAS. **110** (29) 11763 (2013).

[34] M. P. Baden, K. J. Arnold, A. L. Grimsmo, S. Parkins, and M. D. Barrett, Phys. Rev. Lett. **113** 020408(2014).

[35] C. Hamner, C. Qu, Y. Zhang, J. Chang, M. Gong, C. Zhang and P. Engels, Nat. Com. **5** 402 (2014).

[36] L. J. Zou, D. Marcos, S. Diehl, S. Putz, J. Schmiedmayer, J. Majer and P. Rabl, Phys. Rev. Lett. **113** 023603 (2014).

[37] Jürgen Audretsch, Entangled Systems: New Directions in Quantum Physics (WILEY, 2007).

[38] *Quantum Computation and Quantum Information* (Cabridge University Press, 2000).

[39] K. Kim, M.-S. Chang, S. Korenblit, R. Islam, E. E. Edwards, J. K. Freericks, G.-D. Lin, L.-M. Duan and C. Monroe, Nature **465** 590 (2010).

[40] V. annetti, S. Lloyd, and L. Maccone, Phys. Rev. Lett. **96**, 010401 (2006).

[41] A. Sørensen, A. S., Duan, L., Cirac, J. and Zoller, Nature **409**, 63 (2001).

[42] D. J. Wineland, J. J. Bollinger, W. M. Itano, F. L. Moore, and D. J. Heinzen, Phys. Rev. A **46**, R6797(R) (1992).

[43] I. D. Leroux, M. H. Schleier-Smith, and V. VuletiÊ, Phys. Rev. Lett. 104 073602 (2010).

[44] M. H. Schleier-Smith, I. D. Leroux, and V. VuletiÊ, Phys. Rev. Lett. **104** 073604 (2010).

[45] C. Gross, T. Zibold, E. Nicklas, J. Estève, and M. K. Oberthaler, Nature **464** 1165 (2010).

[46] M. F. Riedel, P. Bohi, Y. Li, T. W. Hansch, A. Sinatra, and P. Treutlein, Nat. **464** 1170 (2010).

[47] L. Pezze and A. Smerzi, Phys. Rev. Lett. **102**, 100401(2009).

[48] M. G. A. Paris, Int. J. Quantum Inform. **07**, 125 (2009).

[49] P. Hyllus, O. Gú hne, and A. Smerzi, Phys. Rev. A, **82**, 012337 (2010).

[50] H. Primakoff and T. Holstein, Phys. Rev. **55** 1218 (1939).

[51] *Quantum Optics* (Cambridge University Press, 2013).

[52] R. P. Feynmann, F. L. vernon and R. W. Hellwarth, J. Appl. Phys. **28**, 49 (1957).

[53] S. Schneider and G. J. Milburn, Phys. Rev. A **65**, 042107 (2002).

[54] S. Morrison and A. S. Parkins, Phys. Rev. A **77**, 043810 (2008).

[55] X. Hou and Bambi Hu, Phys. Rev. A **69** 042110 (2004). **tanas** Z. Ficek and R. Tanaś, Phys. Rev. A **77** 054301, (2008).

[56] A. Alvermann, L. Bakemeier, and H. Fehske, Phys. Rev. A 85, **043803** (2012).

[57] G. S. Agarwal, R. P. Puri and R. P. Singh, Phys. Rev. A **56** 2249 (1997).

[58] E. Solano, G. S. Agarwal and H. Walther, Phys. Rev. Lett. **90** 027903 (2003).

[59] *Open Quantum Systems Far from Equilibrium* by Gernot Schaller (Springer International Publishing 2014).

[60] D. Nagy and P. Domokos, Phys. Rev. Lett. **115** 043601 (2015).

[61] G. V. Varada, M. S. Kumar and G. S. Agarwal, Opt. Commun. **62** 328 (1087).

[62] B. M. Garraway, Phil. Trans. R. Soc. A **369** 1137 (2011).

[63] J. A. Mlynek, A. A. Abdumalikov, J. M. Fink, L. Steffen, M. Baur, C. Lang, A. F. van Loo, and A. Wallraff, Phys. Rev. A **86**, 053838 (2012).

[64] B. L ücke, M. Scherer, J. Kruse, L. Pezzé, F. Deuretzbacher, P. Hyllus, O. Topic, J. Peise, W. Ertmer, J. Arlt, L. Santos, A. Smerzi and C. Klempt, Science textbf334, 773 (2011).

[65] V. Vedral and M. B. Plenio, Phys. Rev. A **57** 1619 (1998).

[66] S. Hill and W. K. Wootters, Phys. Rev. Lett. **78**, 5022 (1997).

[67] T. E. Tessier, I. H. Deutsch, and A. Delgado and I. Fuentes-Guridi, Phys. Rev. A **68** 062316 (2003).

[68] C E A Jarvis et al, New J. Phys. **11**, 103047 (2009).

[69] X. Wang and K. Mølmer, Euro. Phys. J. D, **18(3)** 385 (2002).

[70] X. Wang and B. C. Sanders, Phys. Rev. A **68** 012101 (2003).

[71] J Ma, X Wang, CP Sun, F Nori, Phys. rep. **509**, 89 (2011).

[72] J. K. Korbicz, J. I. Cirac, and M. Lewenstein, Phys. Rev. Lett. **95** 120502 (2005).

[73] M. Kitagawa and M. Ueda, Phys. Rev. A **47**, 5138 (1993).

[74] H. J. Lipkin, N. Meshkov, and A. J. Glick, Nucl. Phys. **62** 188 (1965).

[75] N. Meshkov, A. J. Glick, and H. J. Lipkin, Nucl. Phys. **62** 199 (1965).

[76] S. Morrison and A. S. Parkins, Phys. Rev. Lett. **100** 040403 (2008).

[77] S. Morrison and A. S. Parkins, Phys. Rev. A **77** 043810 (2008).

[78] Roy J. Glauber, Phys. Rev. **131** 2766 (1963).

[79] Roy J. Glauber, Phys. Rev. Lett. **10** 84 (1963).

[80] C. R. Rao, Bull. Calcutta Math. Soc. **37** 81 (1945).

[81] H. Cramer, *Mathematical methods of statistics* (Princeton University Press, Prineton, 1946).

[82] M. Frechet, Rev. Int. Stat. Inst., **11** 182 (1943).

[83] G. Darmois, Rev. Int. Stat. Inst., **13** 9 (1945).

[84] R. A. Fisher, Proc. R. Soc. Edinburgh, **42** 321 (1922).

[85] R. A. Fisher, Proc. Camb. Phil. Soc. **22** 700 (1925).

[86] L. Pezzé, A. Smerzi, G. Khoury, J. F. Hodelin, and D. Bouwmeester, Phys. Rev. Lett. **99** 223602 (2007).

[87] L. Pezzé and A. Smerzi, Phys. Rev. Lett. **100** 073601 (2008).

[88] Á. Rivas and A. Luis, Phys. Rev. Lett. **105** 010403 (2010).

[89] A.B. Klimov, C. Saavedra, Phys. Lett. A, **247** 14 (1998).

[90] L. Yu, J. Fan, S. Zhu, G. Chen, S. Jia, and Franco Nori Phys. Rev. A **89**, 023838, (2014).

[91] C. Genes, P. R. Berman, and A. G. Rojo, Phys Rev. A **68**, 043809 (2003).

[92] W. Dür, G. Vidal, and J. I. Cirac, Phys. Rev. A, **62**, 062314 (2000).

[93] S. M. Chumakov, A. B. Klimov, and J. J. Sanchez-Mondragon, Phys. Rev. A **49**, 4972 (1994).

[94] J. C. Retamal, C. Saavedra, A. B. Klimov and S. M. Chumacov, Phys. Rev. A. **55** (3) 2413 (1997).

[95] Phys. Rev. A, **58** (3) 2056 (1998).

[96] D. DiVincenzo, The physical implementation of quantum computation. Fortschr. Phys. **48** 771 (2000).

[97] D. Leibfried, M. D. Barrett, T. Schaetz, J. Britton, J. Chiaverini, W. M. Itano, J. D. Jost, C. Langer, D. J. Wineland, Science **304** 1476 (2004).

[98] C. H. Bennett, G. Brassard, C. Crépeau, R. Jozsa, A. Peres, W. K. Wootters, Phys. Rev. Lett. 70, 1895–1899 (1993).

[99] H. W. Muessel, D. Linnemann, T. Zibold, D. B. Hume, L. Pezzè, A. Smerzi, and M. K. Oberthaler, Science **345** 6195, 424 (2014).

[100] S. Schneider and G. J. Milburn, Phys. Rev. A **65** 042107 (2001).